DOE/ER/40713-1

DOE/ER/40713--1

DE93 013127

Annual Report

Relativistic Heavy Ion Research

Department of Physics and Astronomy
Wayne State University
Detroit MI 48202

October 1, 1991 to September 30, 1992

Forward

This is the first Annual report of the Relativistic Heavy Ion Research effort at Wayne State University. At present the group encompasses the efforts of three regular faculty, (R. Bellwied, T. Cormier, J. Hall) three research faculty (S. Bennett, C. Pruneau , G.Welke) one research associate (Q. Li) and nine graduate students. A significant fraction of this first year has been devoted to recruiting and establishing an appropriate infrastructure. There was, however, some time left to participate in our collaborative research efforts. The experimental work that is reported herein is largely the result the efforts of the E814, E877, E864 and STAR collaborations and thus involves upwards of 300 individuals. It is thus not practical in this format to identify all our collaborators for each of the topics presented. We take the expedient step, therefore, of identifying only the collaboration in each case.

This research has been supported by Wayne State University through the College of Science and the Office of Sponsored Research and by the Department of Energy under grant DE-FG02-92ER40713. All of the work presented here should be regarded as preliminary and should not be quoted or referenced without approval of the appropriate collaboration.

Tom Cormier
October 15, 1992

Table of Contents

I E814/E877 Progress Report

I.1 Transverse Energy Production in 10.7 GeV/c/u Au on Au collisions.

Last spring, Au-nuclei were accelerated up to 10.7 GeV/c/u by the Tandem/Booster/AGS accelerator complex at BNL. The 2.1 TeV beam was delivered to experiments for the first time on August 26, 1992 and was used by the experiments for a 3 week period. Typical beam rates delivered to experiment 877 ranged from a few 1000 to 10000 beam particles per spill. Although such intensities are low, we successfully took data to measure the beam purity, the production of delta rays in the target, and the level of occupancy in the zero degree spectrometer. The main thrust of the data taking, however, was dedicated to a measurement of transverse energy production with the new Au beam.

The beam momentum was 10.7 GeV/c/u instead of the full 11.7 GeV/c/u available in principle. The lower momentum value resulted from the selection of a lower charge state rather than the fully stripped +79 for injection into the AGS.

The beam purity at the E877 target station was measured with a set of two surface barrier detectors positioned into the beam path and was found to be excellent. Over 95% of the beam particles delivered to our experiment had an atomic number 79. Thus the beam purity is found to be quite acceptable for the study of reactions with the gold beam. As for the ^{28}Si induced collision studies however, a set of scintillators and a surface barrier detectors located upstream of the target were used to measure the projectile z (atomic number) for each beam particle and veto the data acquisition for smaller beam fragments. Targets of Al, Cu, Pb and Au with thickness of 2% of an interaction length were used.

The measurement of transverse energy (E_t) production was accomplished with both the target and the participant calorimeters. The data analysis is still underway but preliminary results are already available and shown in Figures 1 and 2. In each case, figures a and b show plots of transverse energy production for Si and Au projectiles respectively. The energy measured with the PCAL has been corrected for both geometrical efficiency and energy leakage outside the calorimeter. Similar corrections still need to be applied to the TCAL data. The leakage correction in the TCAL is quite significant and can amount to an overall factor of two.

The data for the Al, Cu, Au and Pb targets are shown with dash, solid, dash-dot and solid curves respectively in Figure 1 and 2. The E_t spectra have the now familiar shape dominated by the collision geometry. The steep rise seen at very low E_t corresponding to peripheral reactions is followed by a plateau and terminates for the most central collisions at high E_t with a rapid drop. The data taken with the Au-beam show a steady increase of transverse energy production for increasing target size. A similar increase of transverse energy production for increasing target size is observed with the Si beam. Neither set of data indicate a saturation of the transverse energy production for increasingly large system.

In fact, the E_t production achieved in central Au + Au collisions is remarkably large, up to a maximum of nearly 320 GeV into the PCAL's acceptance alone. This is to be compared with the E_t production measured[1,2] in central Al + Si collisions, 40 GeV or so. The ratio of E_t produced in central Au + Au to the E_t produced in central Si + Al is 8. As the beam momentum for Si and Au were different, a small correction to that ratio has to be applied to take into account the linear increase of E_t production with the center of mass energy .

After such a correction we conclude that the E_t production scales as $A^{1.1}$ where A is the size of the system. The E_t production is thus found to increase faster than the size of the colliding system. This is in sharp contrast with the prediction of the model FRITIOF[3] shown in Figure 1b as open squares. FRITIOF [3] assumes that only primary collisions lead to the production of transverse energy and therefore predicts and E_t scaling linearly as A which clearly underestimates the measured E_t production. The data are well reproduced however by calculations with the RQMD[4] and HIJET models shown with stars and open crosses respectively in Figure 1. Both these models include rescattering of the secondaries.

Detailed RQMD calculations have predicted that energy densities in excess of 15 times the normal density can be attained in Au on Au collisions whereas the predicted maximum energy density predicted for Si + Si does not go beyond 10 times the normal nuclear density. At AGS energies, nuclear matter is essentially opaque and, as the size of the colliding system is increased, both the increased number of colliding nucleons and the rescattering of the secondaries combine to produce increasingly higher energy densities. The effect is quite important as the RQMD prediction suggest that the achieved energy and baryon densities are large enough and possibly last long enough to permit the formation of a Quark Gluon Plasma.

Work is currently proceeding to confirm both these preliminary experimental results and the RQMD calculations. The present data by no means prove the existence of the formation of a QGP, however they demonstrate the great interest in the AGS Au beam as a laboratory to study very hot and dense nuclear matter which are two key ingredients for the formation of a QGP.

1) J. Barrette etal. E814 Collab. Phys.Rev.Lett. 64 (1990) 1219.
2) J. Stachel and G.R. Young, Ann.Rev. Nucl.Part.Sci. 42 (1992).
3) B.Andersson etal.Phys.Reports 97 (1983)
4) H.Sorge etal. Phys.Lett. 243 (1990) 7.

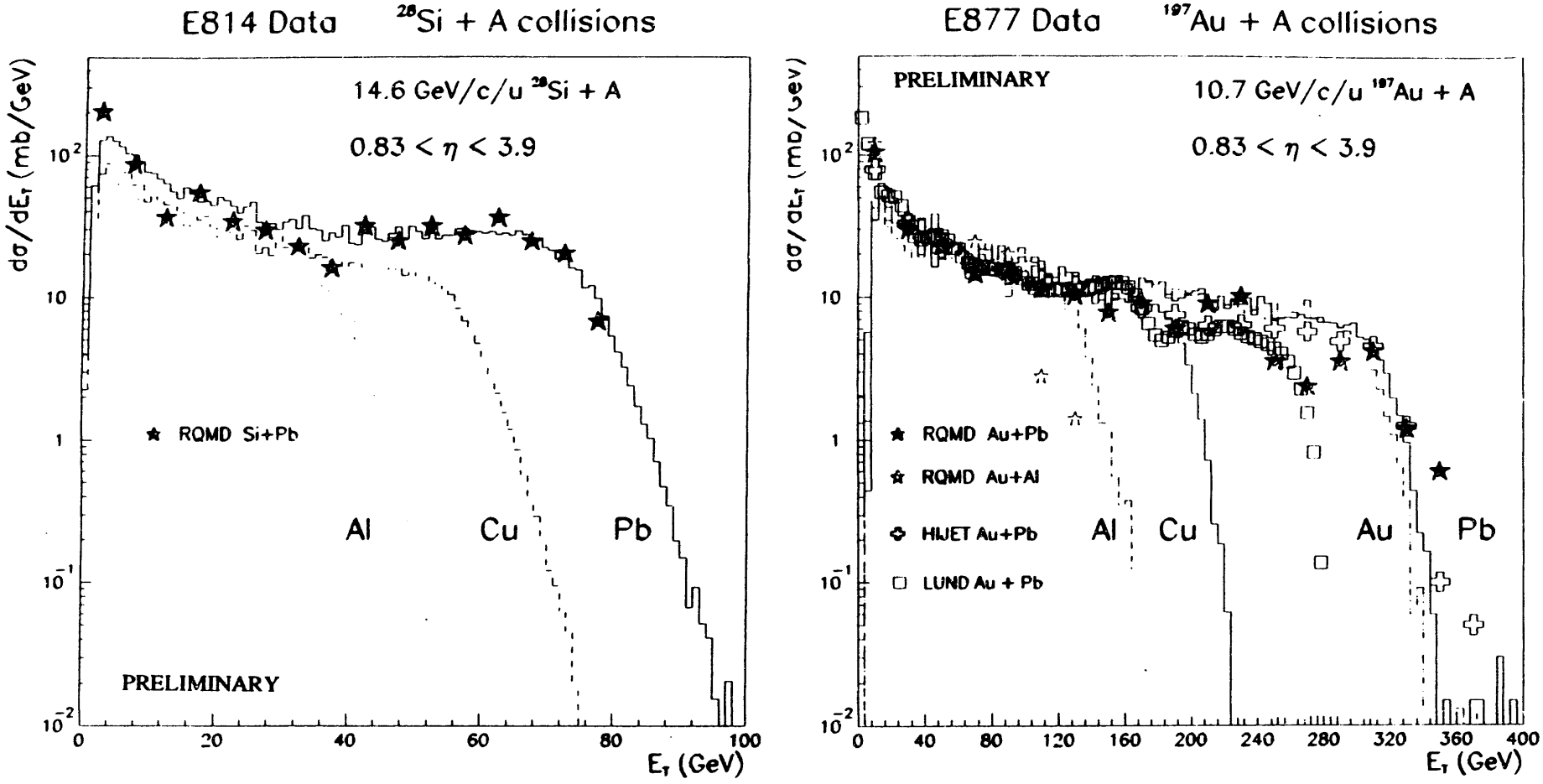

Figure 1. Transverse Energy (E_T) Production measured with the PCAL: Left: 14.6 GeV/c/u Si+Al, Cu, Pb Right: 10.6 GeV/c/u Au+Al, Cu, Au, Pb. The general shape of the spectra is dominated by the collision geometry. Peripheral collisions lead to small E_T production whereas head-on (central) collisions produce the largest E_T. A steady increase in E_T for central collisions is observed for both projectiles with increasing target size suggesting that full stopping is achieved at AGS energy. The data are compared with HIJET (open cross) and RQMD (stars) calculations. Both the HIJET and RQMD calculations are in good agreement with the Au+Pb data supporting the conclusion that complete stopping is reached in Au+Pb collisions. In contrast, the LUND (FRITIOF) calculation clearly underestimates the E_T production for the same system.

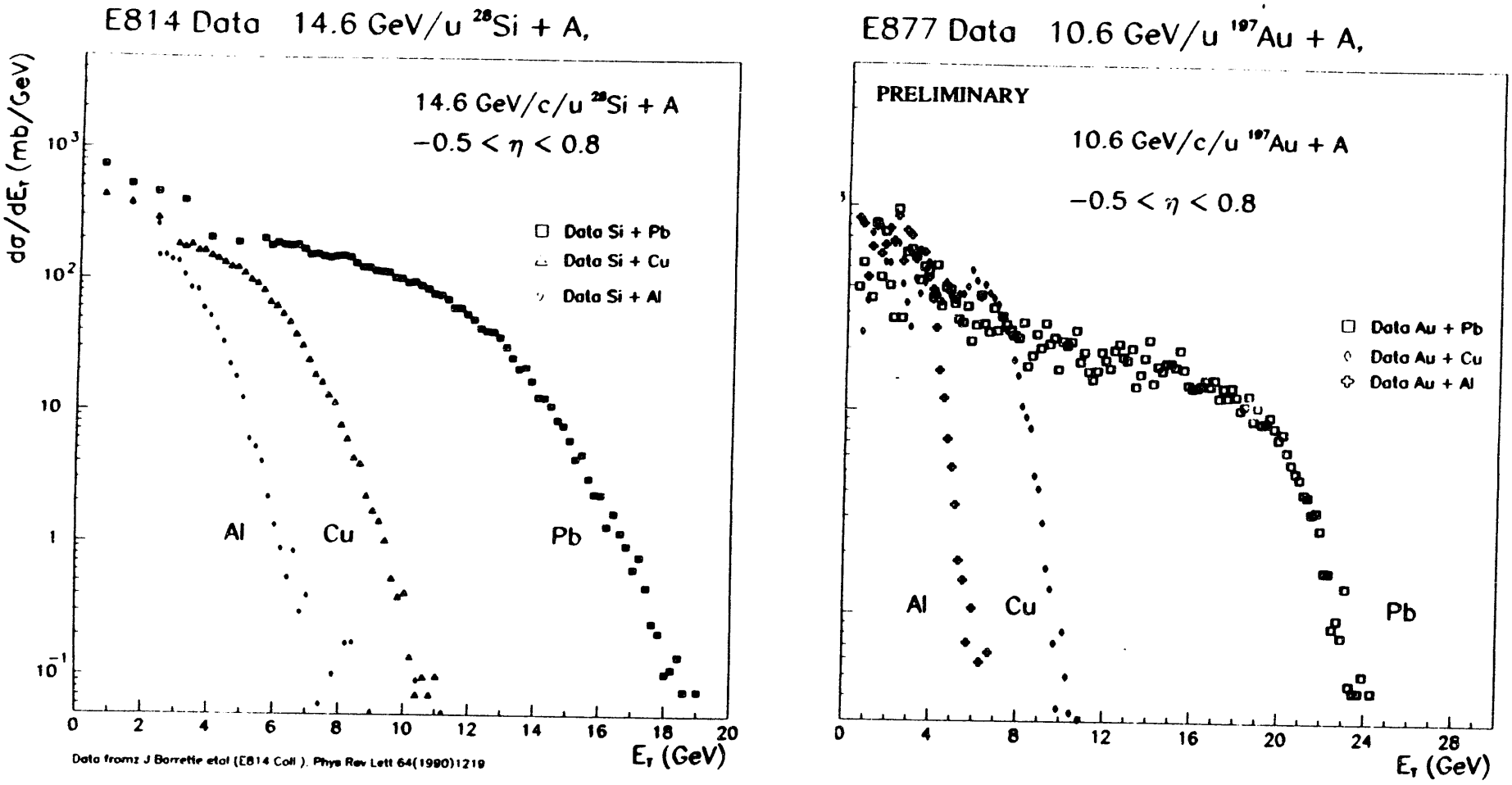

Figure 2. Transverse Energy Production measured with the TCAL: Left: 14.6 GeV/c/u Si+Al, Cu, Pb Right: 10.6 GeV/c/u Au+Al, Cu, Au. The increase in E_T production with increasing target size is much more prononced in the TCAL acceptance than in the PCAL. The energy flow shifts towards lower rapidities for heavier targets, an indication that the projectile nucleons and the particles produced in the primary nucleon-nucleon interactions undergo subsequent dissipative collisions with target nucleons (rescattering).

I.2 Preliminary Studies on the feasibility of flow measurement with the E814 Participant Calorimeter.

ARC [1] and RQMD [2] Monte Carlo calculations have suggested that relativistic reactions of heavy nuclei such as Au + Au involve a very large number of secondary nucleon-nucleon, pion-nucleon, pion-pion etc collisions. They demonstrate that substantial equilibration may be achieved which may lead to macroscopic, collective behavior predicted on the basis of fluid dynamical models [3] and suggest that collective flow may be observed at AGS energies. For small and/or asymmetric systems, no flow effects are predicted [4] or seen [5] but RQMD calculations predict strong and measurable flow effects for heavy systems such as Pb on Pb at 10 GeV/c/u.

Experimentally, the measurement of flow poses quite a few challenges. Successful methods used to measure flow range from tracking and measuring the momentum of all charged particles with a Time Projection Chamber to the use of extensive neutron detector arrays [6]. The Wayne State group is now considering the use of the E814 Participant Calorimeter (PCAL) to measure energy flow. Obviously with such a device, individual tracks and particle energies cannot be measured. However it might be possible to measure azimuthal asymmetry of the transverse energy production as a function of pseudorapidity and phi and therefore get a measurement of the predicted bounce-off and squeeze-out effects.

Before attempting such a measurement, we will study whether the granularity and the energy resolution of the PCAL permit a reasonable measurement of such effects. Our group has now assembled the software tools to study the feasibility and accuracy of a flow measurement with the PCAL. These include the RQMD and the PROPHET codes. The former is a relativistic heavy ion collision event generator that features realistic space time propagation of the colliding particles and rescattering of secondary particles produced in primary nucleon-nucleon collisions. The latter is a calorimeter simulator based on GEANT. It is especially useful for the simulation and quick propagation of showers in sampling calorimeters such as the PCAL. Both these codes are now running on our VAX/SGI cluster .

1) ARC, T.J. Schlagel etal, Phys. Rev. Lett. 68 (1992) 2743 and private communication.
2) RQMD H. Sorge et al, Phys. Lett. 243 (1990)
3) H. Stocker and W. Greiner, Phys. Rep. (1986) 137.
4) H. Sorge etal. Nucl. Phys. A498 (1989) 567c.
5) WA80 Collab, Z. Phys. C38 (1988) 109.
6) R. Madey etal., INPC Abstracts, Wiesbaden Germany, 1992, P3.5.1 U.Grundinger ed.

I.3 First Results on Delta Ray Production and Charged Particle Multiplicities with the Au Beam at 10.7 GeV/c/A

Experiment E814/E877 in which WSU is a collaborator, is a fixed target relativistic heavy ion experiment at the Brookhaven National Laboratory (BNL) Tandem-AGS accelerator complex. A schematic diagram of the apparatus in this experiment is shown in Fig. 1. The majority of work done with heavy ions at BNL has been done with 14.6 GeV/c/nucleon ^{28}Si but at the end of the Spring 92 heavy Ion beam period the AGS delivered its first relativistic beam of Au ions (10.7 GeV/c/nucleon) to the experimental areas. The successful development and delivery of a relativistic Au beam at the AGS is a significant step in the heavy-ion collider program at BNL.

Although the Au beam was initially for machine test purposes, the experiments on the floor took advantage of it to get their first look at collisions using an Au beam. In Experiment E814 , which officially became E877 with the first delivery of an Au beam, calorimetric measurements using the PCAL, TCAL, and Ucals observed the energy flow from Au induced collisions while the silicon charged particle multiplicity detector measured the charged particle production from the same collisions.

An important point in the program of quantifying the charged particle multiplicity measurements is to understand the production of atomic delta-ray electrons caused by the simple passage of the relativistic Au beam through a target. For a Si projectile, we previously measured a delta-ray multiplicity of from 4--5/projectile in targets ranging from Al to Pb, each of which had a thickness corresponding to approximately 2% of a nuclear interaction length for a Si projectile. The results for a non-interacting (beam triggers) Au beam are significantly different as is shown in Fig. 2. where the preliminary raw multiplicity, as yet uncorrected for all instrumental effects, reveals an average multiplicity near 170. A multiplicity of this magnitude is consistent with expectations as delta-ray production is proportional to the projectile charge squared. Delta rays constitute a background for both trigger and physics applications of the Si-multiplicity detector. The consequence for the accurate quantitative measurement of the charged particle multiplicity is that very thin targets must be used to reduce the contribution from delta-rays.

In Fig. 3 we show the angular (pseudorapidity) distribution of the delta-rays produced by the Au beam for various total multiplicity cuts. The shape of the angular distribution is virtually independent of the absolute multiplicity measured.

An example of the charged particle multiplicities (uncorrected) seen online from the E877 multiplicity counter is shown in Fig. 4. Included in the distribution shown in Fig. 4 are the delta-rays discussed above. In this figure, one unit of multiplicity represents one struck pad of the counter (we cannot tell if a pad has had more than one particle pass through it) out of the 1024 active pads in the detector; implying that at large multiplicities, significant corrections for multiple hits in a single pad will be necessarily increase the highest multiplicities. We plan to make this correction but the magnitude of the multiple hit correction required will also entail considerable uncertainty. The present detector geometry is clearly not well suited for multiplicitty measurements with the Au beam. For the Si beam, where we have significant experience with this analysis, the correction was much smaller (about 20% in the worst case).

We have just begun the detailed analysis of the above data but the need for a better multiplicity detector is already indicated as discussed above. During the last beam period, we tested such a detector. It has the same pad layout as the detector discussed above but uses an analog readout system to measure the energy deposited in each pad. This allows us to determine the number of particles hitting each pad. The tests indicate that the detector and readout system work as expected but that the system would not give a reliable trigger when using thick targets because of the large

number of delta-rays produced and the amount of energy that some of them can deposit in the detector. A final decision regarding an upgraded detector will be made in the near future and should be installed in time for the next Au beam time.

Figure Captions:

1). Diagram of the E814/E877 experiment. The beam enters through a hole in the backwall of the Target Calorimeter. Large angle fragments from a beam-target collision are measured by the Target Calorimeter, Participant Calorimeter and the Silicon Multiplicity Detector. Small angle fragments pass through an aperture in the Participant Calorimeter. To be measured by the combination of magnet, drift chamber, and calorimeter elements located further down stream.

2). δ-ray cross section (arbitrary units) seen by the E877 silicon multiplicity detector from the passage of a non-interacting 10.7 GeV/N Au projectile through a 2% Pb target.

3). Normalized angular distribution of δ-rays produced a 10.7 GeV/N Au projectile passing through a 2% Pb target. The various curves are for different multiplicity intervals of figure 2. The distribution is independent of the multiplicity.

4). The on-line multiplicity (no-corrections) seen from 10.7 GeV Au + Au collisions. The figure is the sum of data taken with different triggers each of a different weight. Charged particle multiplicities with over 500 hits in a 1000 element detector are seen.

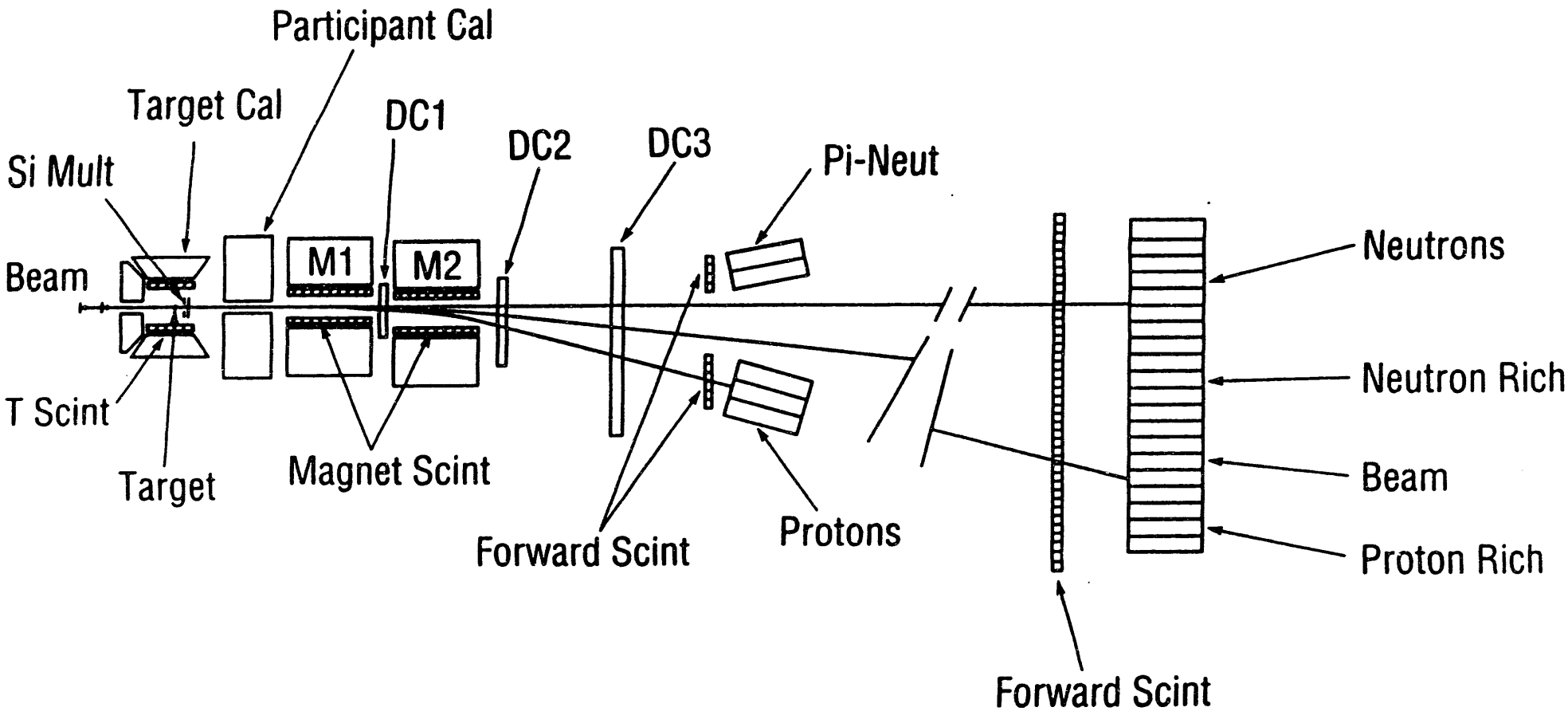
Participant Cal
Target Cal
DC1
DC2
DC3
Pi-Neut
Si Mult
Beam
M1
M2
Neutrons
Neutron Rich
Beam
Proton Rich
T Scint
Target
Magnet Scint
Forward Scint
Protons
Forward Scint

Figure 1

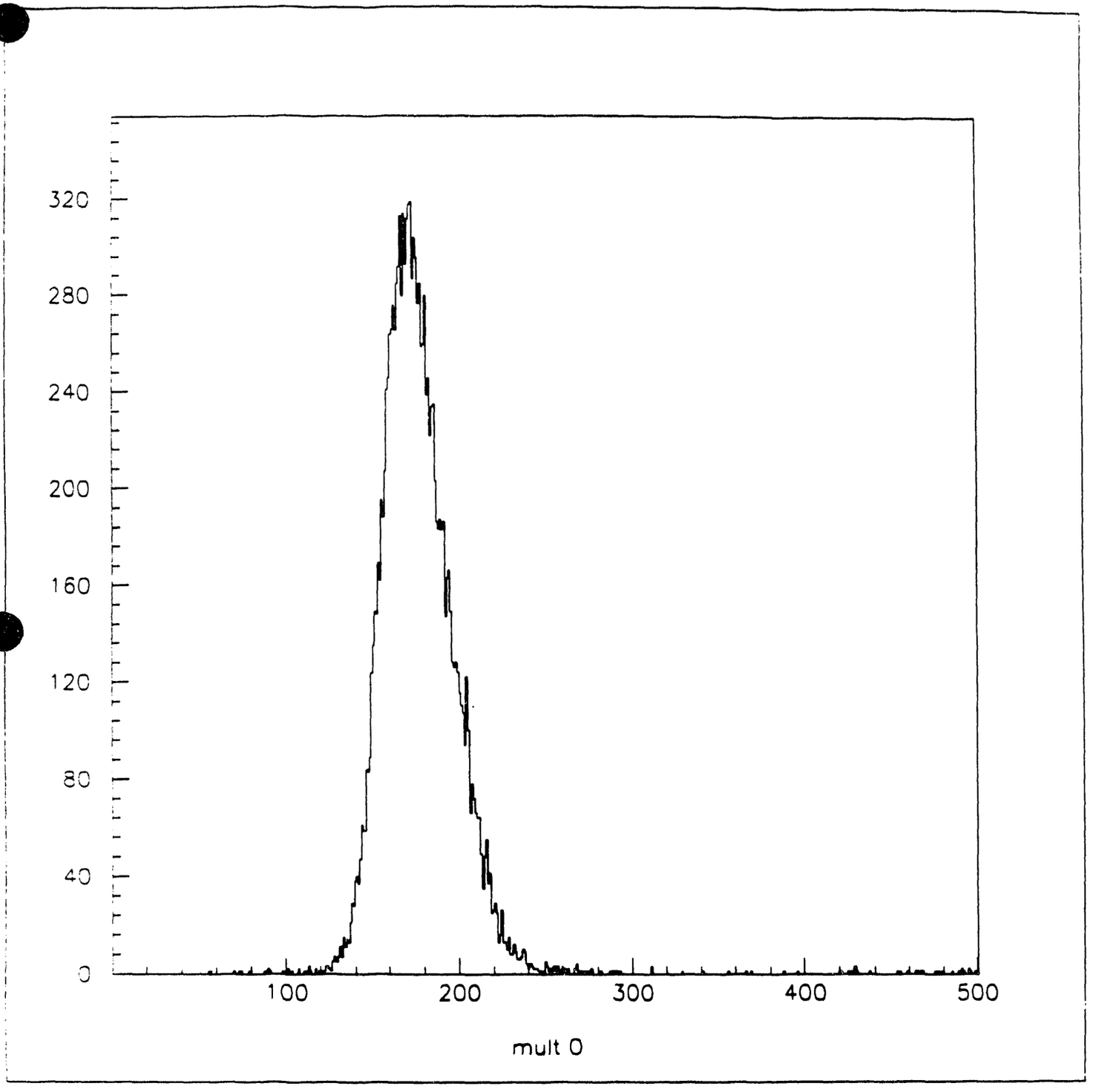

Figure 2

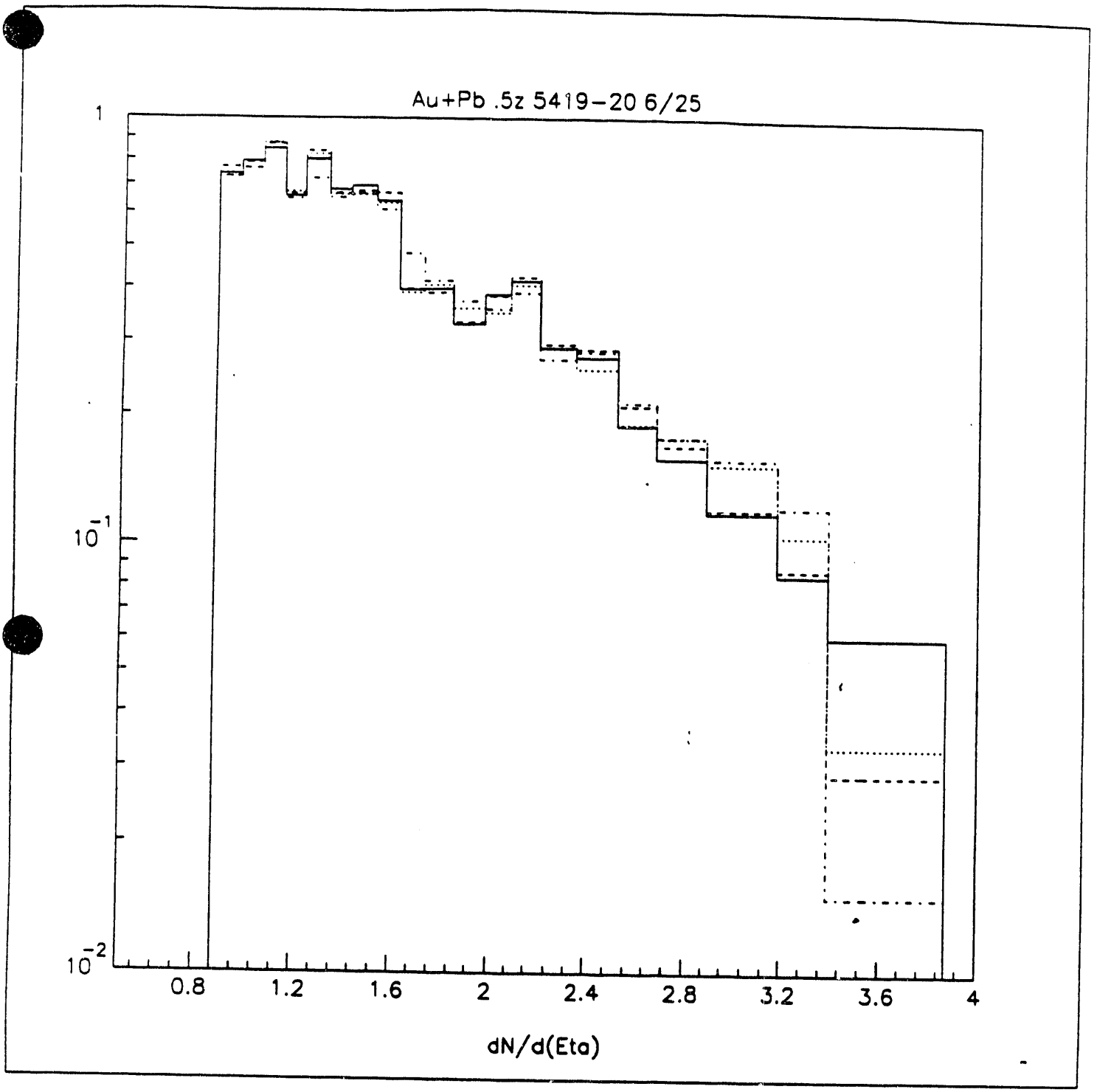

Figure 3

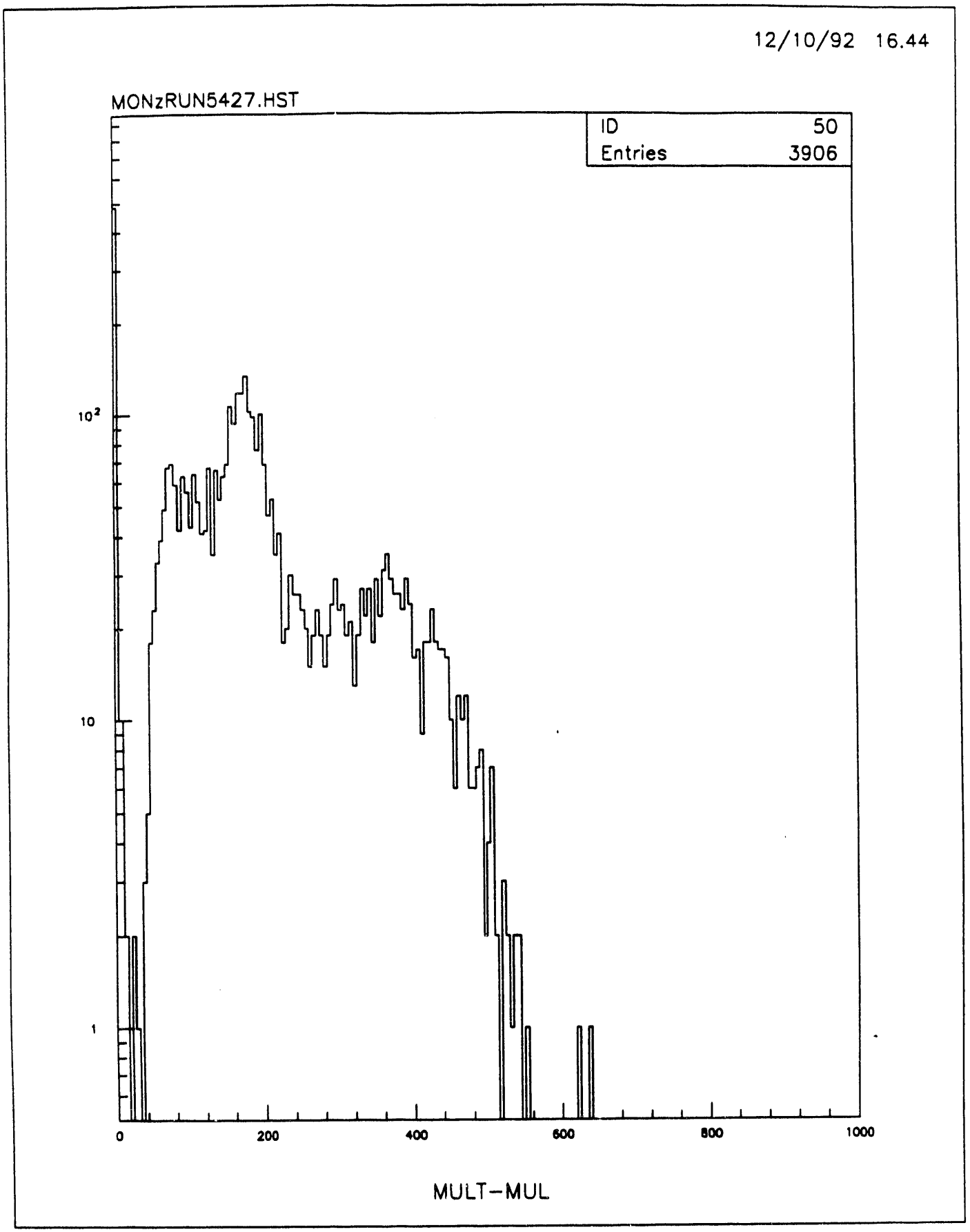
12/10/92 16.44
MONzRUN5427.HST
ID 50
Entries 3906
10²
10
1
0
200
400
600
800
1000
MULT-MUL

Figure 4

I.4 Preliminary Results from the E877 Telescope

In the 1992 beam time of Experiment E877, we measured for the first time the emission of particles in the backward direction. The device used was a scintillator telescope, described in Section IV.1. A measurement of the energy loss in one of the thin scintillators compared to one of the neighboring 17 cm thick blocks yields the particle identification capability of the device. Fig. 1 shows such a dE vs E spectrum from Si + Pb at 14.6 GeV/c for particles that stop in the first thick scintillator block. After linearization, the spectrum is projected onto the particle identification-axis. Fig. 2 and 3 shows a linearized ID-spectra. In Fig. 2 an experimental ID spectrum is overlaid with a GEANT simulation of the energy loss for pions, protons and deuterons. The intensities of the particle groups in the simulation have been chosen to roughly fit the data. Note however, that the experimental ID spectrum is obtained from calibrated data and thus the concurence of the peak positions with those of the simulation provide an unambiguous identication of pions, protons and deuterons. All GEANT physics processes as well as the full detector response, including for example the photo multiplier pulse shape and ADC gate width, are included in this simulation. The incorporation of the pulse shape and gate width are essential for inclusion of the proper fraction of pion and kaon decay energy in the energy response of the detector. Fig. 3 shows a deconvoluted fit for the three assigned particle species. The line shapes used in these fits are taken from smooth functions fit the GEANT simulation. The deconvolution shown in figure 3 implies a signicant kaon yield as well as triton and heavier particles. The kaon yield is too small to be separated from the pion Landau tail and the background using only dE/dx information. The inclusion of time of flight and delayed decay information is expected to greatly improve this situation. The present analysis is based on 1/3 of the measured Si+Pb data.

The background in the present data is due to delta electrons, hadronic interactions, decay in flight and the decay of pionic and kaonic atoms formed by the negative charged Kaons and pions. Further studies of the background are in progress and improvement appears possible with modest detector changes for coming runs. Delta electons, particularly those from up stream beam defining devices are a minor problem with the Si beam data discussed here. This problem becomes a major concern with the Au beam, however.

A number of physics issues can be addressed at the present state of the analysis. For example, we have begun preliminary studies of heavy particle ratios in the backward hemisphere . With the present statistics we attempt only a measurement of the d/p ratio. The complete run analysis including the silicon detectors and time of flight will allow a study of fragment ratios up to the alpha particle. These ratios are being compared to a calculation based on the statistical decay of a compound nucleus close to the ground state (cold target fragmentation). The heavy fragments are not expected to have a significant component that originates from the isotropic fireball (participants). The present measurements are thus a relatively pure determination of the fragmentation process itself.

We have begun to study the variation of our d/p ratio with centrality. In the E814 set up this can be done in a number of ways using charged particle multiplicity, transverse energy in the TCAL and/or PCAL and "zero degree" ratio energy in the UCAL. the latter method most easily gives the widest impact parameter range going all the way from very peripheral to central collisions. Figure 4 shows our prliminary fits to particle ID spectra as a function of UCAL energy bin (1= 300-500 GeV, 2= 200-300 GeV, 3= 100-200 GeV, 4= 0-100 GeV). Some small corrections for range variations need to be applied to the extracted ratios. Qualitatively the trend is clear, however, and is shown in figure 5. Both deuteron and pion yields relative to protons increase with centrality (small zero degree energy). In the case of the deuteron yield, at least two factors vary with centrality in a manner which is expected to influence the yield. The first is the increase in target fragment excitation energy which is expected with increasing centrality. The second is the

variation of the mass of the surviving target fragment as a function of centrality. A simple geometrical model can be used to estimate the mass of the target fragment. For peripheral collisions (energy in forward calorimeter above 300 GeV) the almost complete Pb nucleus survives the initial collision, whereas for central collisions (energy in forward calorimeter below 100 GeV), the residue corresponds to the spectator mass which is around A=120. It is interesting to note that the initial neutron to proton ratio of the target fragment is expected to be that of the original Pb target. Thus the A=120 "fragment" which, crudely speaking, survives a central collisions is rather neutron rich. Preliminary statistical model calculations have been performed and presently a parameter sensitivity study is in progress.

The pion yield is also observed to increase relative to protons with increasing centrality. In this case, however, where the pion and proton sources are likely to be quite different, the absolute yield of pions will be the most informative. That analysis is still in progress.

Besides the particle ratios , we also measure the inverse slope of the particle cross sections for deuterons, protons, and pions. Sample spectra as dN/dp^3 are shown in figure 6 for central collisions selected by E(UCAL) < 100 GeV. Boltzman "temperatures" extracted from such spectra as a function of UCAL selected centrality are shown in figure 7. Within errors (not shown) the resulting inverse slopes are independant of centrality.

The E814 experiment showed early on that in the forward direction this "temperature" parameter which, assuming a statistical equilibrium, would correspond to the Boltzmann temperature, is a function of rapidity. In the region of beam rapidity, the protons obviously do not interact significantly and therefore, do not emerge from an equilibrium state. These protons stay essentially cold so that one finds a strong dependence of the slope on rapidity in this region. Fig. 8 shows the measurements of E814 in the forward direction, analyzing the Si+Pb data in the spectrometer of the 1992 beam time along with a summary of E802 results for both pions and protons. The present data from our telescope provides the points for protons and pions at the largest negative rapidity. As was already quite apparent in our spectra of figure 6, there is a large systematic difference in the "temperature" parameter of protons and pions. The temperature variation with rapidity, y, is described by $1/\cosh(y-y_0)$. Y_0 is found to be between the nucleon-nucleon center of mass rapidity of 1.72 and the Si+Pb overlap center of mass rapidity of 1.2.

The big advantage of the scintillator telescope is its sensitivity to pions and possibly kaons. Beyond matters related to target fragmentation, we also want to extract the yields and spectra of produced particles in the backward hemisphere. We believe that the E877 telescope is the only device that will be able to do this in the AGS energy domain. This kinematic region is strongly suppressed for produced particles in the absence of re-interactions of primaries. We are thus most interested in measuring the kaon yield at back angles. At least one explanation of the enhanced k/π ratio observed at the AGS relies on strong rescattering. Simulations which take into account an amount of rescattering of participants and produced particles RQMD and ARC are able to reproduce many features of the data. In these calculations, the main channels that contribute to the large k/pi ratio are pion absorption by resonance formation and kaon production by pion final state interaction (e.g. $\pi+N \rightarrow K+\Lambda$). These channels are strongly populated in the simulations. The best test of strong rescattering processes is to measure this effect in the backward hemisphere. Initial attempts to isolate the Kaon production are in progress. Fig. 3 shows quite clearly that even the present analysis implies a very significant kaon yield. Time of flight and other techniques available to us are yet to be applied.

Figure Captions:

Fig. 1).dE vs E spectrum for particles that stop in block 1 of the E877 backward telescope.

Fig. 2).solid: linearized dE spectrum for the particle subset of Fig. 1. dashed: GEANT simulation of dE/dx for pions, protons, deuterons. Landau distributions and detector response were included. The yield in the simulation is normalized to the yield in the data. The linearization process used is identical to the linearization process for the experimental data.

Fig. 3).data from Fig. 2 overlayed with deconvoluted fits for the three identified particle species.

Fig. 4).deconvoluted fits as a function of centrality for the data represented in Fig. 2. The energy in the forward spectrometer (UCAL) is used as a measure of centrality. E = 0 - 100 GeV represents the most central collisions, E = 300 - 500 GeV represents the most peripheral collisions.

Fig. 5).particle ratios (d/p, π/p) as a function of centrality resulting from fits in Fig. 4. Centrality 1 is peripheral, centrality 4 is most central.

Fig. 6.) dN/dp^3 spectra for pions, protons, deuterons for central Si + Pb collisions into 143.9 +- 1.9 degree.

Fig. 7.) Boltzmann temperatures from an exponential fit to the dN/dp_3 spectra as a function of centrality for pions, protons and deuterons.

Fig. 8.).comparison of T_B measured in backward hemisphere with data measured by E802 and E814 in forward hemisphere. The data for protons and pions are compared to a function assuming an isotropic fireball decay .

12/10/92 15.35

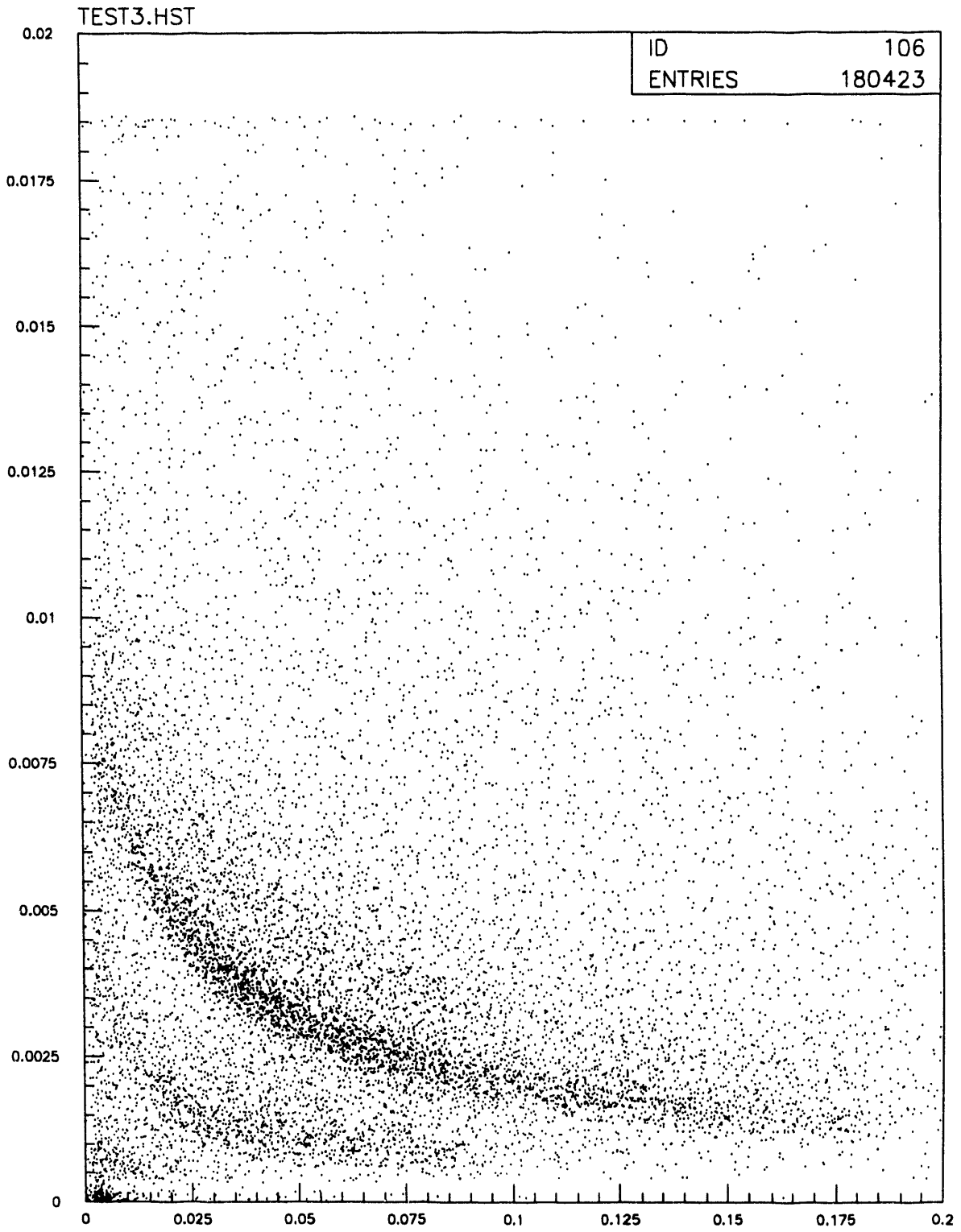

Figure 1

Figure 2

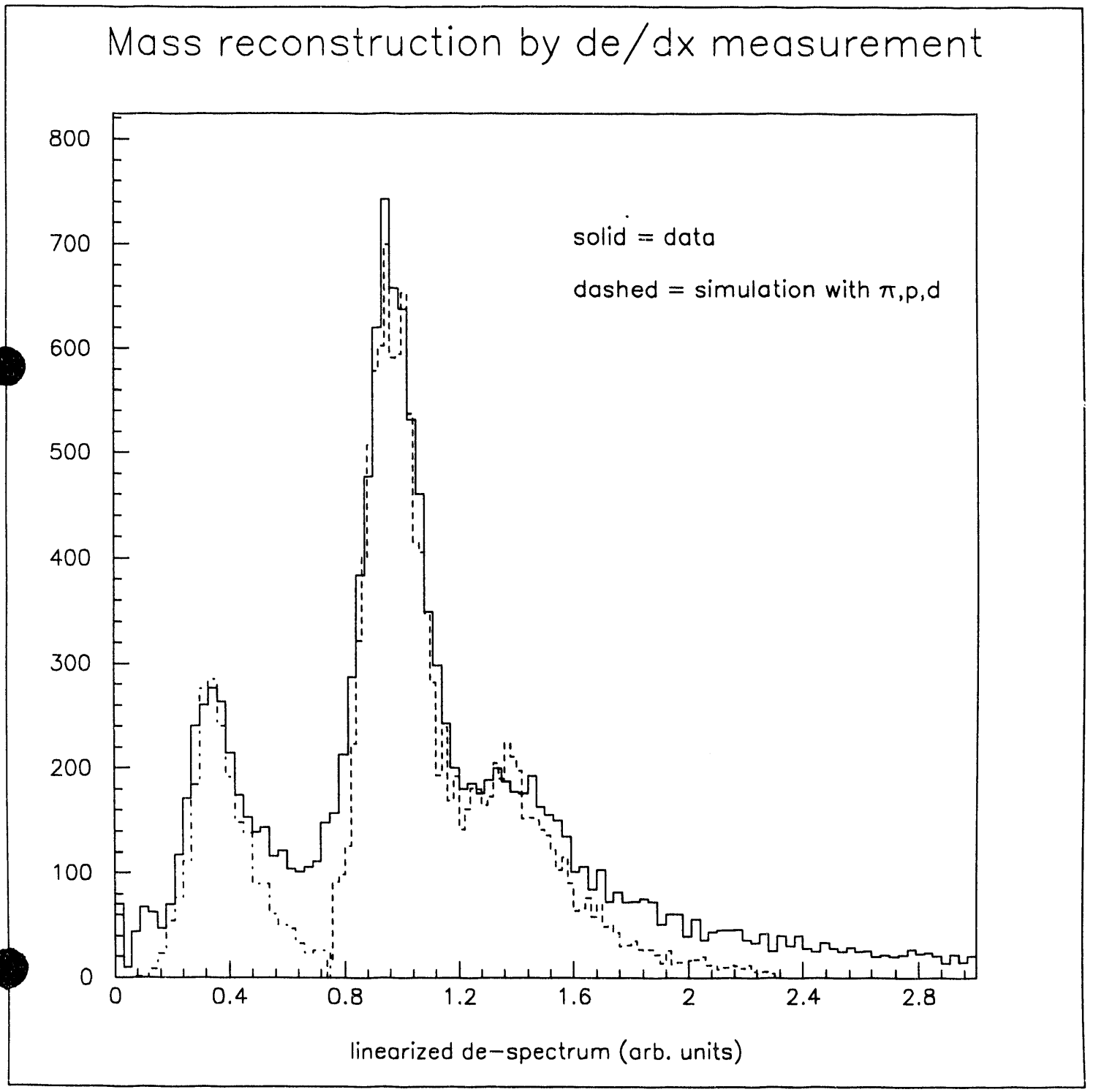
Mass reconstruction by de/dx measurement
800
700
600
500
400
300
200
100
0
0
0.4
0.8
1.2
1.6
2
2.4
2.8
solid = data
dashed = simulation with π,p,d
linearized de−spectrum (arb. units)

08/10/92 10.10

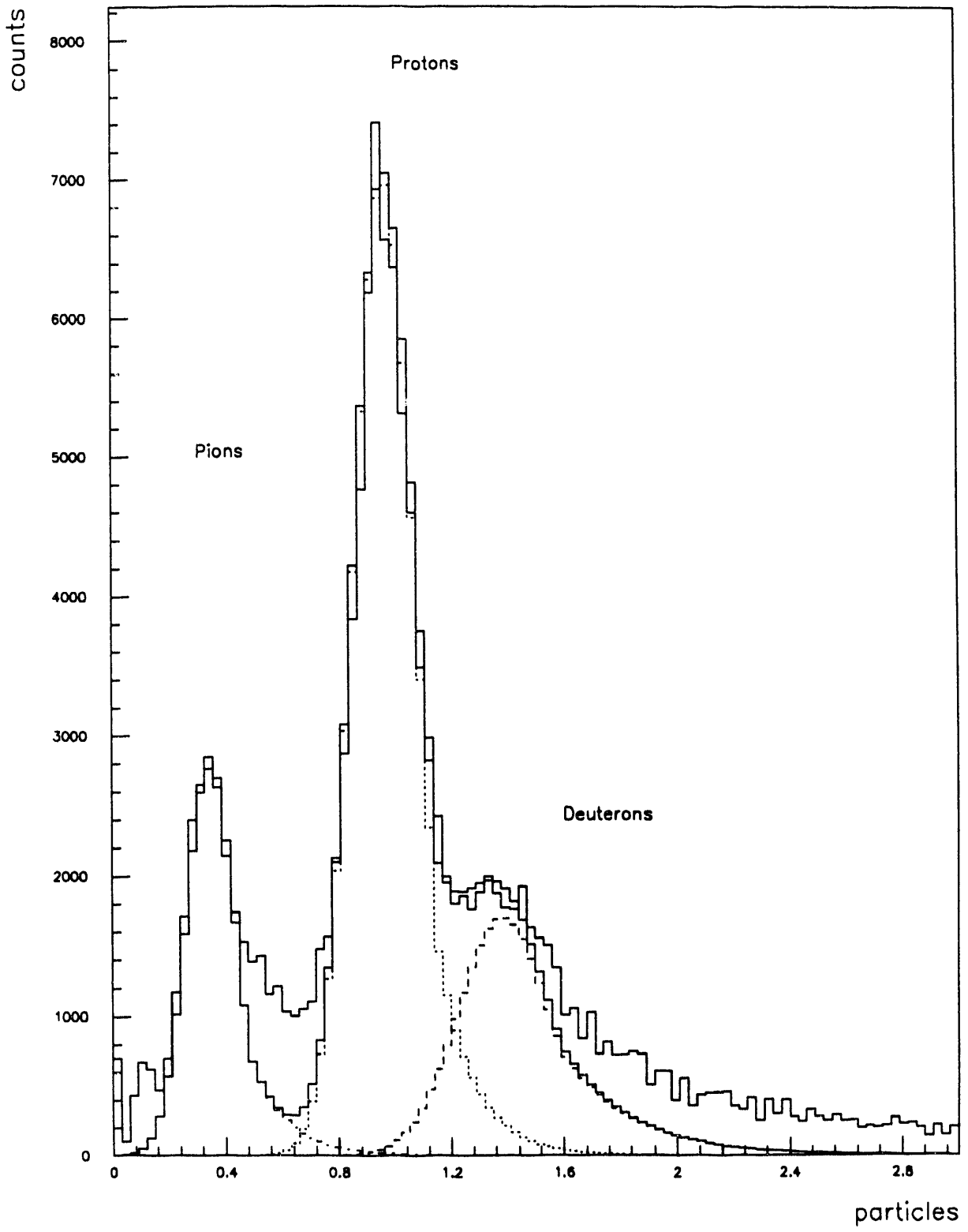

Figure 3

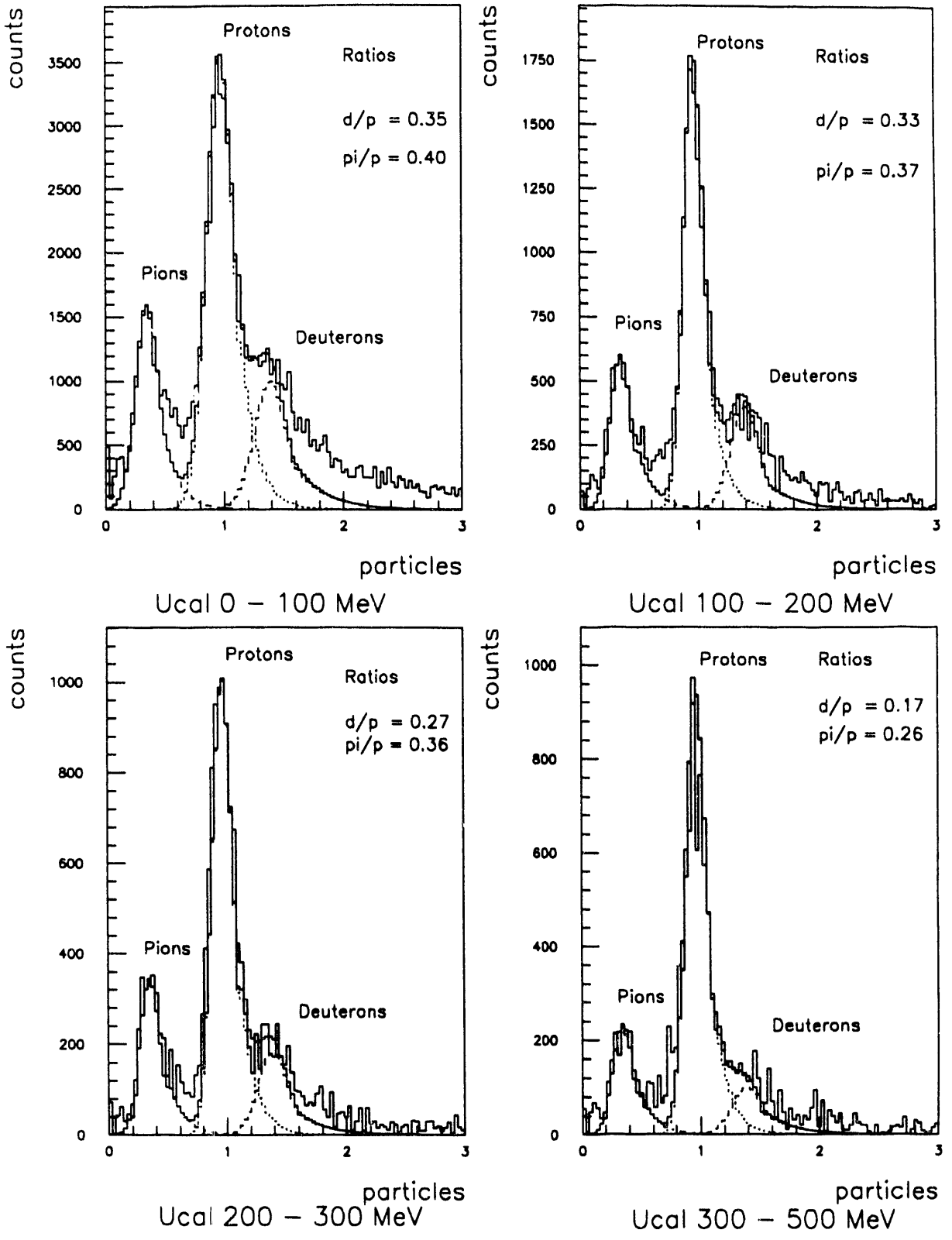
counts
Protons
Ratios
d/p = 0.35
pi/p = 0.40
Pions
Deuterons
particles
Ucal 0 – 100 MeV
counts
Protons
Ratios
d/p = 0.33
pi/p = 0.37
Pions
Deuterons
particles
Ucal 100 – 200 MeV
counts
Protons
Ratios
d/p = 0.27
pi/p = 0.36
Pions
Deuterons
particles
Ucal 200 – 300 MeV
counts
Protons
Ratios
d/p = 0.17
pi/p = 0.26
Pions
Deuterons
particles
Ucal 300 – 500 MeV

Figure 4

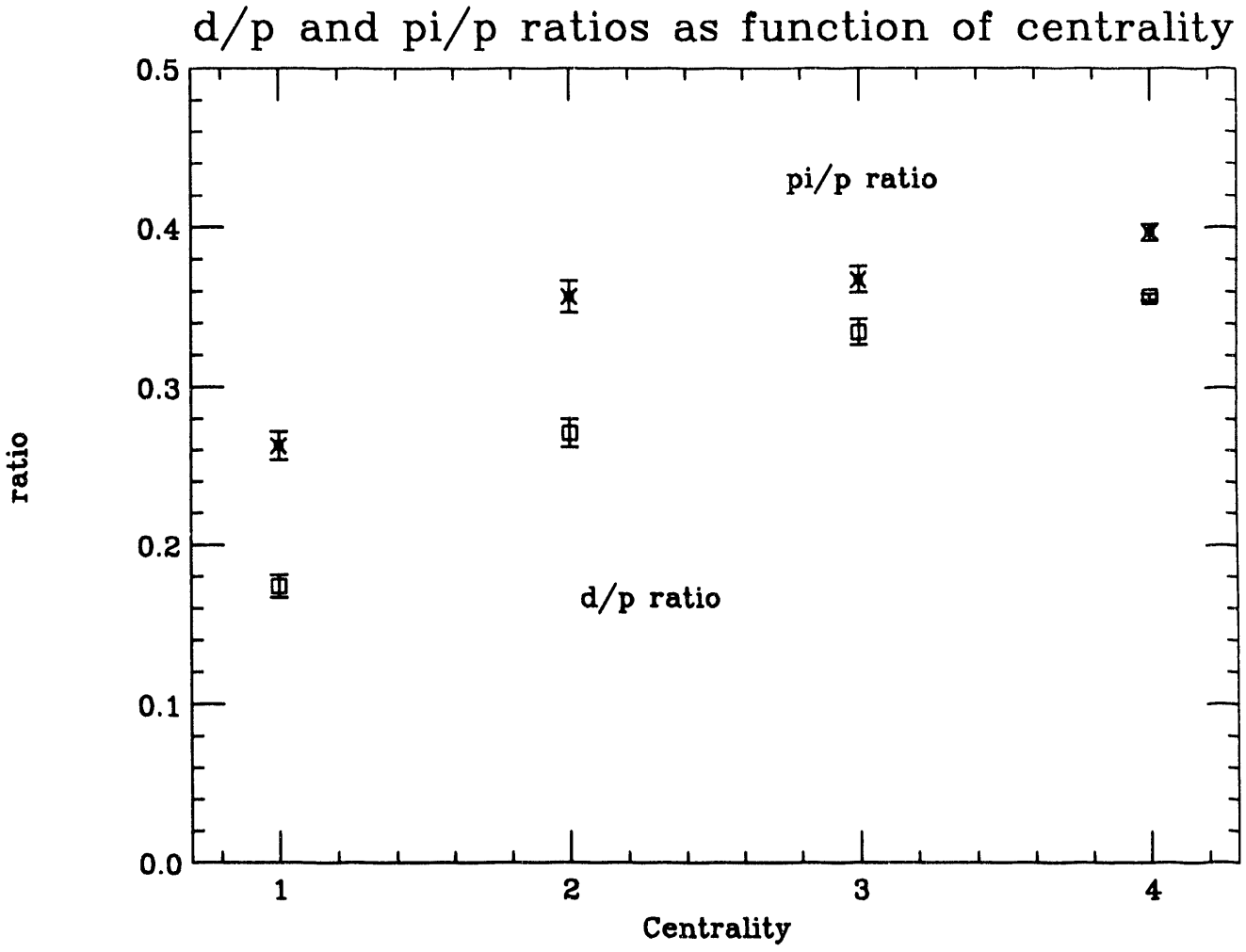
d/p and pi/p ratios as function of centrality
0.5
0.4
0.3
0.2
0.1
0.0
ratio
pi/p ratio
d/p ratio
1
2
3
4
Centrality

Figure 5

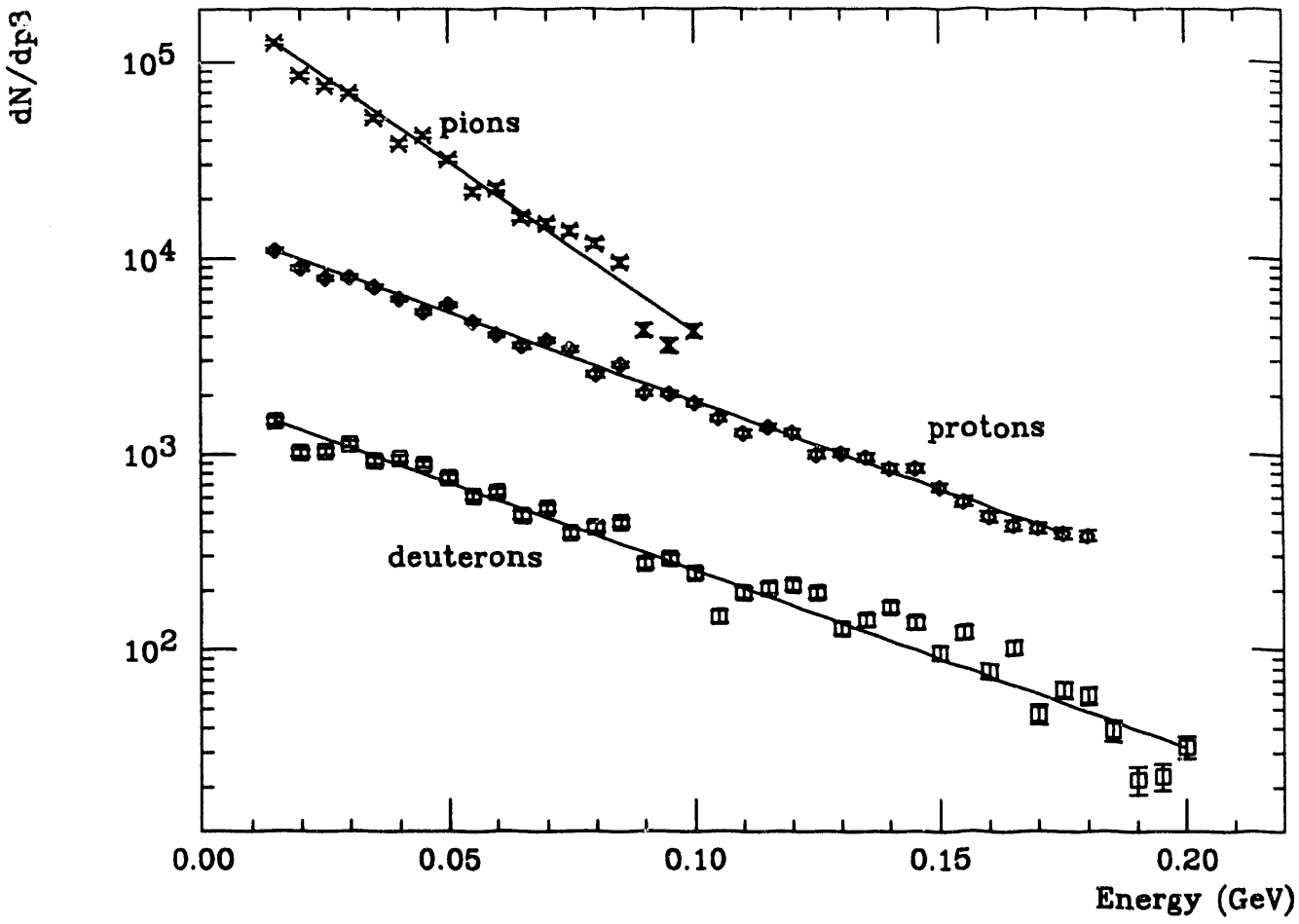
dN/dp3
10^5
10^4
10^3
10^2
pions
protons
deuterons
0.00
0.05
0.10
0.15
0.20
Energy (GeV)

Figure 6

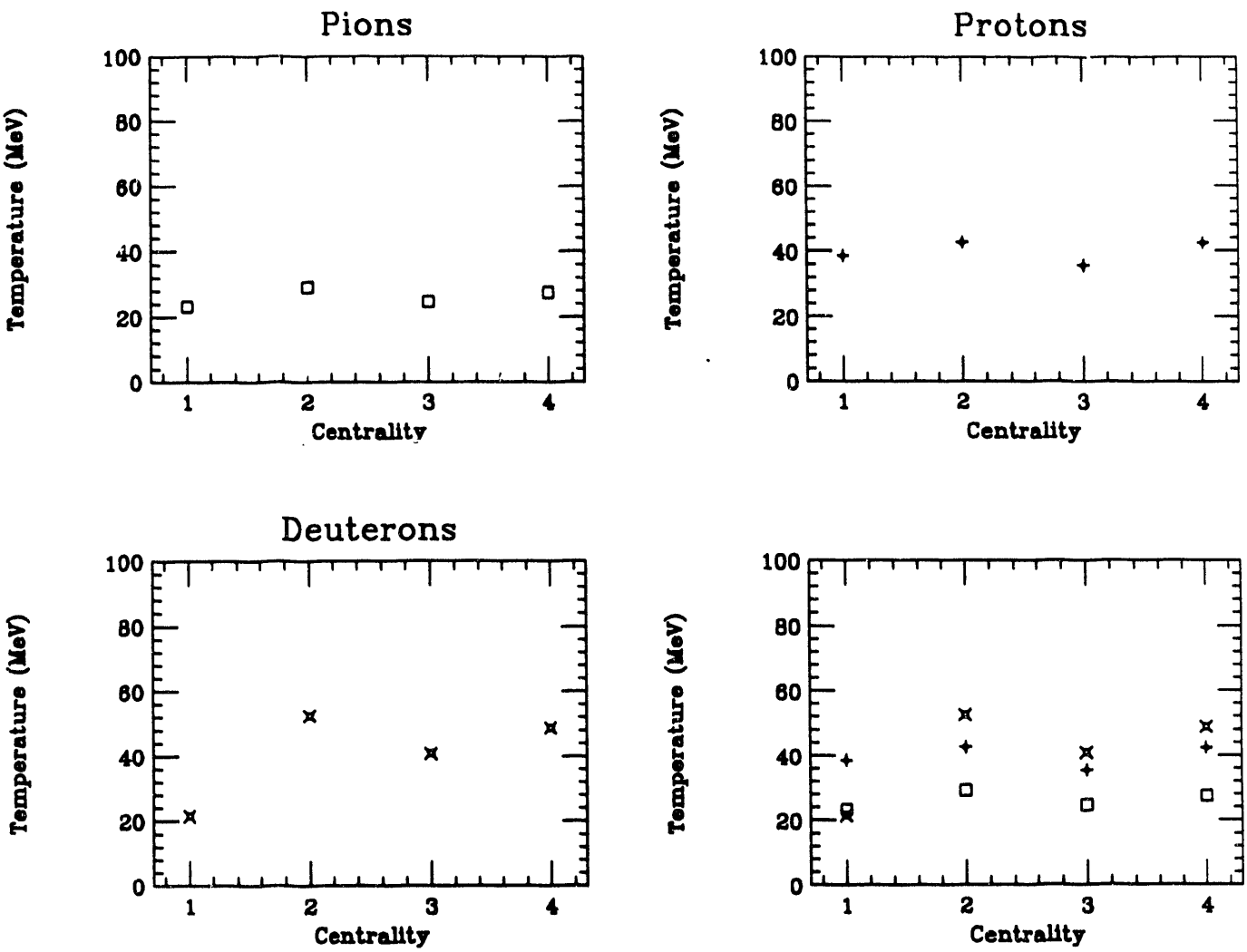
Pions
Protons
Deuterons
Temperature (MeV)
Centrality
0
20
40
60
80
100
1
2
3
4

Figure 7

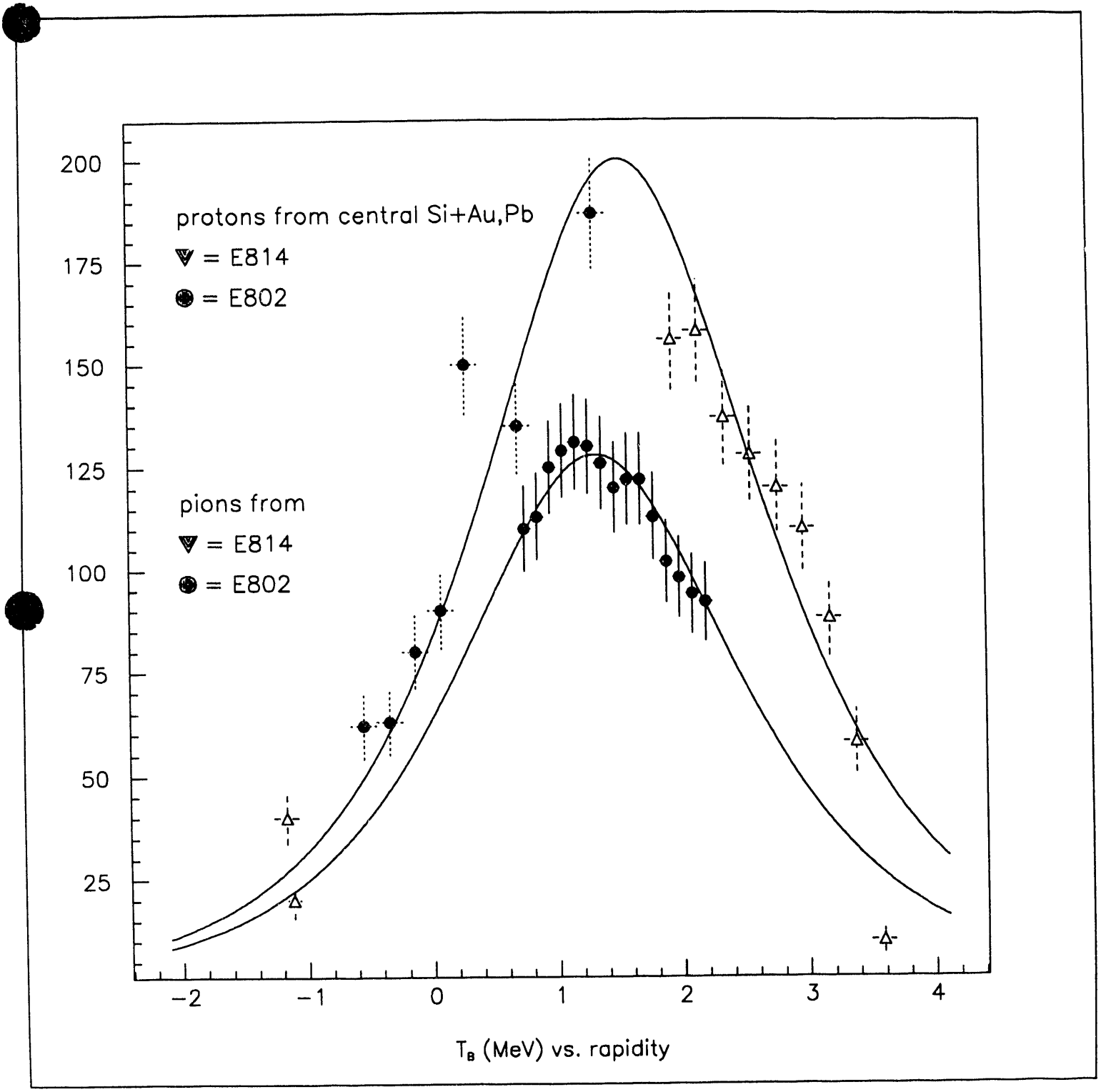
protons from central Si+Au,Pb
▼ = E814
● = E802
pions from
▼ = E814
● = E802
200
175
150
125
100
75
50
25
−2
−1
0
1
2
3
4
T_B (MeV) vs. rapidity

Figure 8

I.5 Low p_t baryon distribution in Si+A1, Pb collisions at the AGS

The p_t distribution measurements for baryons in E814 were finalized with the 1991 beamtime. Previous results were extended to lower rapidity with higher statistics in both systems, the symmetric Si+A1 as well as the highly asymmetric Si+Pb. This permits a determination of the rapidity dependence of the inverse slope parameters plus a complete rapidity distribution for the symmetric system.

Figure 1 shows the phase space distribution (y, p_t plot) for two magnetic fields in the E814 dipoles. One can see that the coverage extends out to over p_t=300 MeV/c for y=3 and decreases to p_t=100 MeV/c for y=2. For the p_t-distributions, the data were binned in rapidity bins of 0.2 from y=1.5 to y=3.9. This range covers the nucleon-nucleon center of mass rapidity (y_0=1.7) up to the beam rapidity (y=3.44). In Figure 2 we show the p_t-dependence as a function of m_t-m_p. The plotted quantity $(1/m_t^2)$ $(dN/dm_t dy)$ is proportional to the invariant cross section, which permits a determination of the source "temperature" from the inverse slope of an exponential fit exp $(-m_t/T)$. At midrapidities the curves reveal a single exponential behavior, whereas close to beam rapidity the data can be described by a two component fit. This second component can be related to the onset of a beam rapidity component due to 'punch-through' protons that traverse the target without significant interaction. The 'temperature' value for this beam rapidity component is around 7 MeV. The high temperature component is strongly rapidity dependent. Figure 3 shows this dependence for both measured systems. The different symbols represent different trigger conditions listed as the observed charged particle multiplicity and the corresponding fraction of the geometrical cross section. Theres is at best a very slight dependance of the temperature on the centrality. The solid line shows a calculation based on an isotopic fireball. This approach assumes a purely kinematical dependence of the temperature following $T \propto 1/\cosh(y-y_0)$. y_0 seems to be in between the nucleon-nucleon center-of-mass rapidity of 1.72 and the center-of-mass rapidity for the Si+Pb overlap volume of 1.2. A detailed analysis (Figure 4) of the centrality dependence reveals a slight increase of the average p_t with decreasing impact parameter (i.e. higher multiplicity), which might hint at the onset of transverse hydrodynamical flow. Our group will try to correlate this effect in the forward direction with a detailed flow measurement utilizing the fully symmetric calorimeter devices around the target. This has been discussed in section I.2.

For the symmetric Si+A1 system we attempted to calculate a full rapidity distribution based on our p_t-measurements. This requires a.) the integration of the full p_t-spectrum and b.) the measurement of all rapidity bins. We chose the Si+A1 system because for a symmetric system the rapidity distribution can be mirrored around mid-rapidity. For Si+A1 we measured the p_t-distributions from y=1.5-3.9. Only the bins above y=2.4 could be integrated, because the p_t coverage in the lower bins was too small to allow a reliable extrapolation to high p_t. Figure 5 shows two extrapolations to mid rapidity based on the systematic uncertainty in the p_t-extrapolations for the y-bins from 1.5 to 2.4. This rapidity distribution is then mirrored around mid rapidity to allow the determination of the shape of dN/dy as well as the integrated yield. These data are compared to model calculations based on RQMD and ARC. RQMD overshoots the yield around midrapidity and both calculations predict peaks at target and beam rapidity. These peaks which would hint at a certain amount of spectator mass are not seen in the data. Still the overall agreement between these models, which require a relatively high baryon density ($\rho > 1/fm^3$) even in Si-induced reactions, is quite good. These simulations predict a much higher density over a larger time scale for Au-induced reactions.

Figure Captions

FIG. 1 Acceptance of the spectrometer in the y versus P_t plane for two magnetic fields.

FIG. 2 Proton spectra as a function of transverse mass for rapidity bins of width 0.2 and central Si + Pb collisions (σ/σ_{geo} = 2%). Spectra have been multiplied with increasing powers of 2.5 with decreasing rapidity. The dotted lines are the results of exponential fits with slopes as shown in Fig. 2. The long dashed lines shown for the four lowest rapidity bins indicate the range of extrapolation.

FIG. 3 Temperature parameters T_B, as a function of rapidity, for different centralities. Dashed lines indicate the upper and lower limits for the extrapolations. Solid lines are predictions using the isotropic fireball model .

FIG. 4 The mean proton transverse momentum (Pt) as a function of charged particle multiplicity, for different rapidities.

FIG. 5 Proton rapidity distributions for central Si + A1 collisions (σ/σ geo = 0.2%). Solid (open) points are data using measured (extrapolated) slope constants. The solid line for $y \leq 1$ represents data reflected about midrapidity, the two separated lines indicate the upper and lower limits due to extrapolation. The histograms without and with solid dots are the RQMD and ARC predictions, respectively.

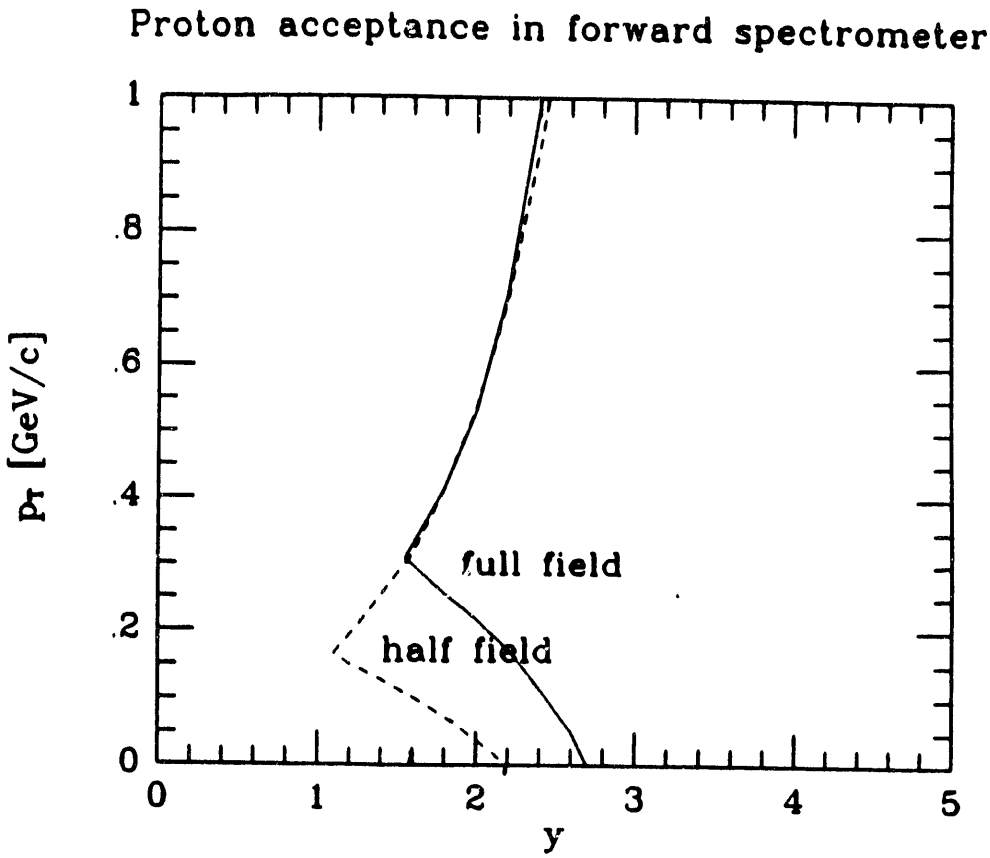
Proton acceptance in forward spectrometer
p_T [GeV/c]
1
.8
.6
.4
.2
0
0
1
2
3
4
5
y
full field
half field

Figure 1

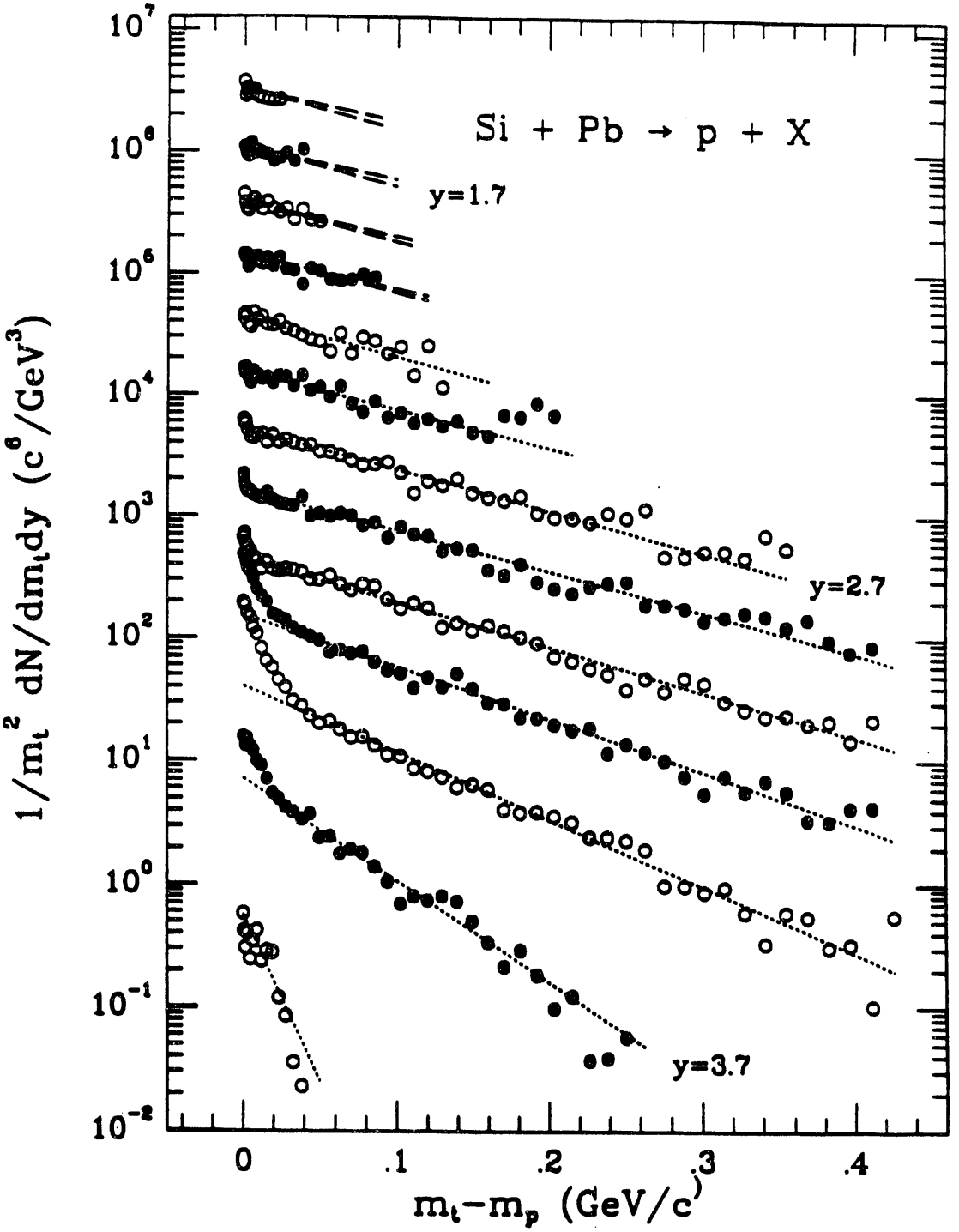
Si + Pb → p + X
y=1.7
y=2.7
y=3.7
$1/m_t^2\ dN/dm_t dy\ (c^6/GeV^3)$
$m_t - m_p\ (GeV/c^2)$
10^7
10^6
10^5
10^4
10^3
10^2
10^1
10^0
10^{-1}
10^{-2}
0
.1
.2
.3
.4

Figure 2

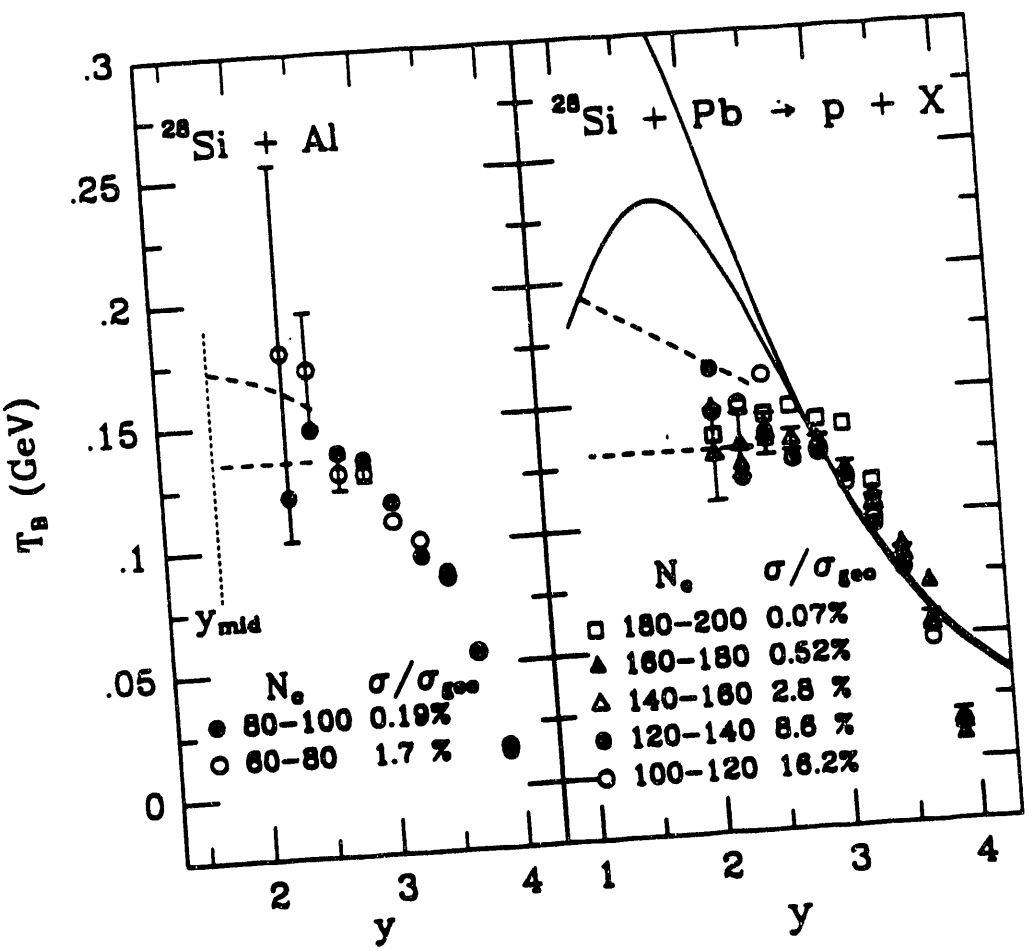
^{28}Si + Al
^{28}Si + Pb → p + X
T_B (GeV)
.3
.25
.2
.15
.1
.05
0
y_{mid}
N_c σ/σ_{geo}
80–100 0.19%
60–80 1.7 %
N_c σ/σ_{geo}
180–200 0.07%
160–180 0.52%
140–160 2.8 %
120–140 8.6 %
100–120 16.2%
2
3
4
y
1
2
3
4
y

Figure 3

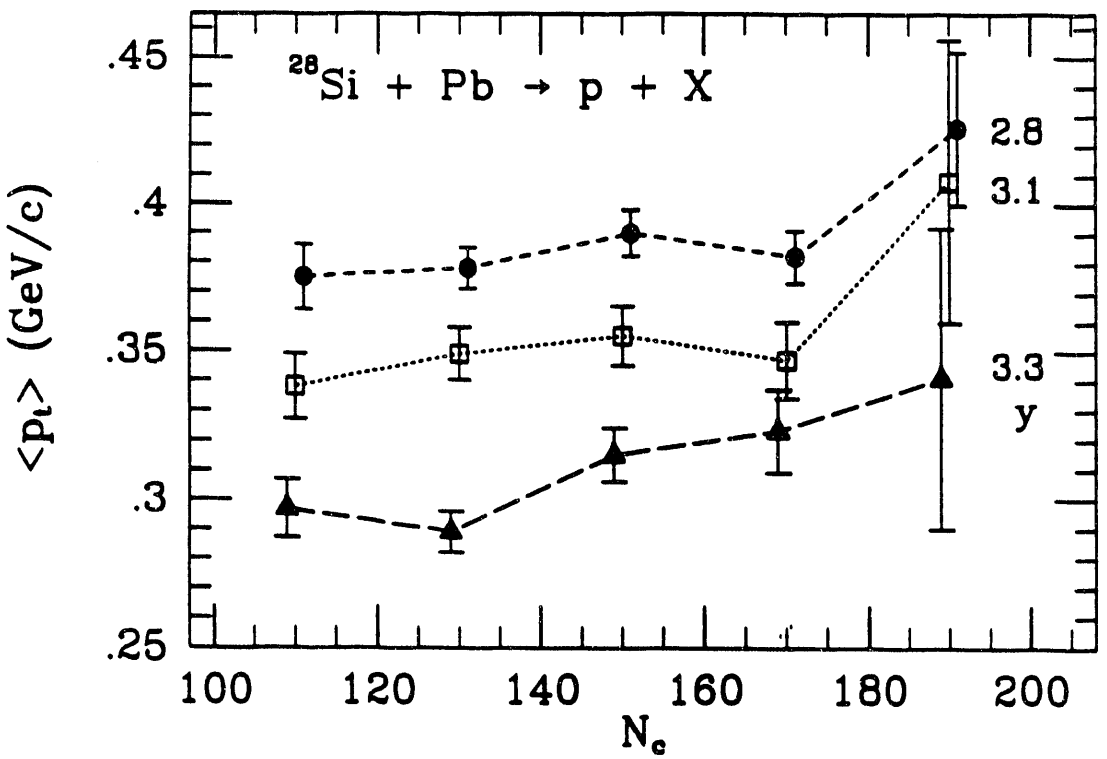

Figure 4

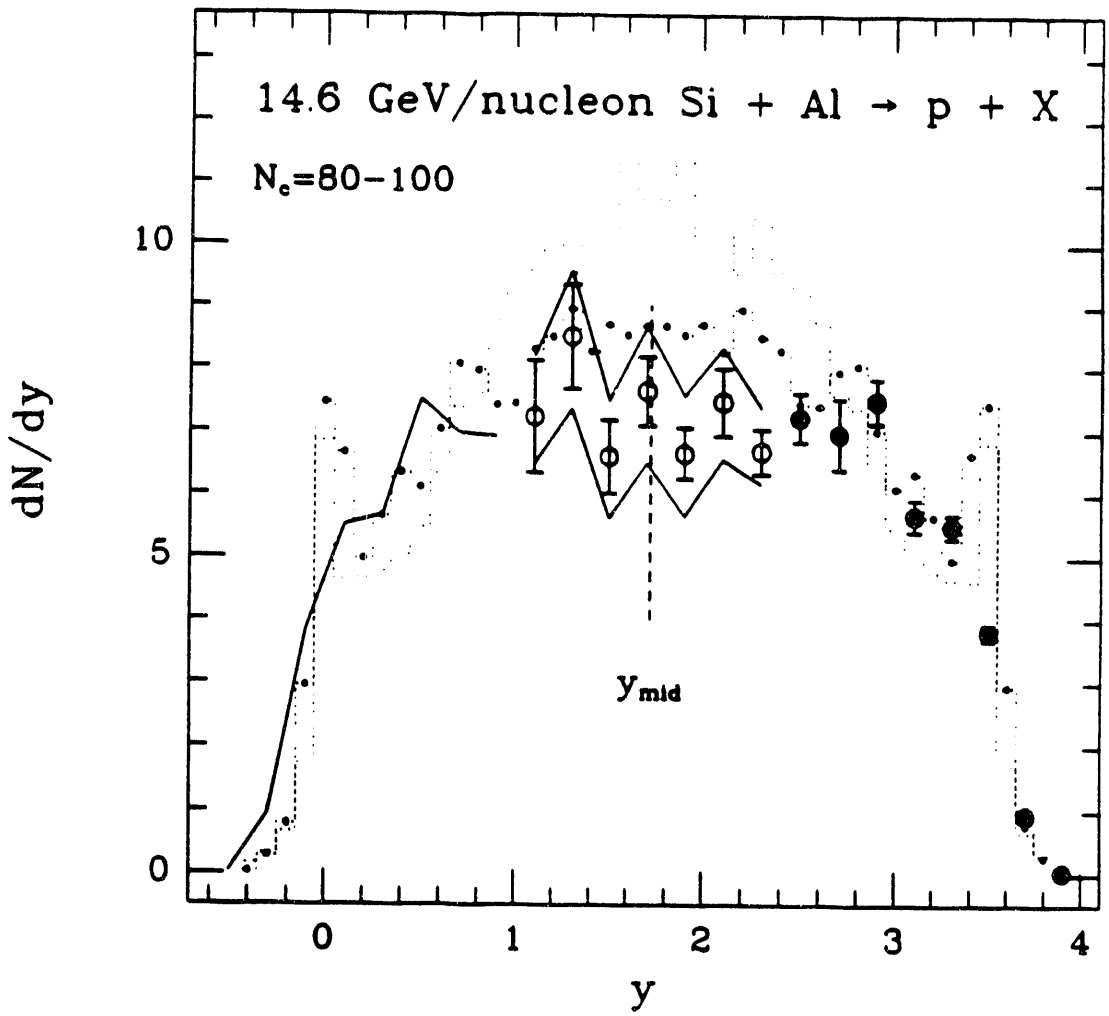

Figure 5

Data were accumulated using a mix of triggers. Targets of natural Al, Cu and Pb were used with a thicknesses between 1.2% and 2.4% of a nuclear interaction length for protons. Here we discuss only briefly the results obtained with the two calorimeters and the multiplicity detector.

The transverse energy distributions ($d\sigma/dE_t$) and spatial transverse energy distribution ($dE_t/d\eta$) have been obtained with both calorimeters for all three targets. The transverse energy production at forward angles, measured using the PCAL, appears insensitive to the target species as the distributions for the three targets are similar in shape. At backward angles however the E_t spectra have smaller slopes for the heavier target indicating strong rescattering effects at target rapidities.

The multiplicity distributions measured with the MULT detector are quite interesting. Although this detector covers essentially the same angular range as the PCAL, the multiplicity spectra obtained with the three targets are quite different both in shape and magnitudes. The Pb spectra has a lower slope and extend to quite large multiplicity relative to the lighter targets. It also shows a broad peak at low multiplicity which is not seen with the Al and Cu targets. The striking difference between the target dependence of E_t distributions and multiplicity distributions can probably be attributed to the higher sensitivity of the MULT detector to very slow target fragments. Detailed GEANT simulations are currently underway to confirm this conjecture.

The E_t data have been compared to predictions from the models HIJET and RQMD. In their latest versions, both these models include rescattering of the secondaries and both models reproduce the TCAL and PCAL data quite well. Work is still underway to compare the multiplicity data with the predictions of the above two models. In addition the data will also be compared with the predictions of FRITIOF.

II. Progress on AGS Experiment E864

Experiment E864, also known as the ECOS, (Exotic Composite Object Spectrometer) has recently received final funding approval. Our group joined this experiment some 10 months ago and have since assumed full responsibility for the Hadronic Calorimeter in this experiment. The full ECOS apparatus, which is a large acceptance forward spectrometer with three layers of straw tube tracking, three layers of high granularity time of flight hodoscopes and a hadronic calorimeter, is designed to search for exotic composite objects potentially produced in relativistic Au+ Au collisions at the AGS. One of the primary motivations for the experiment is the search for strange quark matter in the form of single multi-quark bags (in the sense of the MIT bag model). Early work by Jaffe, Chen and Kermin and others pointed out that such multi-quark bags will have greatly enhanced stability if they have significant strange quark content. In essence, building multi-quark bags out of three flavors of quarks avoids much of the energy penalty that is forced on one from the Pauli principle when only u and d quarks are used in multi-quark bags. The resulting multi-quark, strangeness enhanced, bags would produce quite a striking experimental signature if they were stable enough to pass through our tracking system. Such objects include, for example, massive particles with very low electric charge. A very sensitive mass spectrometer, capable of measuring particle mass to charge ratios with a resolution of about 3% has thus been designed as shown in Figure 1. First experimental runs with approximately 25% of the tracking system in place are scheduled for 1994 with the complete spectrometer ready for data taking in 1995.

II.1 Hadronic Calorimeter Project

The projected sensitivity of E864 for charge 1 strangelets is better than one background count in 10^{11} interactions. To achieve this level of sensitivity, the Hadronic Calorimeter must supply an independent measurement of the mass of all candidate particles, reconstructed solely from the calorimeter energy deposit and time of flight. To provide an independent mass measurement with the best possible resolution, the calorimeter must be designed simultaneously for good hadronic energy resolution and good time a flight resolution. After a careful study of various design possibilities, the collaboration has settled on a spaghetti calorimeter option similar to that used in the SPACAL prototype project.

Beginning with an extensive set of SPACAL test beam results, a series of simulations of the SPACAL calorimeter geometry have been undertaken in order to calibrate our simulation software. These studies of the SPACAL calorimeter were performed in advance of design modification studies that were required to optimize a spaghetti calorimeter device for the relatively low energy range encountered at the AGS. The present design calls for approximately 1,000 towers, each 10 centimeters by 10 centimeters in cross sectional area by 117 centimeters in depth. The construction technique which is illustrated in Figure 2 calls for stacking groved lead plates and fiber layers held together with optical quality cement. An individual tower will contain 47 layers of lead and 47 layers of 47, 1mm diameter, fibers (2209 fibers per tower). GEANT studies of modules based on this design lead us to expect timing resolution shown in Table 1. It is interesting to note that the time resolution is predicted to degrade as the particle energy increases from 2 to 12 GeV from approximately 280 picoseconds to over 400 picoseconds. This effect is understood in terms of the increased lateral shower extension for higher energy particles which produces a considerable spread in the timing of the shower. The predicted calorimeter energy resolution based on GEANT calculations (calibrated to SPACAL results as described above) is shown in Figure 3. At 4 GeV, for example, the resolution is predicted to be in the range of 20 to 25% and thus is expected to be the dominant contribution to the mass resolution of the calorimeter. Figure 4 shows a simulated

mass spectrum of over 70,000 neutron clusters in the calorimeter. The conclusion from this analysis is that the present calorimeter design will provide a rejection power approaching 1 in 40,000 for mass one background objects in a search for strangelets with mass greater than 6 GeV. This rejection power is more than a factor 4 greater than required to achieve the overall sensitivity proposed for the experiment.

We have begun prototype construction based on our present design. A number of mechanical prototypes of 9 inch long towers have been assembled to date to test various construction scenarios. One of these mechanical prototypes was used to take a first look at cosmic ray events and this is shown in Figure 5. Using this 9 inch prototype and cosmic rays, we have begun to study various couplings scenarios between the photo multiplier tube and the tower, various techniques for polishing the fibers and most importantly, we have begun to study the influence of the epoxy used in the assembly process on scintillating fiber attenuation lengths. In this last category, our preliminary measurements indicate no unusual behavior with regard to the attenuation length. More sensitive tests will be possible, however, once we build a first full size module.

At the present time we are placing orders for the raw materials to assemble up to 13 full size modules. These modules will be assembled during the next 6 months in a production area which has been built for the construction of the full calorimeter. The prototypes will be subjected to the same construction steps that are intended for the full calorimeter. The production area is shown in Figure 6. Approximately 1100 square feet of floor space is utilized to provide assembly line space for up to three parallel module lamination processes. In Figure 6, areas A, B and C provide for ultra-sonic cleaning, rinsing and drying lead plates which are then temporarily stored at area D. Areas labeled E provide space for the actual lamination process devices in which layers of lead and fiber are alternately epoxied in place. Fully laminated modules are subjected to hydraulic pressing in the area labeled F and from thence to the curing area labeled G where modules can spend up to 72 hours at an elevated temperature of approximately 125^{o} Fahrenheit. From the assembly area modules will then proceed to the machine shop for final trimming and polishing of the fiber ends. Finally, the completed modules are moved to an area where they will be tested with cosmic rays and prepared for shipment. The first 13 full scale prototype modules will be used in FY'93 test beam at the AGS.

Figure Captions

Fig 1: Plan and elevation of the E864 spectrometer to be constructed at Brookhaven National Laboratory.

Fig 2: Cross-section through a single calorimeter module showing the high degree of sampling permitted by the 'spaghetti' design of calorimeter. A single module will be constructed from a sandwich of scintillating fiber and grooved Lead sheets (shown in the figure).

Fig 3: The predicted energy resolution of the E864 spaghetti calorimeter calculated by GEANT simulations.

Fig 4: Simulations of the mass reconstruction of over 70,000 neutron clusters in the E864 spaghetti calorimeter. This figure illustrates that less than one event in 10,000 is erroneously reconstructed with a mass greater than 6 GeV.

Fig 5: Energy spectrum for comic rays measured in a nine inch long prototype module for the E864 spaghetti calorimeter.

Fig 6: Floor plan of the E864 spaghetti calorimeter construction facility at Wayne State University.

E864

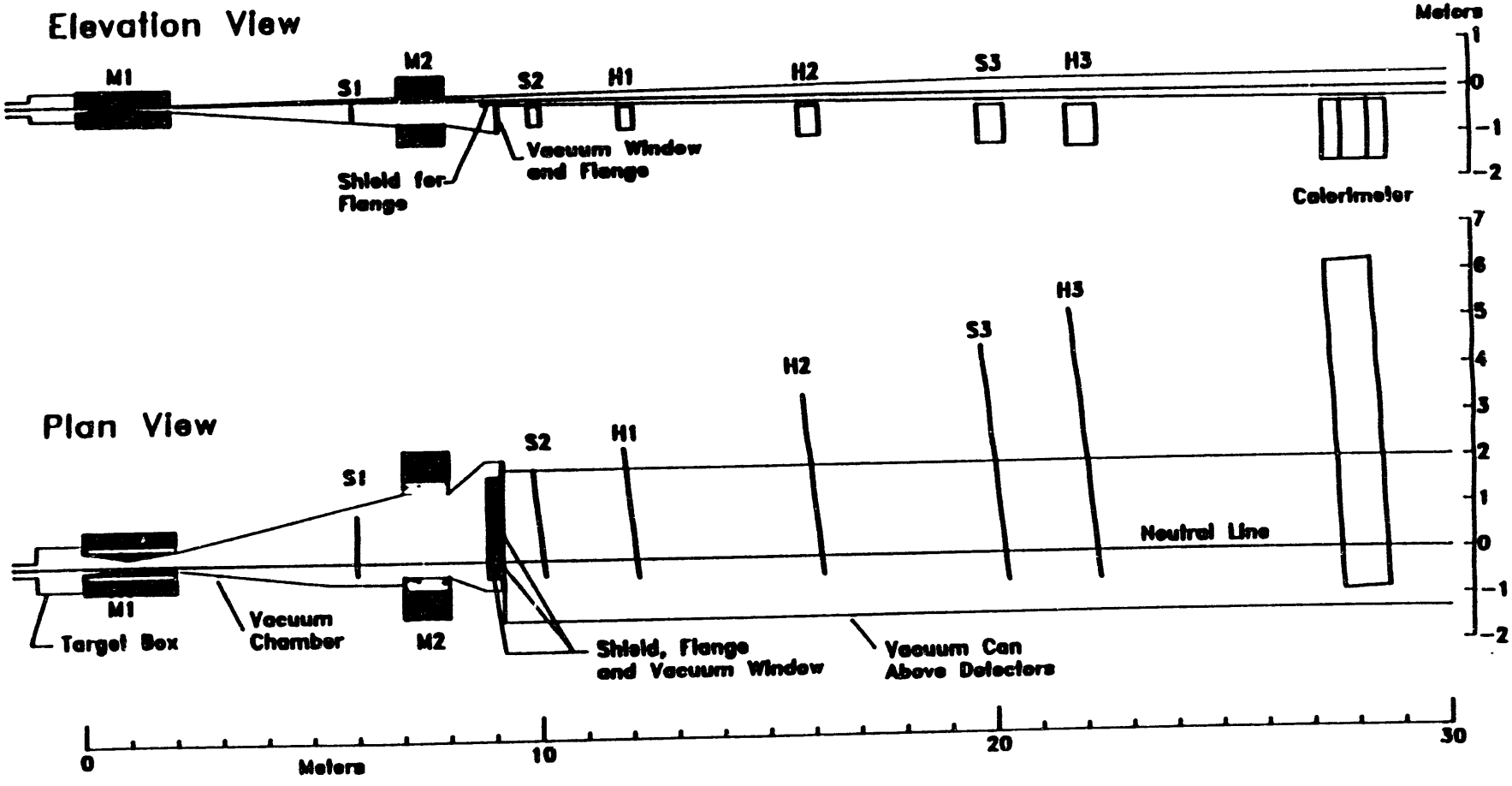

Sections at the neutral line are shown for the magnets, collimators and vacuum chamber. M1 and M2 are dipole spectrometer magnets; H1, H2, H3 are scintillation counter hodoscopes; S1, S2, S3 are straw tube arrays.

Figure 1

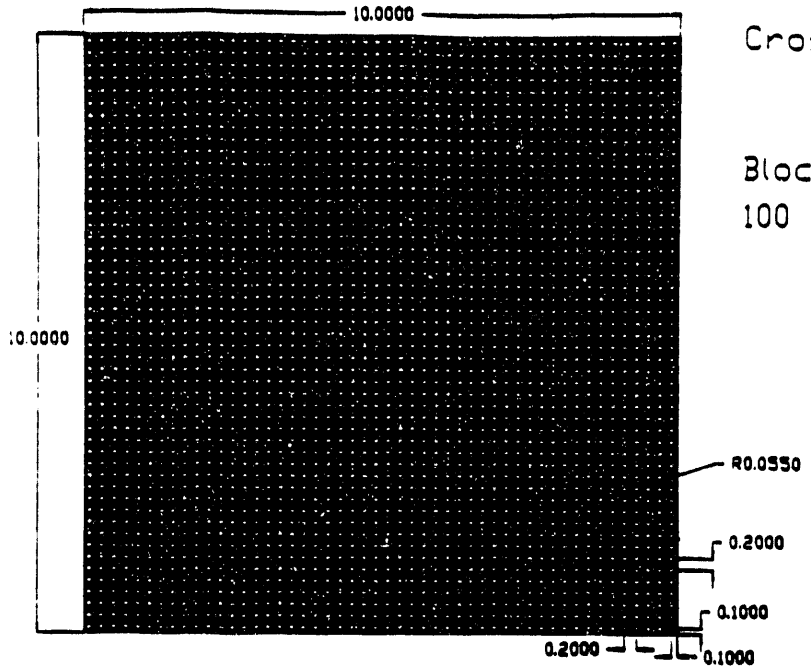

Cross-section of a single calorimeter tower using 1 mm diameter fibers and a lead-to-scintillator volume ratio of about 4:1. (Dimensions are in cm.)

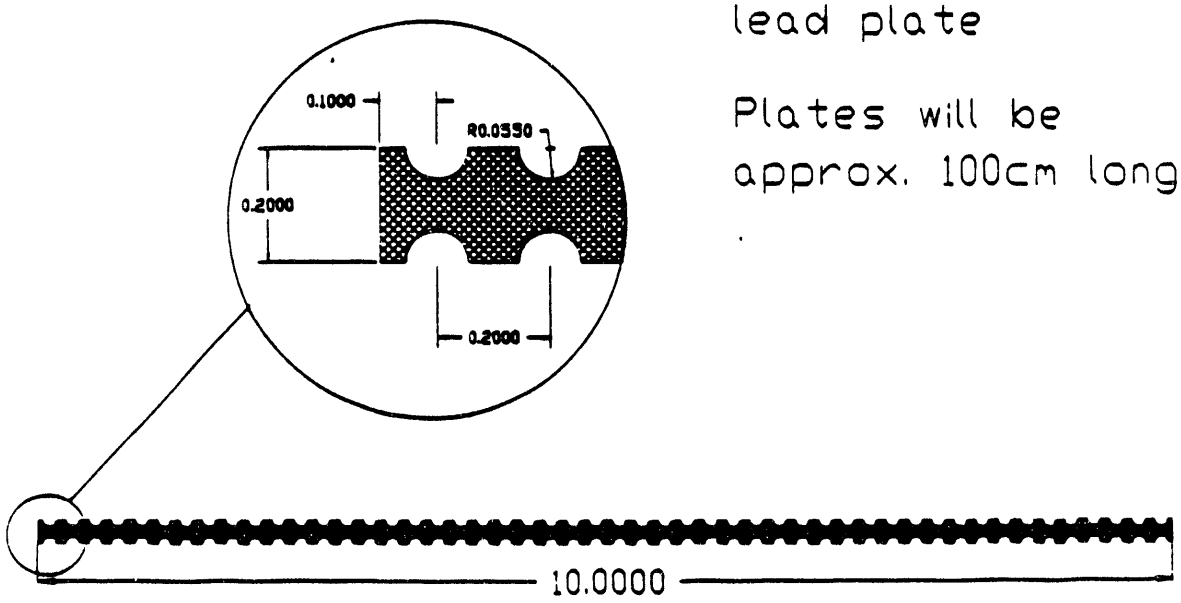

Cross-section of a grooved plate
(Dimensions are in cm.)

Figure 2

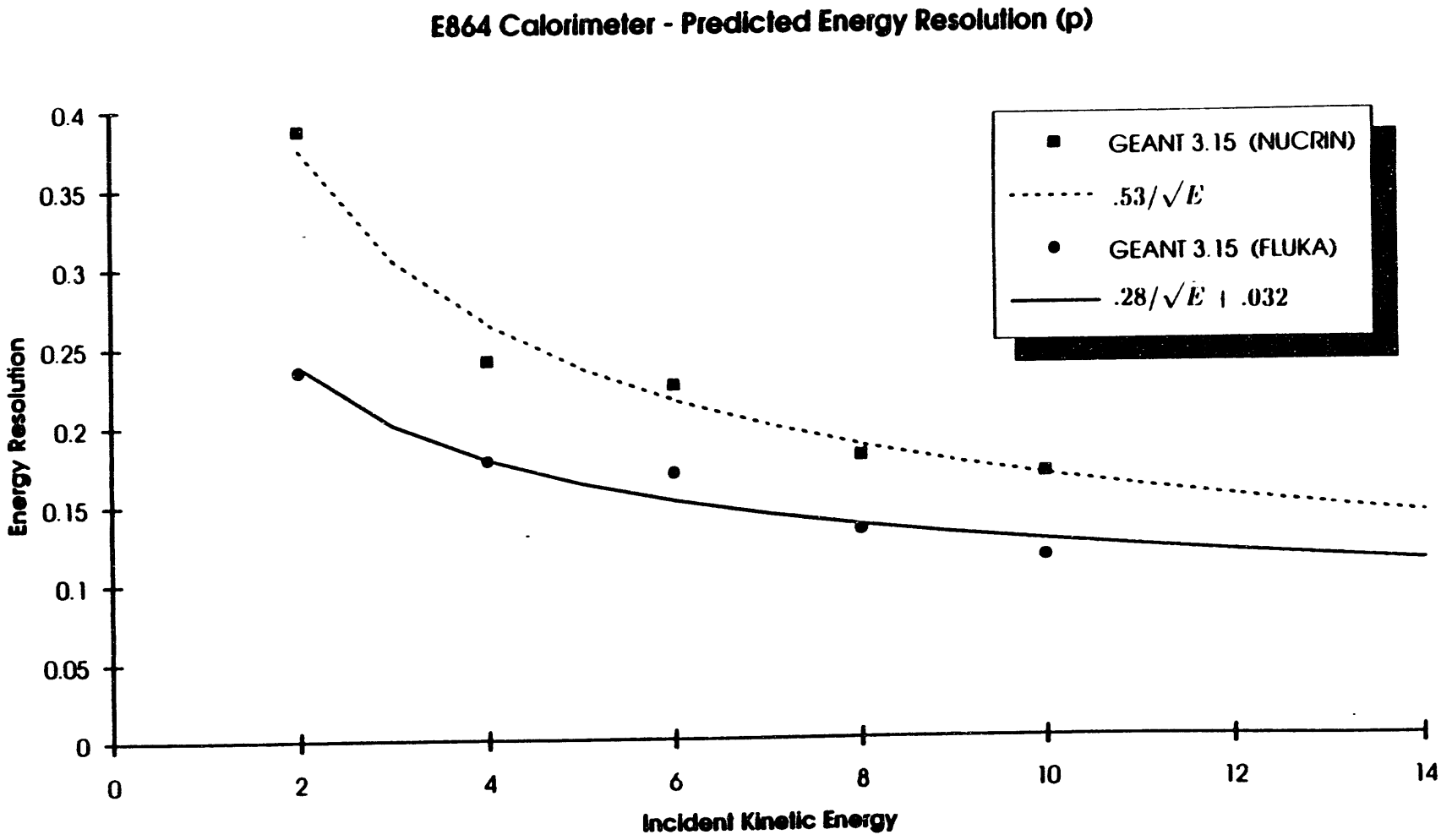
E864 Calorimeter - Predicted Energy Resolution (p)
GEANT 3.15 (NUCRIN)
$.53/\sqrt{E}$
GEANT 3.15 (FLUKA)
$.28/\sqrt{E} \oplus .032$
Energy Resolution
0.4
0.35
0.3
0.25
0.2
0.15
0.1
0.05
0
0
2
4
6
8
10
12
14
Incident Kinetic Energy

Figure 3

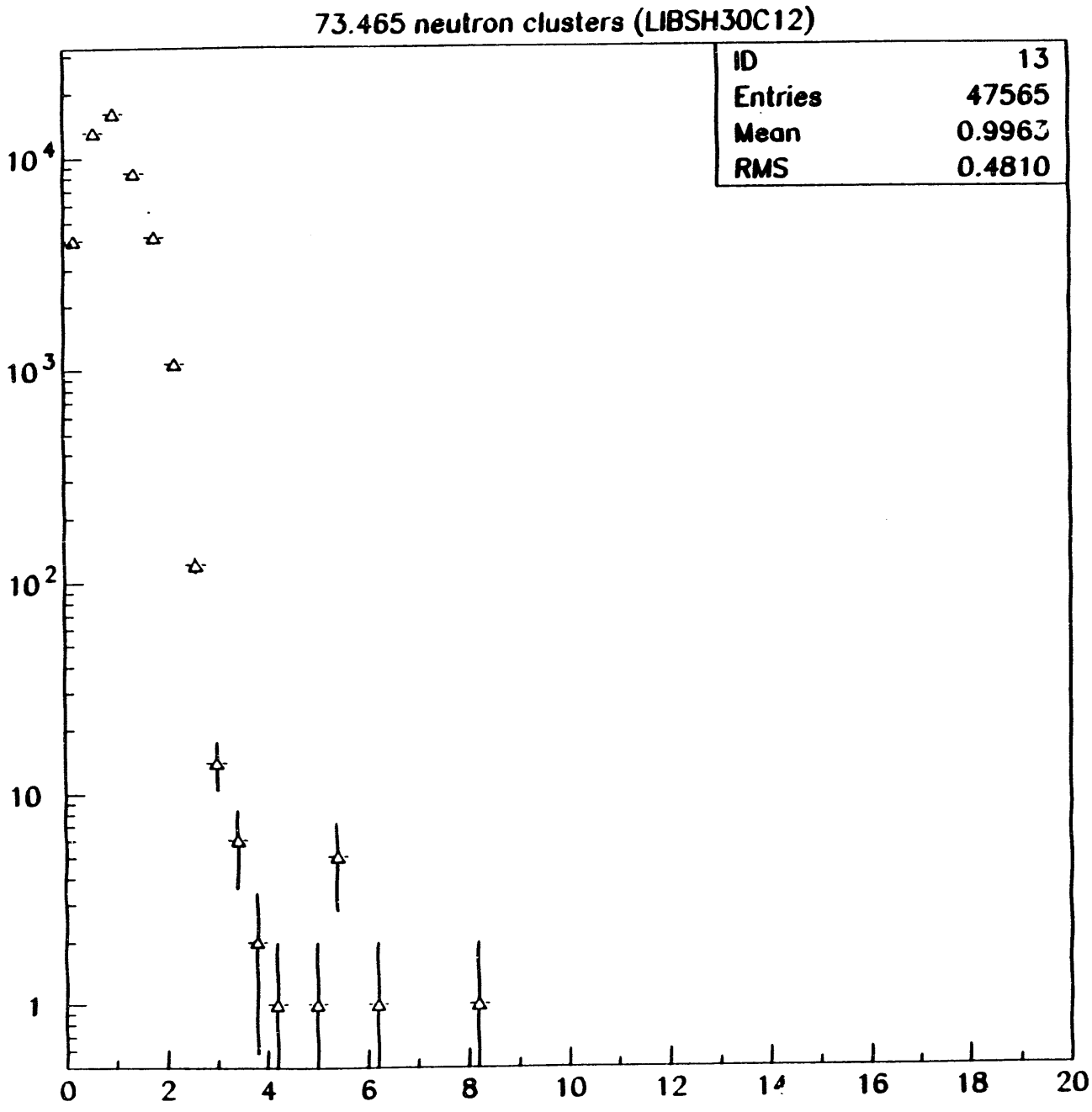
73.465 neutron clusters (LIBSH30C12)
ID 13
Entries 47565
Mean 0.9963
RMS 0.4810
10^4
10^3
10^2
10
1
0
2
4
6
8
10
12
14
16
18
20
Mass (GeV)

Figure 4

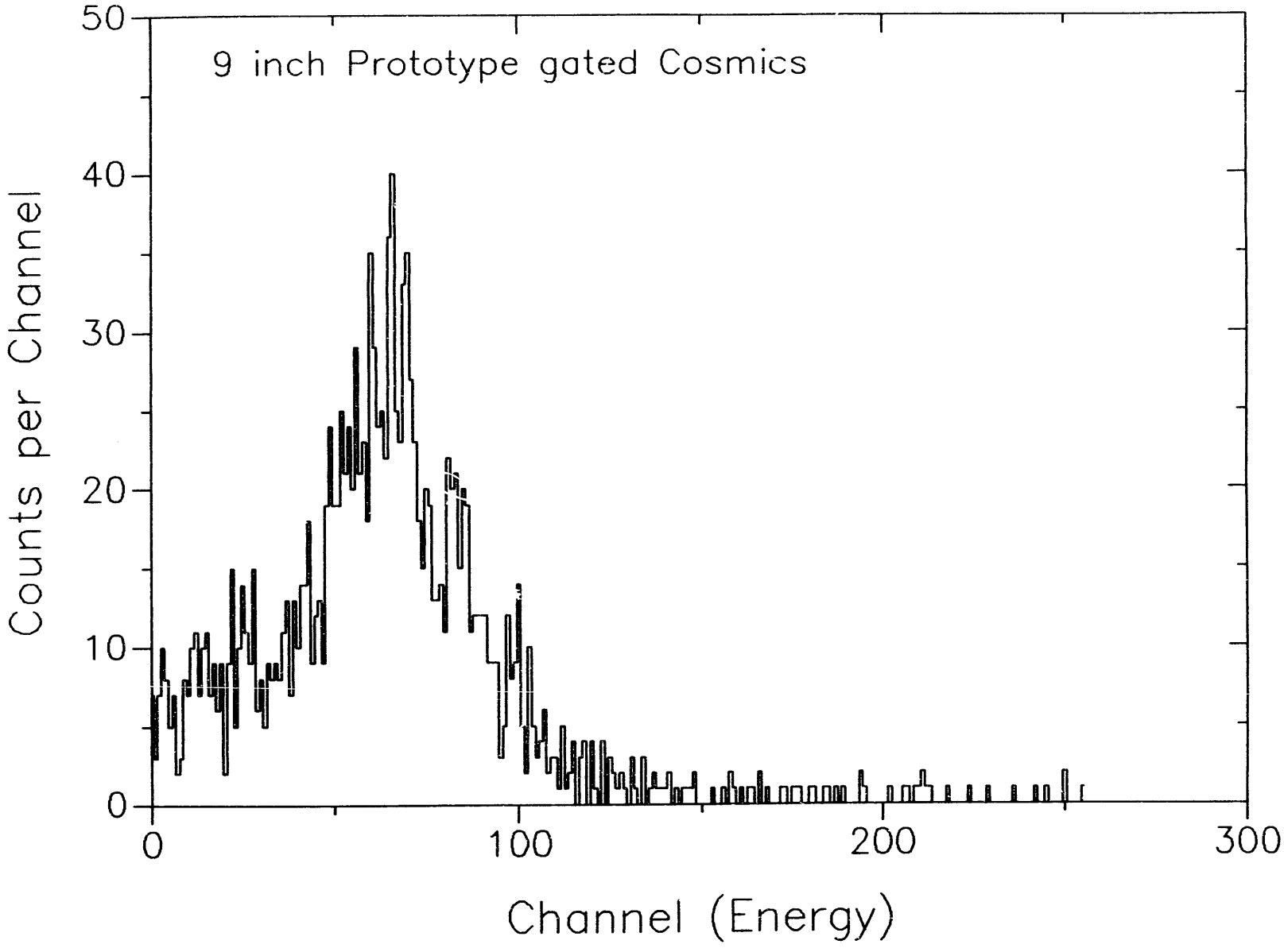
9 inch Prototype gated Cosmics
Counts per Channel
Channel (Energy)
0
10
20
30
40
50
0
100
200
300

Figure 5

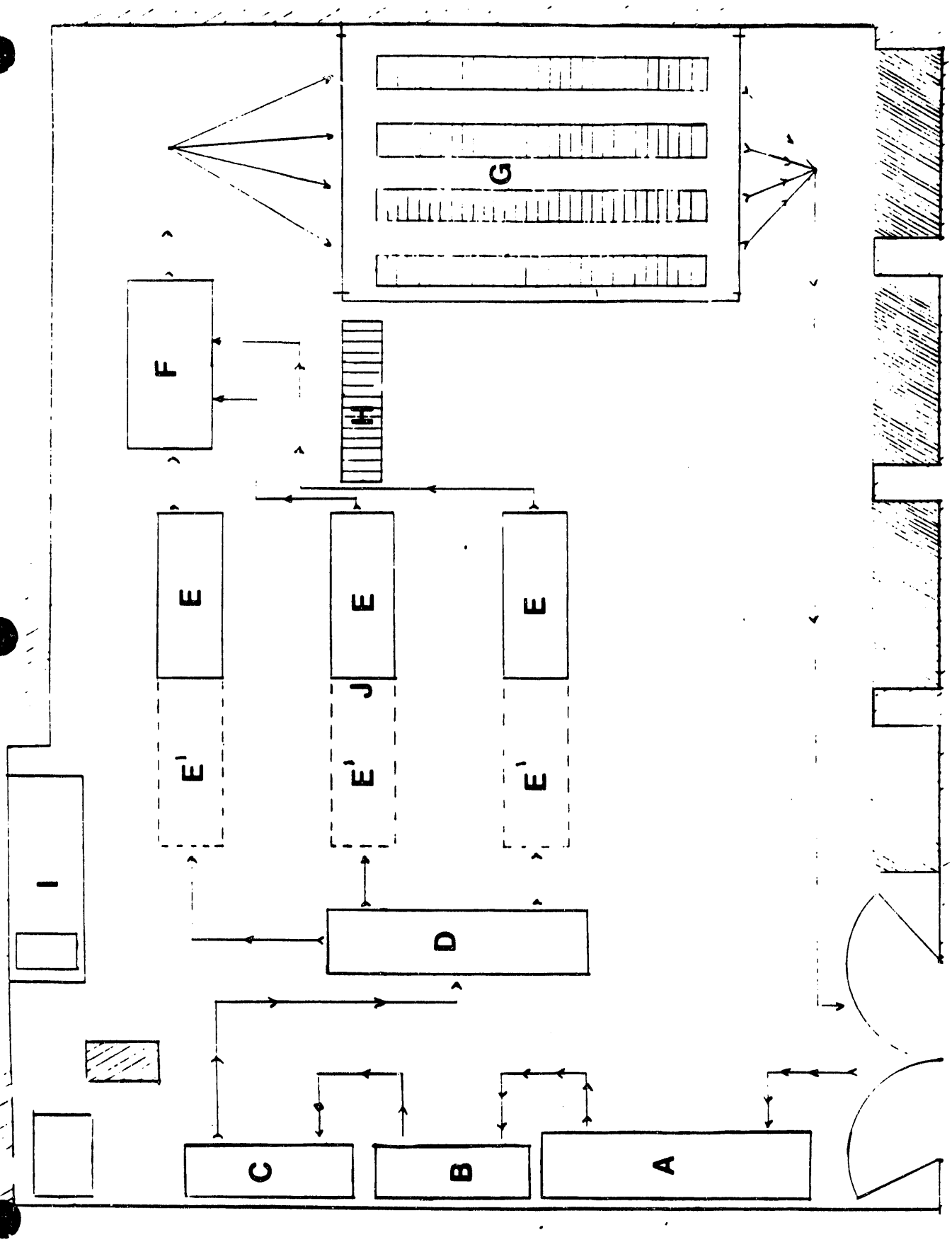

Flow of Pb/Sci through the lamination-curing area (precut/ inspected fibers).

Peak Module Timing

Results of the calorimeter timing simulation. The RMS of the timing distribution for 400 events at each energy is shown in picoseconds for both the uncorrected and slewing corrected distributions.

Energy (GeV)	uncorrected RMS (ps)	corrected RMS (ps)
2	512 ± 18	284 ± 10
4	383 ± 14	377 ± 13
6	396 ± 14	365 ± 13
8	384 ± 14	364 ± 13
10	431 ± 15	423 ± 15
12	413 ± 15	414 ± 15

Side Module Timing

Results of the calorimeter timing simulation for side (next to peak) towers. Δt = t(side) - t(peak) and the RMS for the slewing corrected distributions. The slewing correction used was the same as for the peak tower.

Energy (GeV)	Δt (ns) (corr)	RMS (ps) (corr)
2	−.94 ± .023	794 ± 12
4	−.102 ± .021	753 ± 10
6	−.118 ± .020	728 ± 10
8	−.162 ± .020	765 ± 10
10	−.169 ± .020	726 ± 11
12	−.190 ± .020	704 ± 11

Table 1

III STAR

III.1 SVT Project Evolution and Development in FY92

By the end of 1991, the Relativistic Heavy Ion group at the WSU Physics Department decided to join the STAR RHIC collaboration. With the beginnings of some expertise in Si technology (two of us: Tom Cormier and Rene Bellwied worked on the Si-strip detector for TALES/SPARHC, two of us: Jerry Hall and Claude Pruneau worked on Si-pad detectors for E814 and OASIS), we decided to join the Silicon Vertex Tracker (SVT) group in STAR. A chronology of our work on this project to date is as follows: Shortly after joining the SVT project, we participated in a test beam time with a prototype Silicon drift detector at TRIUMF in Vancouver in February 92. This beam time was aimed at determining the de/dx capabilities for Si drift detectors and a first result of these measurements can be seen in Fig. 1. It was the first time an energy loss distribution for 300 MeV/c pions was obtained with a Si-drift detector. This so-called STAR 0 detector was a prototype designed and manufactured by Pavel Rehak at Brookhaven National Lab. It has a drift length of 1.6 cm and 32 anode output channels. These first dE/dx look very encouraging and further more extensive testing is planed for the next generation prototypes.

In March of 1992, one of us, (Rene Bellwied) was assigned by the STAR management to participate in the conceptual design committee (CDC) of STAR. The responsibility of this committee of seven people was to down scale the physics program of STAR with respect to the available resources. After two months of meetings and discussions, this committee decided to propose the so-called STAR baseline design which meets the 30 million dollar requirement set by the DOE. The baseline detector concept consists of the TPC, the magnet, trigger detectors and the DAQ. The committee also felt that a SVT available at day one of RHIC running would enhance the physics capabilities of STAR in a tremendous way. The committee, therefore, decided to suggest an alternative financing of the SVT based on R+D money for the first 3 years from 1993 on. This is also in agreement with the assessment that the SVT is the major R+D project in STAR. It is based on a new technology in Si detectors (Si drift) and therefore, requires the most attention in the R+D phase. The CDC was also responsible for the conceptual design report (CDR) which was due in June, 1992. During this time, the CDC worked closely with the interim project leaders.

Right after the publication of the CDR, the STAR management shifted the project leadership for the SVT to Wayne State University. Since the beginning of July, Rene Bellwied functions as the SVT project leader. Since the vesting of the project management at WSU, we have invested considerable effort in developing a consensus driven management structure for the SVT project. Most recently, work plans, R+D project plans, milestone and prototype plans have been worked out to assure a successful cost and scheduling review for the SVT by RHIC and the DOE.

At the present time, participating institutes include BNL, LBL, WSU, OSU, U of Washington, U of Arkansas, and Warsaw. All in all, the SVT group consists of 36 people from these seven institutions at this stage. We are in close contact with 2-3 other interested groups in the United States and Europe.

III.2 SVT software results from 1992 by WSU

The WSU simulation group (Joe Bielecki, Gabriel Roger and Rene Bellwied) started a new project by trying to utilize the SVT for stand alone tracking for low transverse momentum particles. The physics of low momentum particles is an interesting field, in itself, and one of the smaller RHIC

collaborations (PHOBOS) is working on an experiment for RHIC that will address these physics issues only. The main topics are:

a) The low p_t enhancement detected by several groups at the AGS and CERN in heavy ion reactions.

b) The correlations of low p_t particles which might be attributed to localized plasma formation.

c) Intermittence effects in low p_t correlations.

d) The enhancement of HBT efficiency compared to the TPC measurements.

e) The complete phase space coverage with SVT and TPC for the decay of secondaries and resonances like the phi-meson.

f) The measurement of unusual low p_t particle ratios, which might hint at the formation of a cold QGP.

The simulation effort at WSU was aimed at determining how many of these relevant physics issues can be determined with a high resolution tracking device like the SVT in a stand alone mode. The second part of the simulations determined how effective an integrated tracking device (SVT+TPC) can be operated. The tracking efficiency in the TPC decreases drastically below 200 MeV/c because these low momentum tracks are bent by the solenoidal magnetic field in a way that they do not hit all the pad rows in the TPC. We, therefore, attempted to track these particles by applying a helix fit to the spacepoints measured in the SVT only. A helix fit requires 4 points, so that in a 3 barrel SVT design, the vertex has to be determined before the helix can be fitted. A vertex measurement is possible without any sophisticated track reconstruction because most of the tracks point back to the primary vertex. By applying this to the spacepoints found in SVT and TPC one can reach a vertex resolution of 150 microns. The suggested tracking code for the SVT is attempting to connect spacepoints from the inside out. That means, each spacepoint on the first layer is connected to the vertex. Then one defines a cone on the second layer into which the first spacepoint has to be connected. This cone is defined by the bending of the lowest measurable transverse momentum particles. Due to interactions in the beam pipe, this lowest p_t is around 40 MeV/c. Besides the bending, the multiple Coulomb scattering (MCS) in the first layer, as well as the vertex and spacepoint resolution contribute to the cone radius. The MCS consists of a component due to the first layer of silicon itself, as well as, tiled areas of Silicon to avoid dead areas on the detectors and the frontend electronics (FEE) which is located between the individual wafers. All this is taken into account in the WSU simulation. We then perform a layer to layer tracking up to the point where each track accumulated 4 points. Then a helix is fit based on a chisquare constraint which is determined by the spacepoint (momentum) resolution of the detector. The requirement of 4 points for the helix makes it impossible to fit secondary vertices (decaying particles) with this algorithm. We, therefore, suggested an upgrade to a 4 layer SVT design.

In Figs. 2 and 3 we show the track efficiencies for the two different designs, which are now under consideration for the final SVT detector. The 4-layer design foresees a fourth layer very close to the beam pipe (R = 3 cm). This allows for a reconstruction of 80% of the primaries which decay in the SVT, because their secondary vertex is before the first layer. All in all around 10% of the secondaries decay in the SVT (the secondaries are dominated by the pion cross section). A breakdown of these numbers reveals that all of the 'relevant' primaries (Ω's,Σ 's, and Ξ's) are reconstructed by the SVT tracking routines. Decaying primaries which are not completely reconstructed include the Λ's, π's, and K's . The measurement of multi strange particles is one of the main physics goals of STAR.

A further, ongoing project in this context is the reconstruction of the D-meson decay utilizing the SVT tracking capabilities. The problem in this case is the determination not only of the secondary, but also the third vertices in this decay chain. The output should be a 5-prong of charged particles. In collaboration with our colleagues at Warsaw University, we tried to postulate a set of phase space constraints which are independent of the physics of a particular Au+Au event. Based on these constraints, one can narrow down the amount of tracks that can contribute to the background for the 5-prong. These simulations are very time and cpu consuming. At the moment, simulations hint at a signal-to-noise ration of 1:1 for 10^6 central Au+Au events. We are trying to improve these simulations by including so called neural network algorithms, based on work done by Gyulassy. An alternative approach suggested by Stroebele and Bellwied proposes just the measurement the vertex of Kaons produced very close to the primary vertex. The D-meson has a $c\tau$ of 300 microns, whereas the SVT will determine the primary vertex down to 150 micron. Assuming a cut between 200 and 400 microns for the secondary Kaon vertex, would allow a determination of the D-meson yield by simply counting the Kaon's produced in this range. The effect of primary Kaons on this D meson signal appears to be very small.

Another important set of data is recovered by the near perfect reconstruction of the K^0_s that is provided by the SVT. Declan Keane et al. showed that this enables STAR to perform a HBT measurement with neutral strange particles which would complement the TPC-HBT measurements of charged Pions and Kaons. Fig. 4 shows the correlation function from a simulated K^0 reconstruction in the SVT.

The second vertex reconstruction in the SVT is crucial to the successful reconstruction of any secondary particle in general, because around 60% of all decaying particles have a component below 200 MeV/c, which would be lost in a pure TPC running mode (e.g. Fig. 5). For particles above 200 MeV/c we will have spacepoints in TPC and SVT. For these tracks the matching between the two vectors which are the result of the two independent tracking codes, becomes crucial. WSU made a first attempt to match from the inside out (SVT to TPC), whereas the groups at LBL and U of Washington tried to match from the outside in (TPC to SVT). A comparison between the two simulations shows that a SVT to TPC matching is favored, if possible. The much better resolution of each spacepoint in the SVT (25 micron compared to 700 micron in the TPC) assures a smaller cone in the layer to match to, and therefore, a smaller occupancy in this part of the TPC. Figs. 6 and 7 show a comparison between the two methods based on the WSU algorithm. Based on these matching efficiencies LBL attempted a comparison of secondary reconstructions with and without the SVT. Figs. 8 and 9 show the results.

After matching the two detectors, we attempted to determine the effect of the SVT on the momentum resolution of all emitted particles. In the low momentum range of particles seen by SVT and TPC, the effect is small because the resolution is dominated by the sagita and the only improvement comes from the improved determination of the vertex. The stiffer the tracks gets, that means the higher the momentum of the particles, the bigger the improvement due to the excellent spacepoint resolution of the SVT. This effect becomes dominant for tracks with almost no deviation from a straight line. Figs. 10, 11 show a simulation of this improvement as a function of momentum.

III.3 SVT Instrumentation

At Wayne State, we are working in close collaboration with Ohio State (Tom Humanic's group) to instrument and maintain one of the three big Si detector development labs for the SVT project. The other labs are located at BNL and LBL. In connection with this laboratory development we are establishing a dedicated electron beam line at our 5 MeV Van De Graff accelerator to serve as an

electron test beam facility for the Si drift detectors. The 3 MeV/c electron beam from this facility is comparable to a 300 MeV/c pion beam except that it is available year round at next to no cost. This modest upgrade will provide a high spatial resolution (on the 10 micron level), low intensity (one particle at a time) electron beam. The upgrade is financed by STAR R+D money. This high spatial precision will enable us to map the response of a Si wafer in each point of the active area. Ohio State and Wayne State have agreed to use this facility in FY93 as part of a joint testing program. The availability of the beam over the whole year allows us to optimize the test program according to the progress. This test beam will complement allocated test beam at TRIUMF and the AGS. Fig. 12 shows a comparison between 300 MeV/c pions (available at TRIUMF) and 3 MeV/c electrons. The electrons are penetrating but they have a slight disadvantage in resolution in all but the first layer. The main application of the electron beam will, therefore, be the study of the complete response of individual detectors over their entire surface and the effect of thermal gradients on this response.

One of the major R&D questions to be addressed at WSU relates to the difficult thermal environment in which the SVT will operate. There are two facets to the problem. The first is the matter of removing the the continuously generated heat load from 80,000 electronic channels which will be buried under their own densely packed cabling. Water or other liquid cooling looks like viable alternative at present but the engineering problems that this will pose are numerous. Assuming an appropriate heat removal system for the bulk of the heat load, the remaining major requirement is the maintenance of temperature stability at the active area of the wafers and minimizing even stable temperature gradients at the wafer surface. The rather strong dependance of drift velocity on temperature suggests that the design goal should be combined spatial gradient and temporal variation approaching a small fraction of a degree.

We have assumed responsibility , in connection with WSU's Institute for Manufacturing Research (IMR), for the study of spatial temperature gradients on the detector surface. Such gradients may be difficult to avoid since the presence of Darlington pairs and voltage grading resistors that are integrated into the silicon wafer produce localized heat sources. In collaboration with the IMR we are able to image detector surfaces in the infrared with 128x128 pixel resolution and a temperature precision in each pixel down to 0.001 degree. This imaging capability is compatible with realistic detector test operating environments. Thus, two dimensional drift time maps of the detector surface can be measured using an electron beam and correlated with simultaneously surface temperature maps.

The installation of a Si test laboratory at WSU is integrated in an effort to install three independent development locations for Si drift detectors. STAR started this process last year by instrumenting a Si-lab at LBL. We also utilize a Si-lab at BNL, which addresses slightly different issues. Besides the electron beam and IR imaging capability, our group will put in place an appropriate read out chain involving CAMAC waveform digitizers . A laser for table top testing tests will be shared with the E864 calorimeter effort. A x-y table allows precision movement of the individual wafers down to the micron level. This first level instrumentation will be complemented by the OSU group which provides a wirebonder and a dedicated laser for wafer testing.

WSU is also responsible for the cabling integration for the SVT signal and high voltage cables. Both components cause serious design challenges. The signals cannot be multiplexed at the detector. At present, therefore, 80000 signal channels that are wire bonded to a read out board in 2.5mm must propagate all the way to the exterior of the TPC housing. Capton-Aluminium cables developed for the SSC are forseen for the path from the detector to the TPC housing where the next level of the electronics is located. These cables provide the smallest addition of material in the vicinity of the detector. Prototypes of these cables with a 200 micron pitch between channel wires are in production. The high voltage cables have to bring 3000 V to each wafer to an area where the detectors overlap to ensure 100% active area. We are working on these problems and we will perform cabling test in the WSU test lab.

III.4 FY93 SVT Pion test beam

The TRIUMF test beam scheduled for March 93 is a continuation of the February 92 beam time at TRIUMF. In '92 we used the STAR 0 detector with 16 instrumented channels. After amplification and shaping, the signals were digitized in a Le Croy 2262 waveform digitizer. One wafer was tested for its dE/dx performance, see Fig. 1. For the FY93 beam time, we will use three to four detectors in a multi layer design. The detectors will be STAR 1 detectors (a wafer of 5x5 cm area) with 24 instrumented channels in each detector. This results in 6 mm active area over each wafer. After aligning these active areas we will attempt to measure the tracking performance of STAR 1 design . For these prototypes, the signals will be read out into a SCA board (Switch Capacitor Array) which will feed the signals, after multiplexing, into an ADC on the same board. This board will be read out in a VME crate. This read out chain is very similar to the final design expected for the STAR experiment. As in FY92 WSU, LBL and University of Washington will be responsible for the data acquisition and analysis for the FY93 beam time.

In preparation for the upcoming test beam at TRIUMF, the WSU machine shop will manufacture the support structure for testing the tracking capabilities of the STAR1 prototypes. These detectors have already designed and manufactured by Pavel Rehak (6 detectors). The plan is to get at least 3 detectors in series in a pion test beam to test the tracking efficiency. The rather extensive support structure, which has to assure alignment in all 3 dimensions, has been designed by the WSU group and it will be machined within the next months. The shop is also tooling up to build ,a full size Aluminum prototype of the final SVT support structure (barrel structure) here at WSU in FY 93.

Figure Captions

Fig. 1: dE/dx distribution for various particles. The solid line represents measurements at 2 GeV/c [1], the dotted line shows SVT TRIUMF data. The dashed line shows expected performance for K,p [1]

1.) J. F. Bak, et al., Nucl. Phys. B288 (1982) 681

Figs. 2/3 Simulated track efficiencies for a.) a 3 layer SVT design. b.) a 4 layer SVT design. The upper two curves in Fig. 2) represent the efficiency assuming a first pass through the SVT algorithm to exclude 'stiff tracks' above P_T = 200 MeV/c. For the part of the spectrum between 40-200 MeV/c, the efficiency as a f(P) is then fitted for a tiled and a non-tiled design. The non-tiled design leads to 11% dead area on the detector which decreases the efficiency accordingly. The third curve in Fig. 2) represent the track efficiency for the full particle spectrum without excluding stiff tracks above 200 MeV/c. Fig. 3 show the track efficiency for the low P_T - part (40-200 MeV/c) in a 4-layer design (tiled and non-tiled).

Fig. 4 Simulated correlation functions for K^0_S interferometry for 10^4 central RHIC events

Fig. 5 Pion spectra from the Ξ^- decay. a.) Momentum distribution, b.) Transverse momentum distribution. More than 50% of the pions are below the tracking threshold for the TPC alone.

Fig. 6/7: Matching efficiencies between TPC and SVT. Fig. 6) Shows the efficiencies by matching from the SVT to the TPC (inside-out). Fig. 7) Shows the efficiency by matching from the TPC to the SVT (outside-in) The two curves on each plot represent presentations of matching efficiencies for a.) The low P_T-subset (40-200 MeV/c) of the particle spectra b.) The full particle spectra

Figs. 8/9 Reconstruction of K^0_S and Ξ^- by an integrated STAR tracking system (TPC + SVT)

Fig. 10 P_t resolution as a function of P_t for both the TPC only and TPC plus SVT.

Fig. 11 Effect of momentum resolution on measured yields at "high" p_t with and without the SVT

Fig. 12 Simulation of the energy loss of 300 MeV/c pions and 3 MeV/c electrons through three consecutive layers of 300 micron Si.

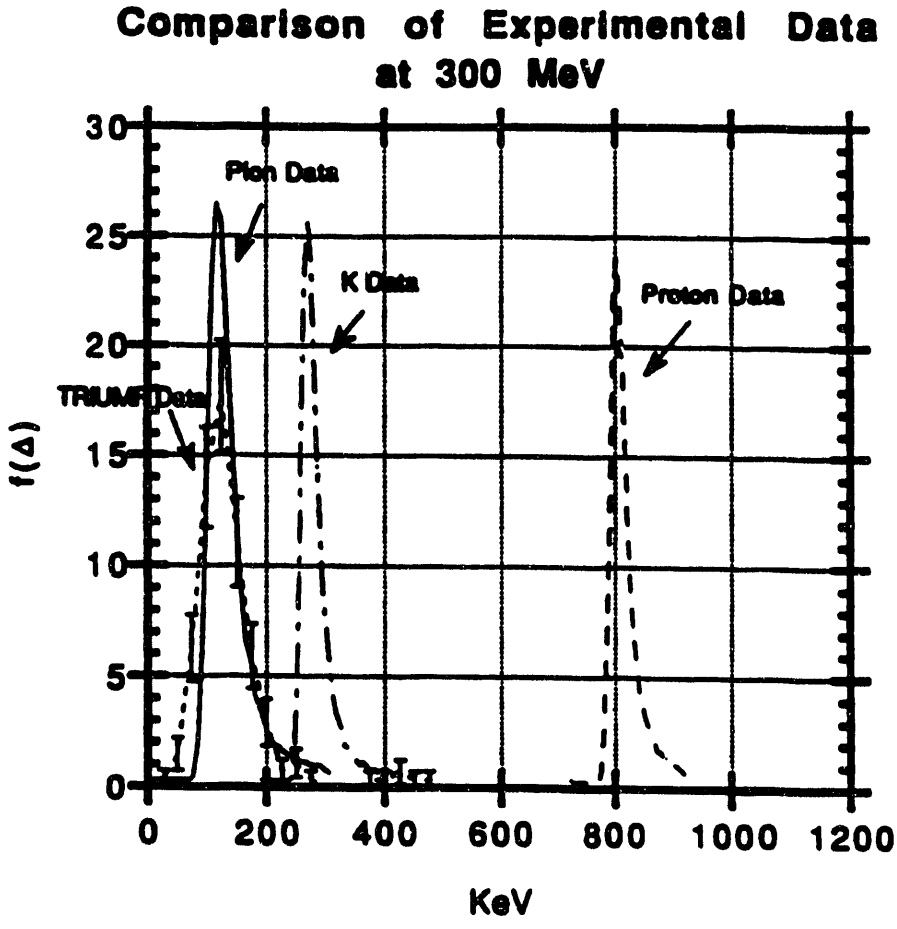
Comparison of Experimental Data
at 300 MeV
Pion Data
K Data
Proton Data
TRIUMF Data
f(Δ)
30
25
20
15
10
5
0
0
200
400
600
800
1000
1200
KeV

Figure 1

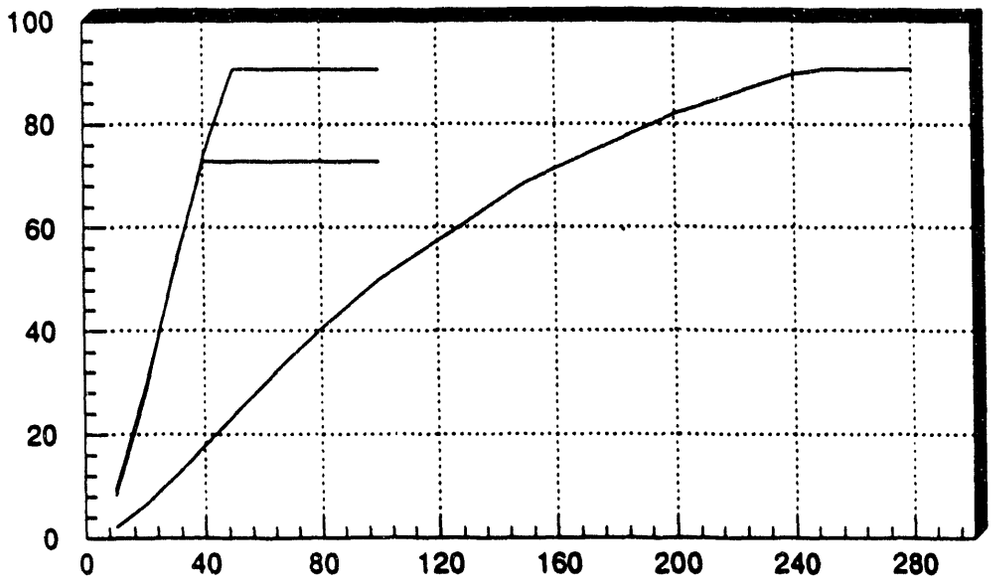

Figure 2

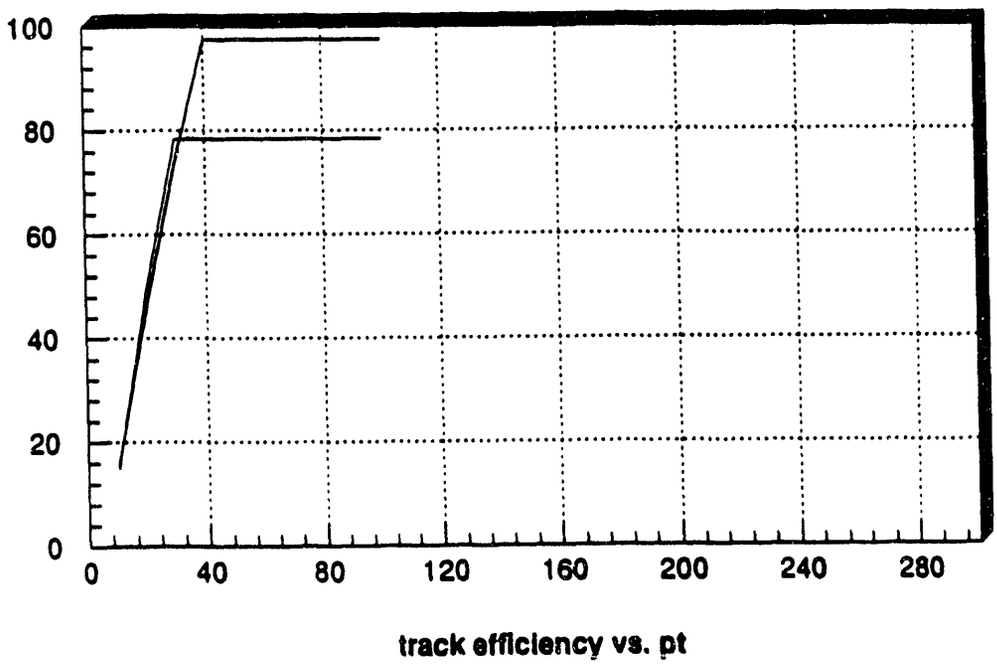

Figure 3

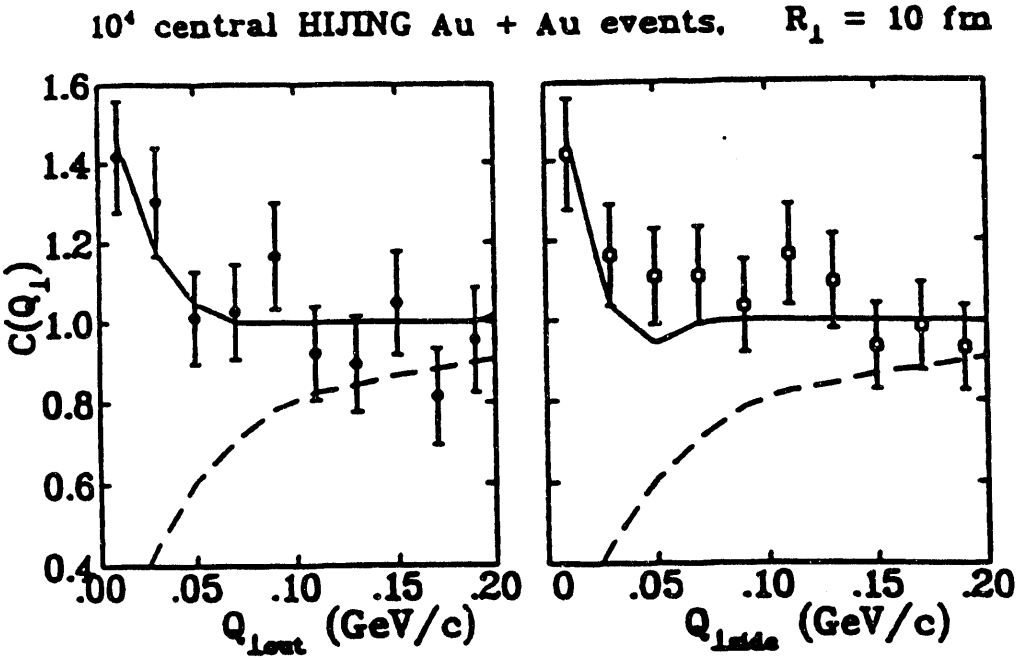
10⁴ central HIJING Au + Au events, R⊥ = 10 fm
C(Q⊥)
1.6
1.4
1.2
1.0
0.8
0.6
0.4
.00
.05
.10
.15
.20
Q⊥out (GeV/c)
0
.05
.10
.15
.20
Q⊥side (GeV/c)

Figure 4

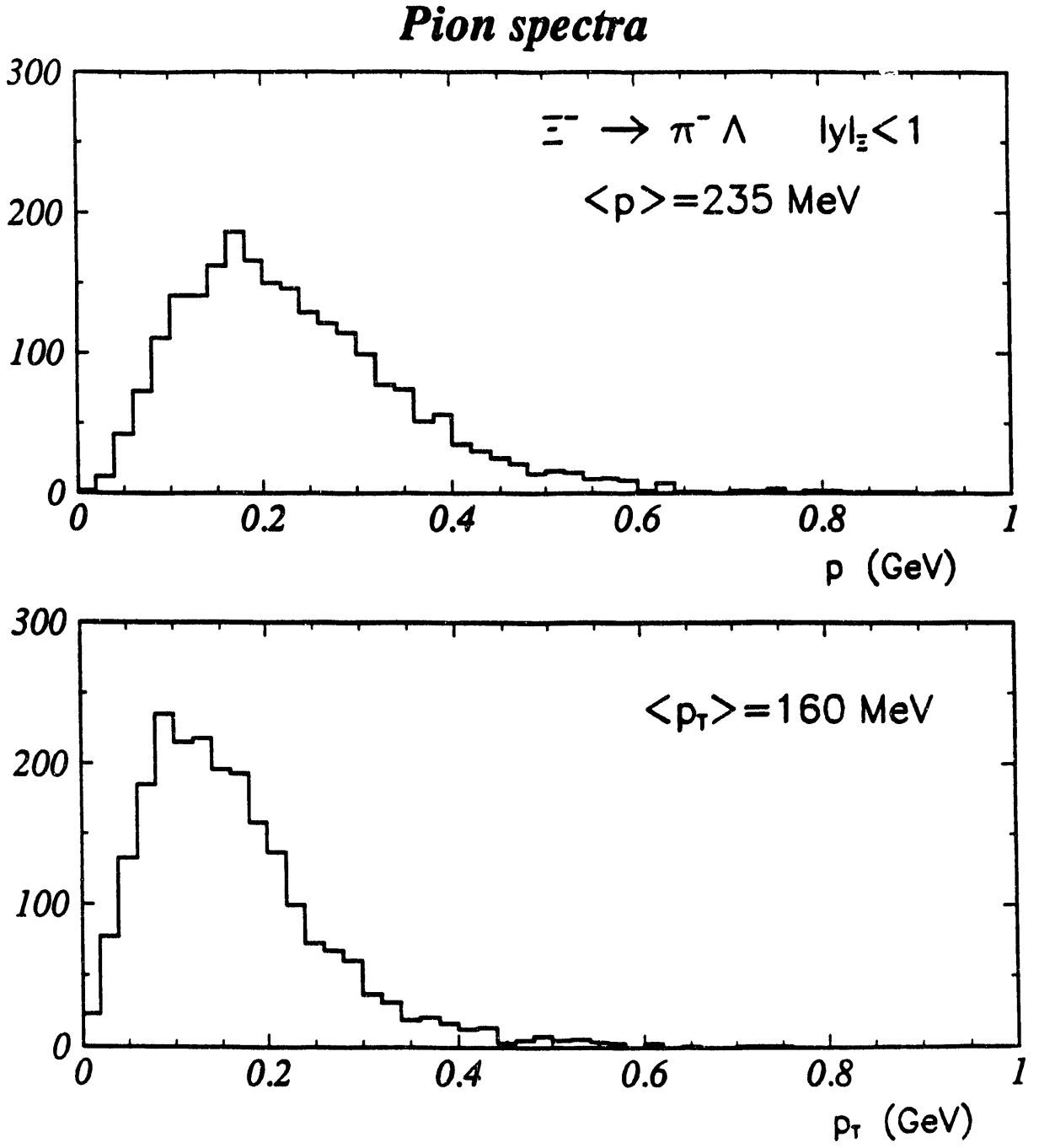
Pion spectra
300
200
100
0
$\Xi^- \rightarrow \pi^- \Lambda$ $|y|_\Xi < 1$
<p>=235 MeV
0
0.2
0.4
0.6
0.8
1
p (GeV)
300
200
100
0
<p_T>=160 MeV
0
0.2
0.4
0.6
0.8
1
p_T (GeV)

Figure 5

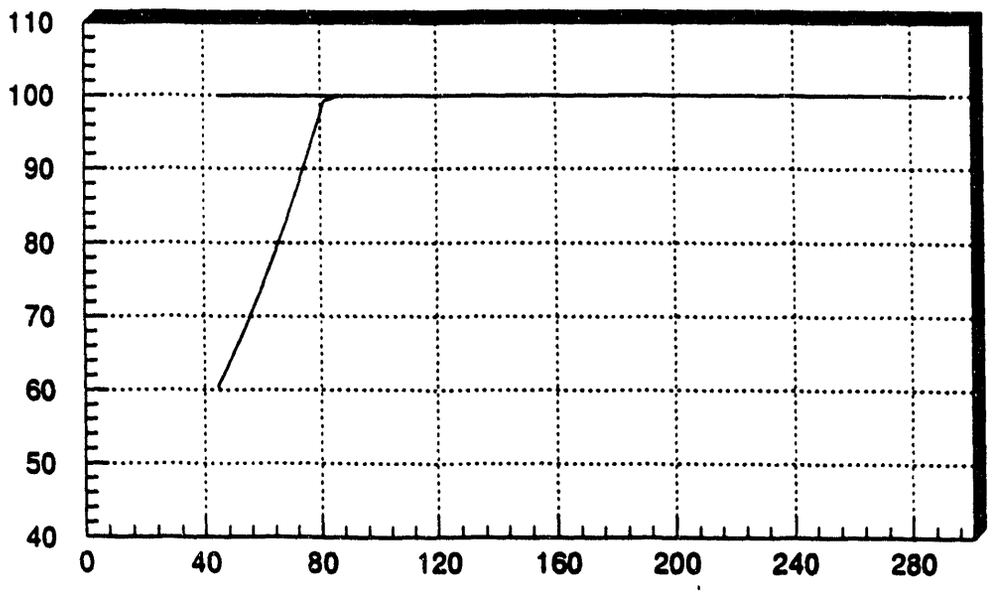

Figure 6

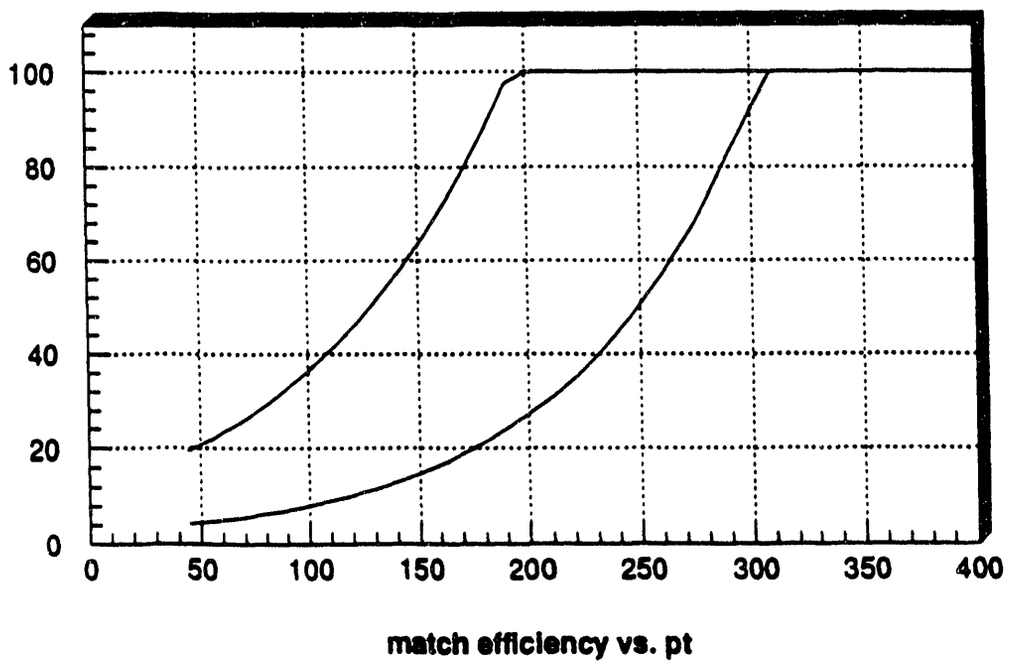

Figure .7

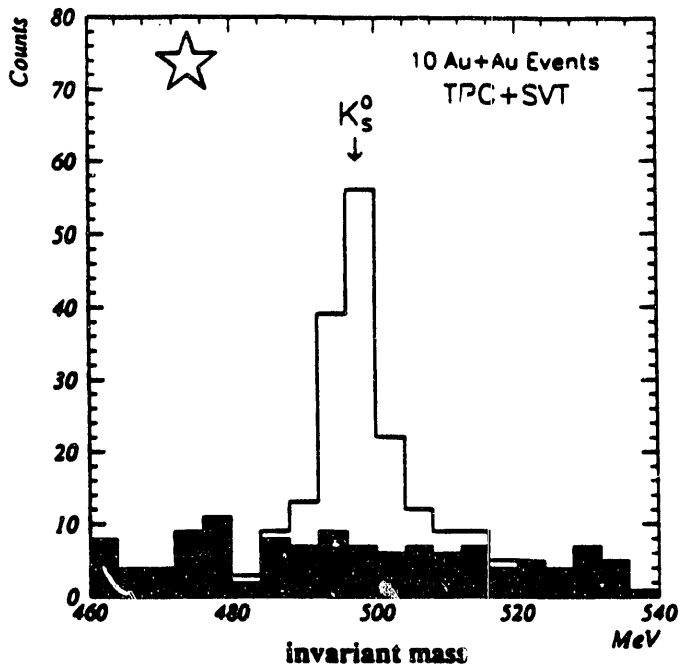

Figure 8

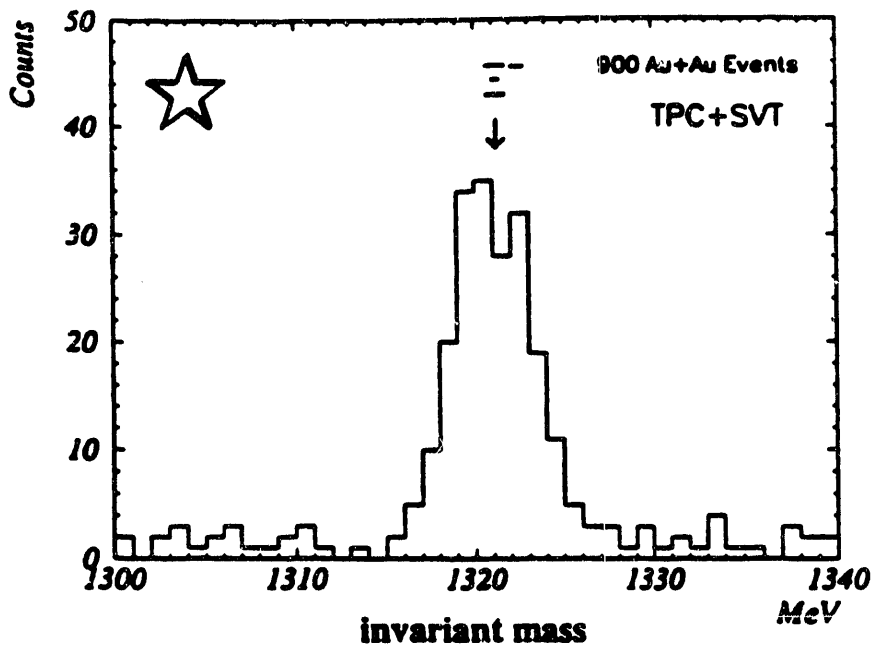

Figure 9

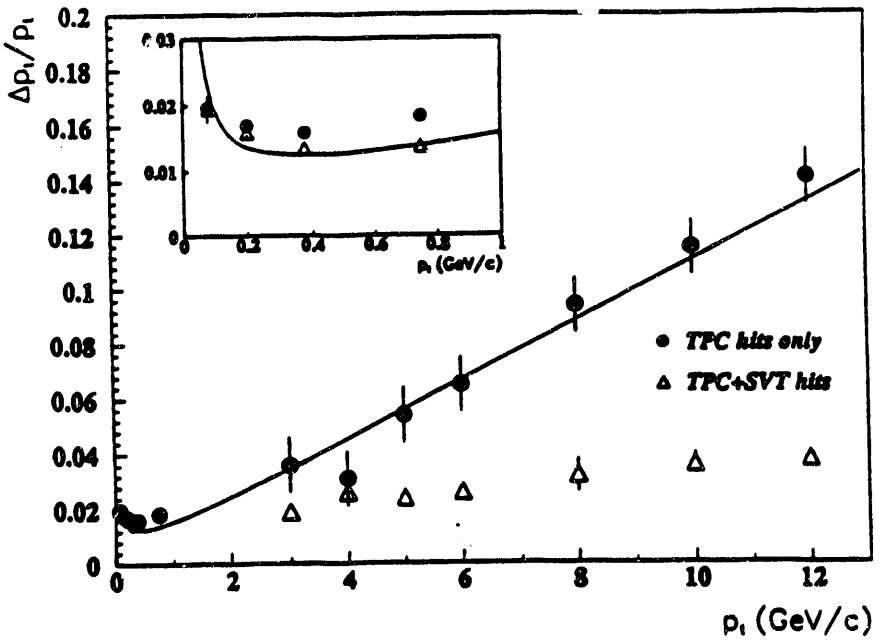

Figure 10

p_t resolution as a function of p_t for both the TPC only and TPC + SVT cases.

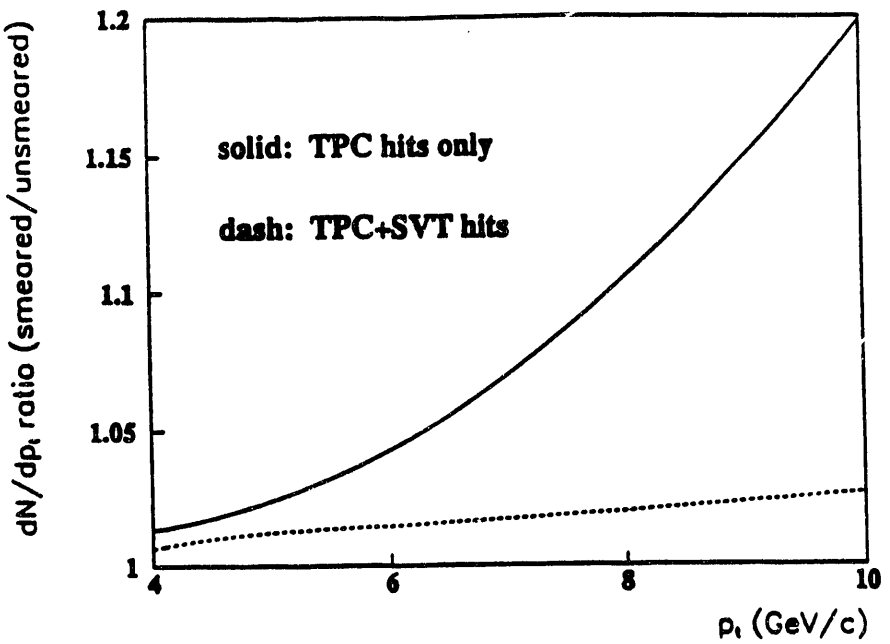

Figure 11

The effect of momentum resolution on the measured yield assuming measurement with TPC alone (solid) and TPC + SVT (dashed).

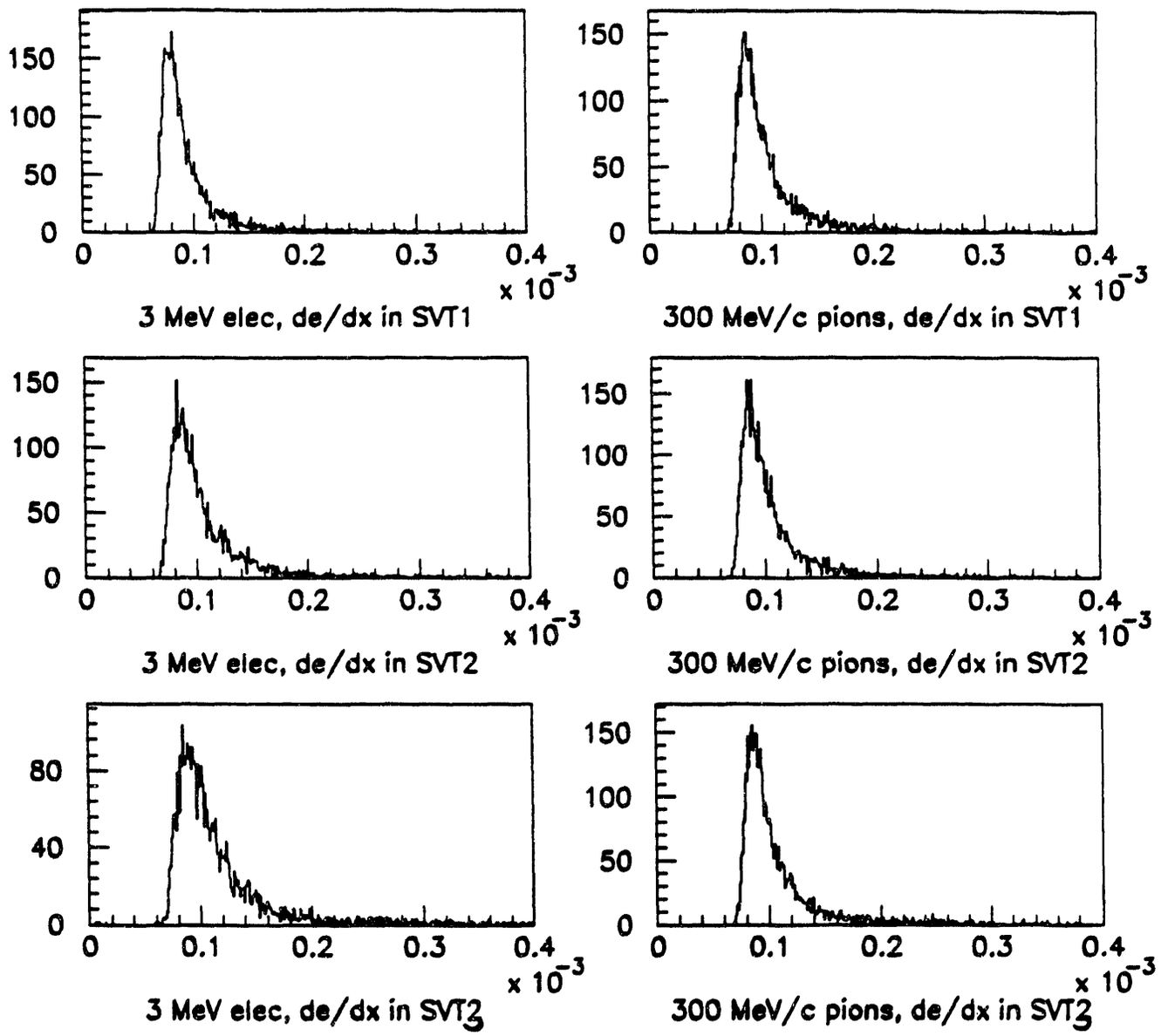
150
100
50
0
0
0.1
0.2
0.3
0.4
x 10^-3
3 MeV elec, de/dx in SVT1
300 MeV/c pions, de/dx in SVT1
3 MeV elec, de/dx in SVT2
300 MeV/c pions, de/dx in SVT2
80
40
3 MeV elec, de/dx in SVT3
300 MeV/c pions, de/dx in SVT3

Figure 12

IV Instrumentation

IV.1 The design and installation of a Target Rapidity Telescope for BNL Experiment 814/877

This year has seen the design and installation by the WSU group of a detector subsystem in the E814/E877 spectrometer at the Brookhaven National Laboratory called the Target Rapidity Telescope. The telescope is placed in the backward hemisphere in the laboratory and the physics reasons for design are two fold. The first purpose is to measure the products of target fragmentation at back angles at AGS energies to determine the ratios of yields for particles, such as p, d, t and alpha's, as a probe of target fragment heating. In E814/E877, the telescope will have the capability of measuring the dependence of these fragment ratios on the centrality of the collision using both our 4π calorimetry and our Silicon multiplicity array. The telescope's second purpose is the detection of produced particles in the backward hemisphere where rescattering could give yields exceeding those expected on the basis of rapidity distributions measured forward of y=0. Recent transverse energy measurements by the E814 collaboration and the π and K rapidity distributions measured by the E802 collaboration suggest considerable interaction does indeed occur between 'spectators' and 'participants' in such collisions.

The desire to measure such a diverse range of particles (π, K, p, d, t, α) over a wide energy range (0 - 200 MeV) dictates the use of an extremely flexible detection system with a high degree of segmentation along the direction of a particle's trajectory. In the present detector, this is provided by a large number (up to 17) dE measurements along a particle's track. Note that in this energy range, ionization energy deposition dominates for all but pions. The detector segments chosen to perform this task in the telescope are shown in figure 1. They comprise: two 22 mm diameter 0.2 mm thick silicon surface barrier detectors, three 22 mm diameter 2 mm thick silicon surface barrier detectors, and six pairs 170 by 170 mm, 5 mm thick NE102 plastic scintillator dE detectors and 170 by 170 mm, 170 mm thick plastic scintillator E detectors. The silicon surface barrier detectors were instrumented using charge sensitive preamplifiers, shaping amplifiers, and Ortec AD811 ADCs. The light output from each of the twelve scintillators was measured by two photomultiplier tubes (PMT) to provide a high light collection efficiency. The E scintillators were coupled directly to 5" diameter PMT's whilst the six dE scintillators were coupled via light guides (due to space considerations) to PMT's. The first dE scintillator was instrumented to provide good (< 80 ps) time resolution for a time-of-flight measurement providing another means of particle identification. The entire telescope is surrounded by plastic scintillator paddles to provide detection of prompt out-scattered radiation following interactions within the detector or for delayed radiation from the decay of stopped particles.

The telescope was mounted at an angle of 143^0 with respect to the beam and at a distance of 80 cm from the target. The solid angle of the telescope was defined by the fifth silicon detector. In order to place the telescope in this position, the rear wall of the E814/E877 target calorimeter was removed.

The purpose of the silicon detectors is to provide high resolution energy measurements (< 30keV) and particle identification for the heavily ionizing particles such as d, t and α's. The plastic scintillator stack is designed to provide identification and measure the energy of the more lightly ionizing particles such as the π^+, K and p. dE plastic scintillators are repeated throughout the telescope because high energy π and K are minimum ionizing over some of their range and thus the initial dE measurements convey little particle identification information. In later analysis a dE-E combination is thus chosen near the end of the particle trajectory. K^+ and π^+ particles can be

distinguished in principal from their anti-particles by requiring a delayed decay signal in at least one of the surrounding plastic scintillators. To enable measurement of this signal each PMT is instrumented with 2 ADC's to permit a simple pulse shape measurement. The ADC integration times for each detector are set to around 20 and 50 ns, with a common start. The ratio of the two energy signals thus permits identification of subsequent decays. Simulations of the detector using GEANT together with the standard HIJET event generator (with re-scattering) indicate that this identification is approximately quite efficient. Further work on this technique is required before it can be confidently implemented.

Figures 2, 3 and 4 shows the simulated energy response of the detector for incident energies of 50, 100 and 200 MeV. The panels show the results for π^+ , π^- , K^+ , K^- and p respectively. The observed resolution for all but protons is determined by the fraction of the decay energy recorded along with the kinetic energy. For K^- in particular, the decay energy contribution precludes particle identification at all energies, while for pions, particle identification becomes impractical significantly above 100 MeV because of hadronic interactions in the detector stack.

Monitoring and gain stabilization of the PMT's, after an initial cosmic ray calibration, is provided by a laser and fibre optic system. A Laser Photonics LN120C nitrogen laser is used to pump a dye cell emitting radiation with a final wavelength of 420 nm, chosen to match the peak response of the PMT's. Each of the E scintillators are connected to the laser system via a light distribution system utilizing AMP 501232-5 plastic fiber optic cable. The laser was run at a repetition rate of about 1 Hz throughout the experiment emitting light equivalent to around 100 MeV in each of the twelve E PMT's. The dE PMT's were not connected as they form only a small contribution to the total energy of an event.

The intensity of the laser emissions varies on a pulse-by-pulse basis and hence some monitoring is required if gain stabilization at the 1% level is to be achieved. This is provided in the current setup by feeding a fixed fraction of the laser output to a PIN photodiode detector instrumented with an Ortec pre-amplifier and spectroscopy amplifier. The PIN diode was chosen for linear response and temperature stability and measurement of the laser intensity was included in the event-by-event data for each laser pulse.

After an initial calibration using radioactive sources, the gain and stability of the silicon detector electronics is monitored using a precision pulser.

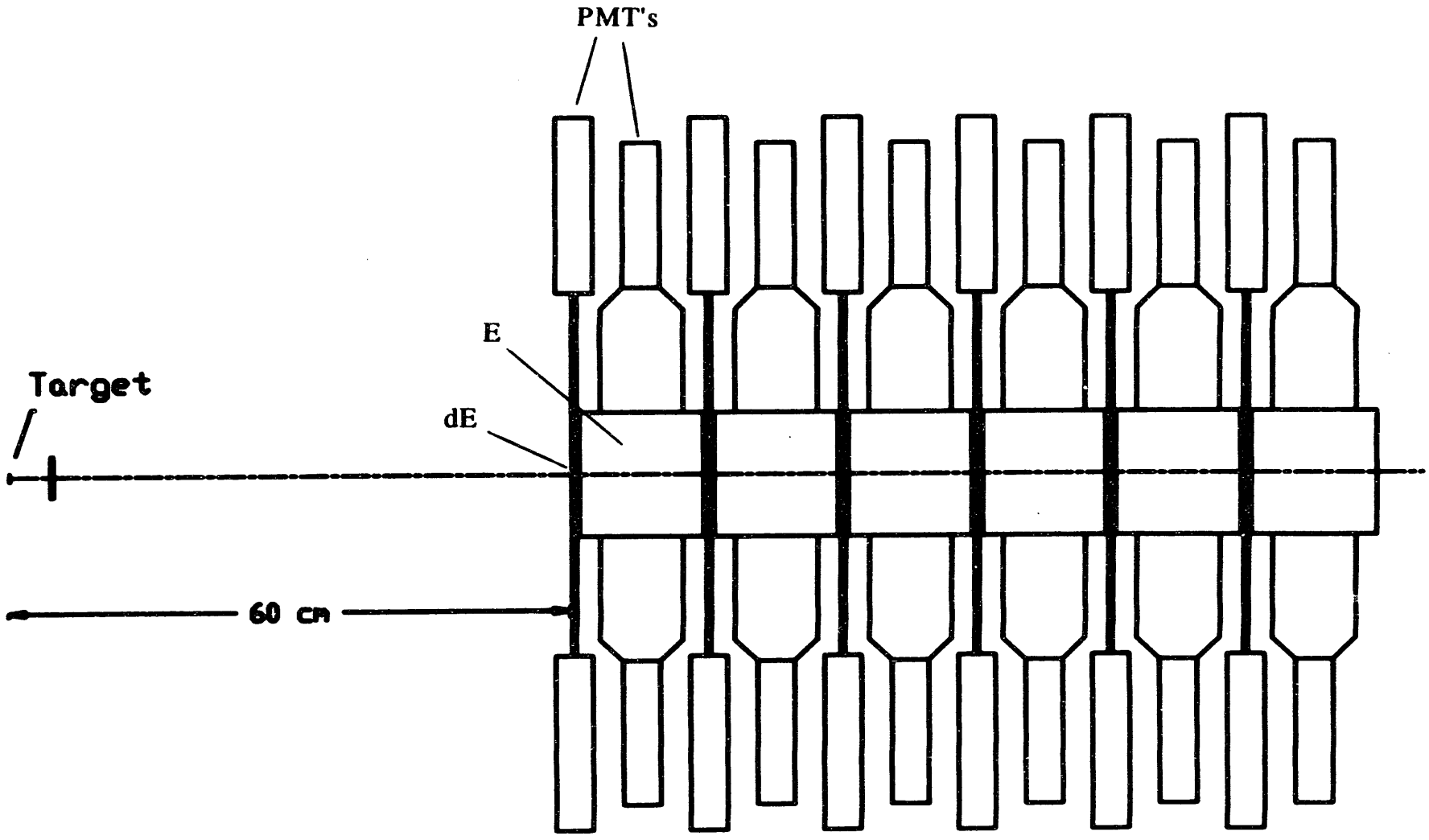

Figure 1. The target Rapidity Telescope of E814/E877

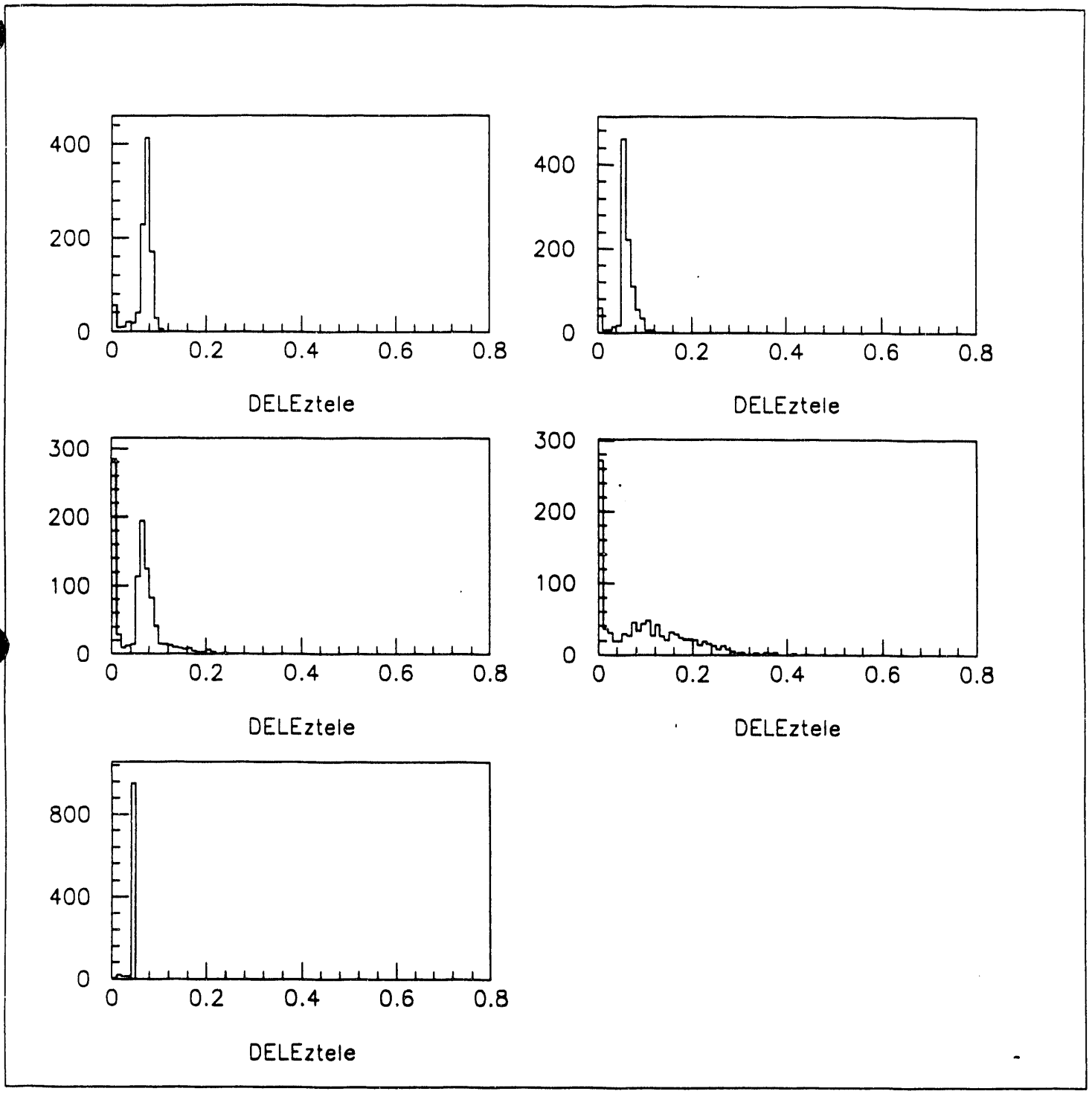

Figure 2. The Simulated Response of the Target Rapiity Telescope to 50 MeV π+, π-, K+, K-, and p

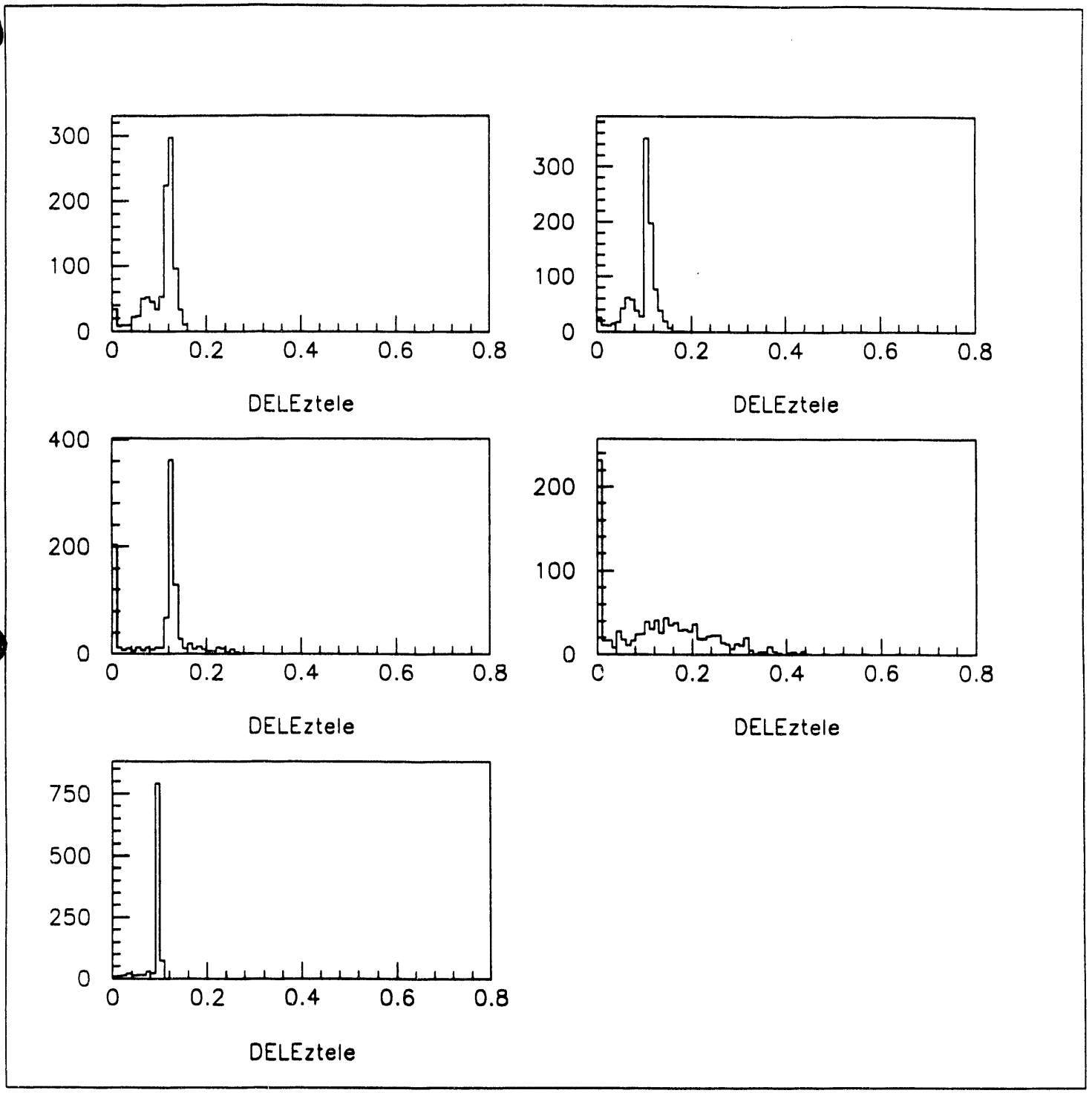

Figure 3. The Simulated Response of the Target Rapiity Telescope to 100 MeV π+, π-, K+, K-, and p

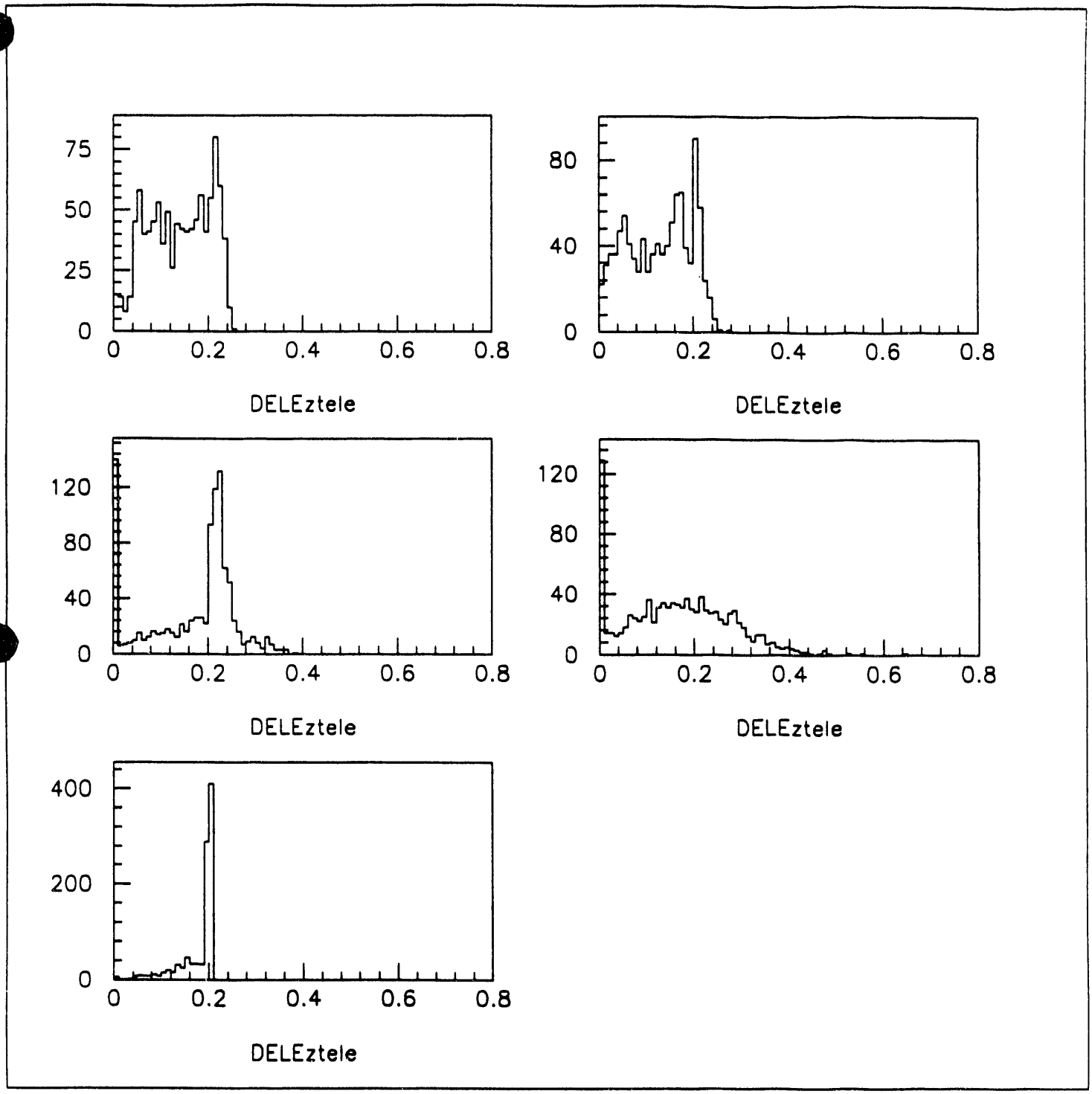

Figure 4. The Simulated Response of the Target Rapiity Telescope to 200 MeV π+, π-, K+, K-, and p

IV.2 Repair Scheme for the E814/E877 Participant Calorimeter

The E814/E877 participant calorimeter (PCAL) at Brookhaven National Laboratory is of a conventional lead/plastic scintillator design incorporating a read out method using wavelength shifting (WLS) fibers. The PCAL is separated into four quadrants as shown in figure 1. Looking downstream, the quadrants are labeled I to IV beginning with the upper left hand quadrant and then rotating clockwise. The layers of scintillator in each quadrant are separated into four azimuthal triangular slices of 22.5 degrees each. These segments are often referred to as pies and are numbered 1 to 16, with pie 1 being the lowest in quadrant I, then rotating clockwise. The pies are segmented radially into eight different size plates of scintillator forming eight towers in each segment. The calorimeter is then longitudinally segmented into four depth sections, two electromagnetic and two hadronic.

Each of the 7552 scintillator plates in the PCAL has a 1.5 mm WLS fiber bonded into one edge. The fibres are routed to photomultiplier tubes (PMT) depending on plate size, azimuthal section, and longitudinal depth from which it originated. In addition, each PMT has a 1.5 mm clear polymethyl methacrylate (PMMA) fiber routed to it from a monitoring port that is part of the optical light source calibration system.

After the June, 1990 heavy ion run, a loss of response was noted in several towers located within pies 6 and 7 of quadrant II. The calorimeter quadrant was subsequently opened on 13th February, 1992 and the problem quickly identified. After visual inspection of the inside of quadrant II, it appears that the movement of a steel block resulted in a number of the WLS fibers breaking near the polyurethane couplers used to support and group fibers towards an appropriate PMT. In most cases the remaining length of WLS fiber is insufficient to allow direct coupling back to the appropriate PMT, though enough fiber remains to ensure that all of the blue scintillation light is wavelength shifted to green, to match the peak sensitivity of the PMT. It is visually estimated that about 150 WLS fibers and 15 clear PMMA optical fibers are no longer routed to their couplers. These WLS fibers represent approximately 2% of all the WLS fibers contained in the PCAL. Some way of extending these WLS fibers must be employed if the symmetry of the PCAL is to be restored for future heavy-ion runs.

In order to investigate techniques for extending these WLS fibers, a visit to the Fermi National Accelerator Laboratory was arranged to consult with Adam Para and Eva Skup, specialists in fiber optic techniques. A number of techniques have been employed to join optic fibers but the most successful appears to be to splice the remaining portion of the WLS fiber to a clear PMMA fiber of larger diameter, a technique also suggested by Joanne Simon-Gillo of Los Alamos National Laboratory. This procedure is achieved by taking the larger diameter fiber and boring a hole a few millimeters deep into one end of the fiber along its axis. The broken end of the WLS fiber is cut using a hot-wire cutter to alleviate stress and then inserted into the hole in the clear fiber. A glue joint is then made using an optical epoxy such as Bicron BC600. The main problem with this technique is that of achieving a bond which has a uniform light transmission for each of the fibers. This is necessary in the PCAL as all of the scintillator plates in one tower are coupled to only four PMTs (one for each depth segment). Any variation between the light transmission of such fibers will directly degrade the resolution of that tower of the PCAL. Current plans are to embark upon a research and development program to determine the best way to meet this requirement. This will include: determination of the optimum techniques for achieving good polishing of the fiber ends, the best methods for applying adhesive in the joint without injecting air bubbles which would scatter the wavelength shifted light, and tests of a number of adhesives and solvents to find one which achieves a bond whose light transmission is stable with time. When these issues have been addressed, the WLS fibers in the PCAL will be fixed in situ at the Brookhaven National Laboratory.

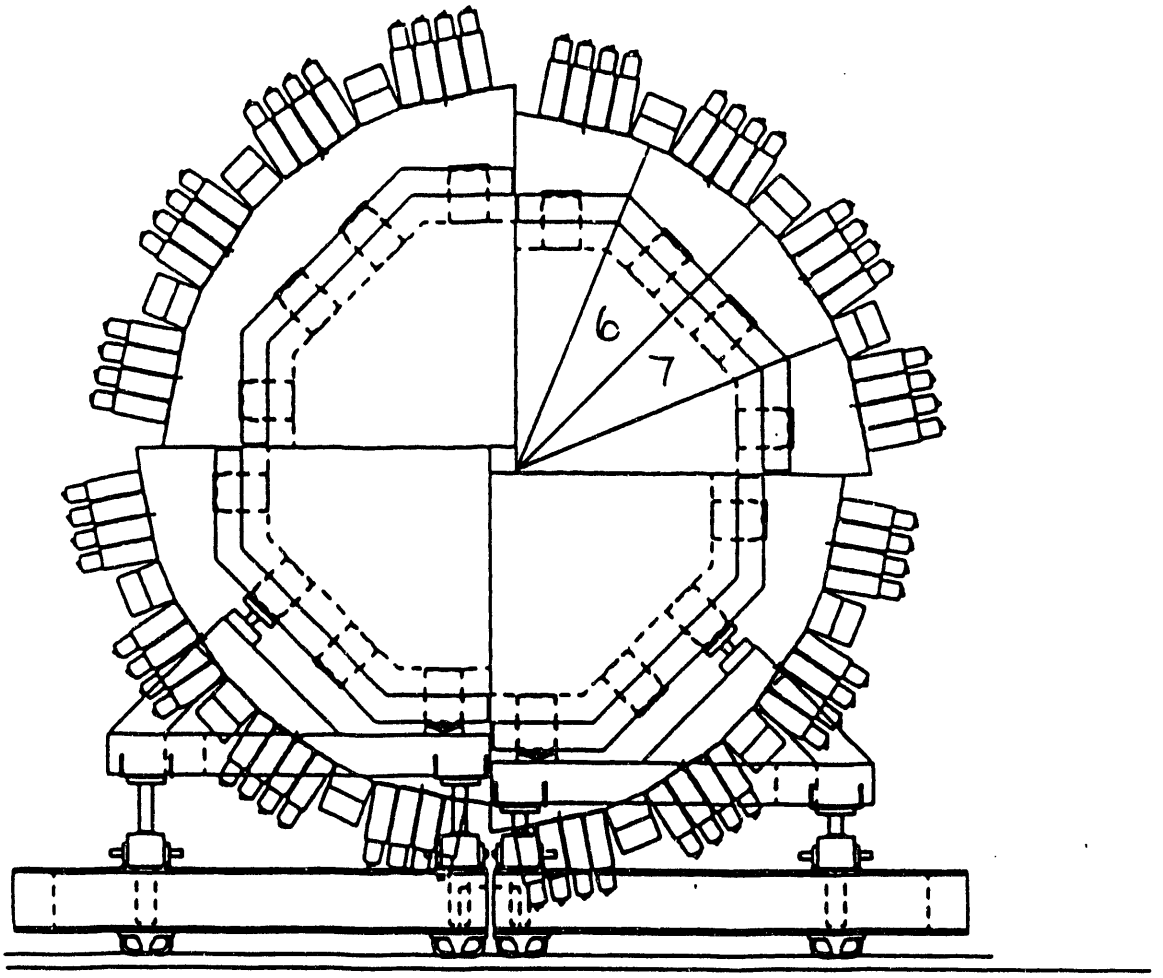

Figure 1: The participant calorimeter of E814. The division of the calorimeter into four quadrants allows for a variable beam aperature size.

IV.3 Relativistic Heavy-Ion Group Computational Facilities

The recent growth of the Relativistic Heavy-Ion Group at Wayne State University has necessitated a rapid expansion of the Group's computational facilities. These facilities (detailed in figure 1), are required to address two main goals: the analysis of event-by-event data from existing AGS experiments at Brookhaven, and the simulation of these ongoing experiments to aid in their data analysis as well as simulation of new experiments planned at Brookhaven.

Analysis of existing event-by-event data from AGS experiment E814/E877 is provided by two VAX 4000-60 workstations. The choice of the VMS operating system for this activity is dictated by the need to maintain compatibility with existing analysis software. The rest of the computational facilities are Silicon Graphics (SGI) UNIX workstations and one mainframe. These are dedicated to simulations of the AGS experiment E864, and the RHIC experiment STAR. Such calculations involve simulation of Gold-Gold collisions at energies of 10.7 GeV/A and 100 GeV/A respectively, and are extremely computationally expensive, requiring the full 42 MFLOP CPU capabilities of the SGI 4D/440S. To further augment these computing facilities, two additional SGI Indigo R4000 workstations and five X-terminals have recently been ordered.

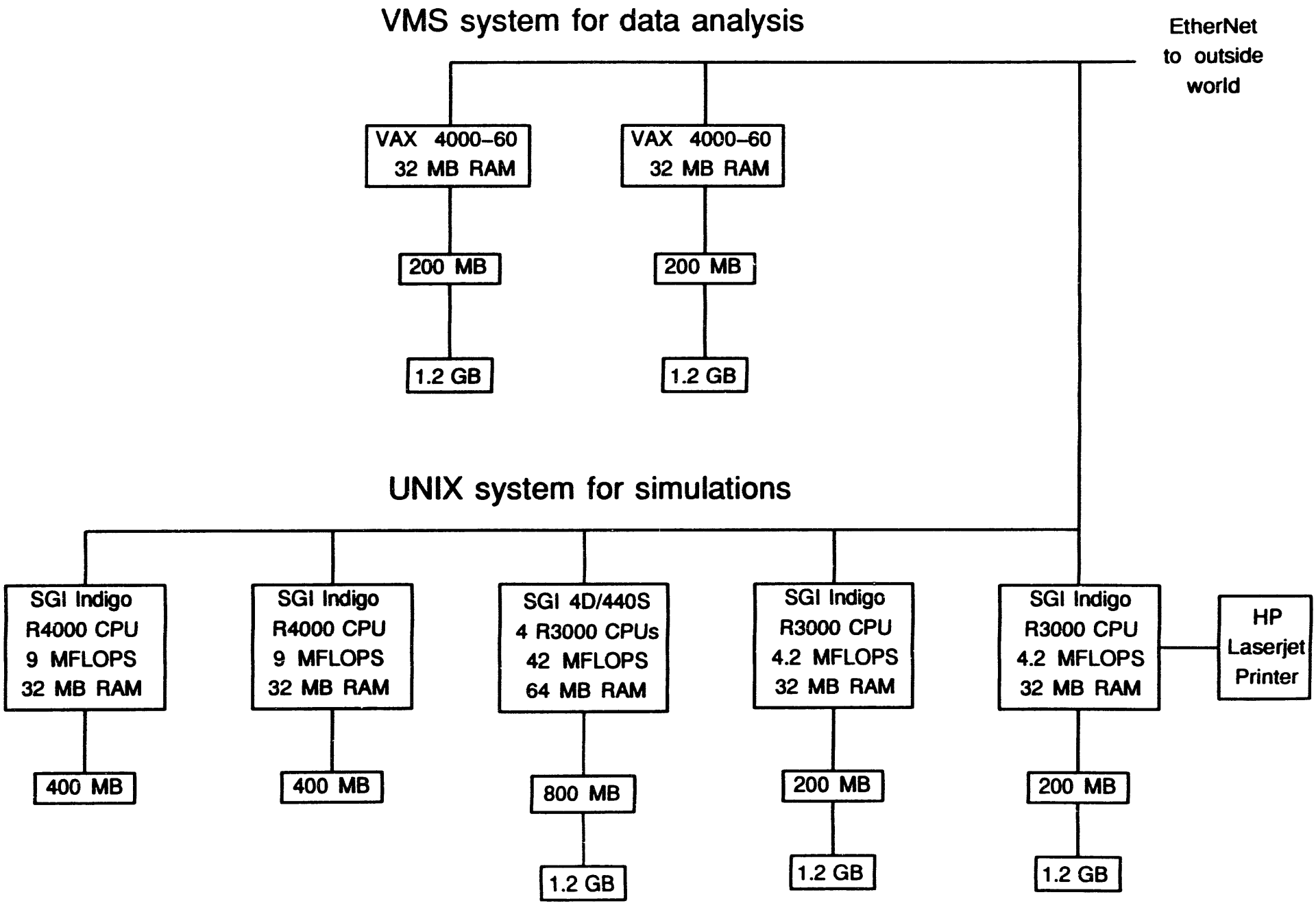
VMS system for data analysis
EtherNet to outside world
VAX 4000-60 32 MB RAM
VAX 4000-60 32 MB RAM
200 MB
200 MB
1.2 GB
1.2 GB
UNIX system for simulations
SGI Indigo R4000 CPU 9 MFLOPS 32 MB RAM
SGI Indigo R4000 CPU 9 MFLOPS 32 MB RAM
SGI 4D/440S 4 R3000 CPUs 42 MFLOPS 64 MB RAM
SGI Indigo R3000 CPU 4.2 MFLOPS 32 MB RAM
SGI Indigo R3000 CPU 4.2 MFLOPS 32 MB RAM
HP Laserjet Printer
400 MB
400 MB
800 MB
200 MB
200 MB
1.2 GB
1.2 GB
1.2 GB

V. THEORY

V.1 Bosonic kinetics: thermalization of mesons and the pion $p_\perp$ spectrum in ultrarelativistic heavy ion collisions[1-4]

Gerd M. Welke, in collaboration with H. W. Barz,[1] G. F. Bertsch,[2] P. Danielewicz,[2], H. Schulz,[3] M. Prakash,[4] and P. Schuck.[5]

Negative particle and π^0 spectra from ultra-relativistic heavy ion collisions at CERN show a markedly enhanced low transverse momentum component when compared to corresponding minimum bias pp spectra.[5] As one possible source of this effect, we have considered the rôle of quantum correlations in the evolution of the hadronic phase of the collision, as included in a bosonic Boltzmann equation

$$\frac{Df_1}{Dt} = -\frac{1}{1+\delta_{12}}\frac{g_2}{2E_1}\int d\Gamma_2 d\Gamma_3 d\Gamma_4\,(2\pi)^4\delta^4(k_1+k_2-k_3-k_4)|T_{12}|^2\{f_1f_2\tilde{f}_3\tilde{f}_4 - f_3f_4\tilde{f}_1\tilde{f}_2\}\,. \tag{1}$$

This equation becomes a coupled set if more than one particle species is considered. The factors $\tilde{f}_i \equiv 1 + f_i$ imply that if collisions are frequent and effective enough to thermalize the system during the expansion phase (and/or if the initial phase space occupation large enough) considerable low momentum peaking will result in the final state. Our investigations have specifically addressed

1. The development of a new test-particle method to solve Eq. (1).[1,2] To test this procedure, both the collision rate in equilibrium and approach to the equilibrium Bose-Einstein distribution function were considered.

2. An application to the simplest scenario in which all secondary mesons consist of pions only. The $\tilde{f}$-factors are then be maximized, and this picture is a zero-order test of the effect of quantum correlations. The initial phase space distribution was guided by pp data (for small source sizes one expects negligible Bose correlation effect) in a Bjorken-like picture,

$$\frac{d^6N}{dy_b\,dr_\perp^2\,dy\,dp_\perp^2} = \mathcal{N}\left[\exp\left[\beta m_\perp\cosh(y-y_b)\right]-1\right]^{-1} \times\ \theta(\Delta y_b/2+y_b)\,\theta(\Delta y_b/2-y_b)\int_{-\infty}^{\infty}dz'\,\rho_O(r_\perp^2+z'^2)\,, \tag{2}$$

where y =rapidity, $p_\perp^2 = m_\perp^2 - m_\pi^2$ is the transverse momentum, $r_\perp$ = transverse position, ρ_O = empirical projectile baryon density, and y_b is a (flat) boost rapidity. Note that the initial distribution is not even locally equilibrated. The parameters appearing in (2) were fixed from NA35 and NA22-EHS pp data at central rapidities.[5,6] The initial phase space occupation depends linearly on the effective hadronization time τ_0 of the pions (since $z = \tau_0^{eff}\sinh y_b$; the magnitude of the low-$p_\perp$ enhancement may thus be expected to depend sensitively on τ_0^{eff}. Fig. 1(a) and (b) show the results of a calculation with $\tau_0^{eff} = 7$ fm/c. The calculations thus show a strong correlation effect and suggest

$\tau_0 \lesssim 7$ fm/c. The magnitude of the peaking also depends sensitively on τ_0^{eff} (Fig. 1(c)) – shorter hadronization times imply stronger peaking.

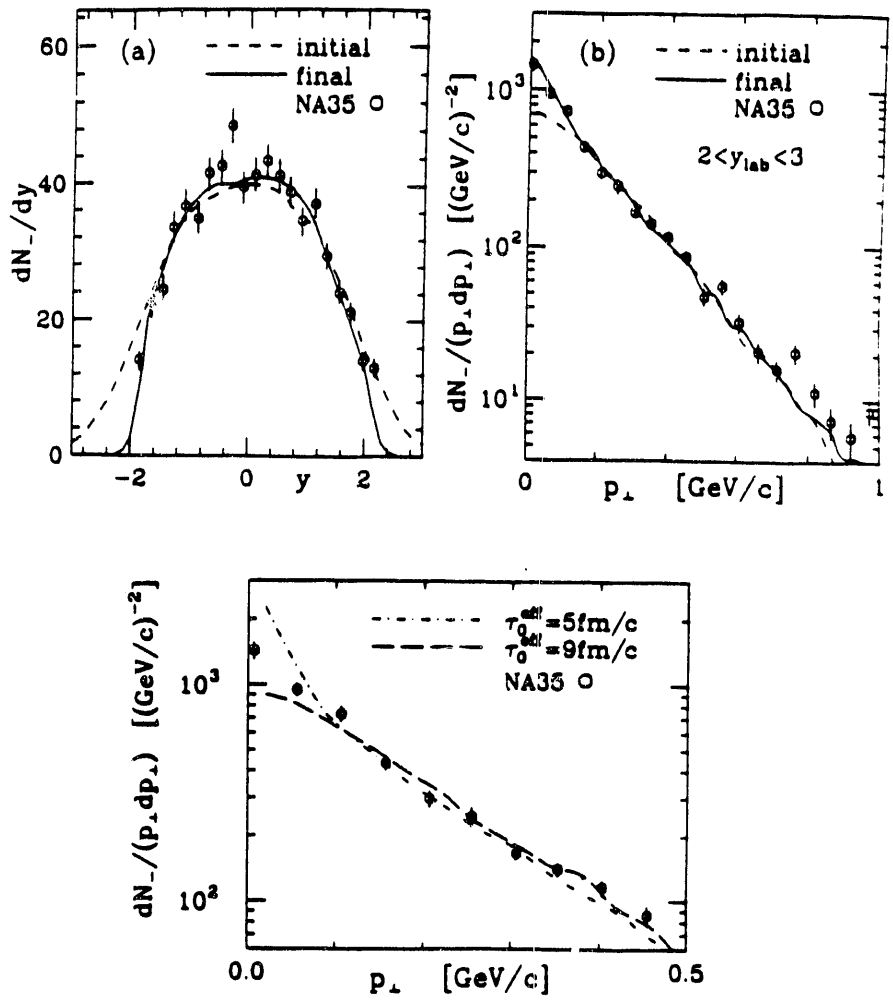

FIG. 1 (a) Rapidity distribution (dashed=initial, solid=final, circles=NA35 data). (b) Pion transverse momentum spectrum (dashed=initial, solid=final, circles=NA35 data). Both figures are for $\tau_0^{eff} = 7$ fm/c and $\beta^{-1} = 135$ MeV. (c) Pion transverse momentum spectra for different pionization times.

3. An investigation[3] of the effects of the dense medium on the scattering cross-section in Eq. (1). The equation for the T-matrix there is of the Bethe–Goldstone type, and the influence of the medium may partially be accounted for via phase space occupancy factors

f. For a seperable interaction,[7] the in-medium T-matrix in channel α is

$$T_\alpha(k,k',P,s) = \frac{V_\alpha(k)\,V_\alpha(k')}{s - M_\alpha^2 - \int_0^\infty dk\,k^2\,\frac{V_\alpha^2(k)\,\langle 1+f_1(k)+f_1(-k)\rangle_{angles}}{4\pi^2\omega(k)(s-4\omega^2(k)+ic)}} \quad . \tag{3}$$

Fig. 2, for the case of a thermal system (T = 150 MeV and μ = 130 MeV), shows how strong the suppression due to these medium effects can be, particularly at low $\sqrt{s}$. The cross section is now essentially inversely proportional to $\langle 1 + f_k + f_{-k}\rangle^2_{angles}$. Indeed, it is found that at sufficient particle density, the scattering rate in a *Bose* gas *with* in-medium effects is equal to the scattering rate in a *Maxwell* gas with *no* medium effects. Repeating the calculations with σ_{med}, the pionization time required to produce peaking consitent with data shrinks to 4.5 fm/c,[4] for which case the average pion density in the c.m. frame is ~ 0.5 fm^{-3} at the time the central rapidity region has hadronized.

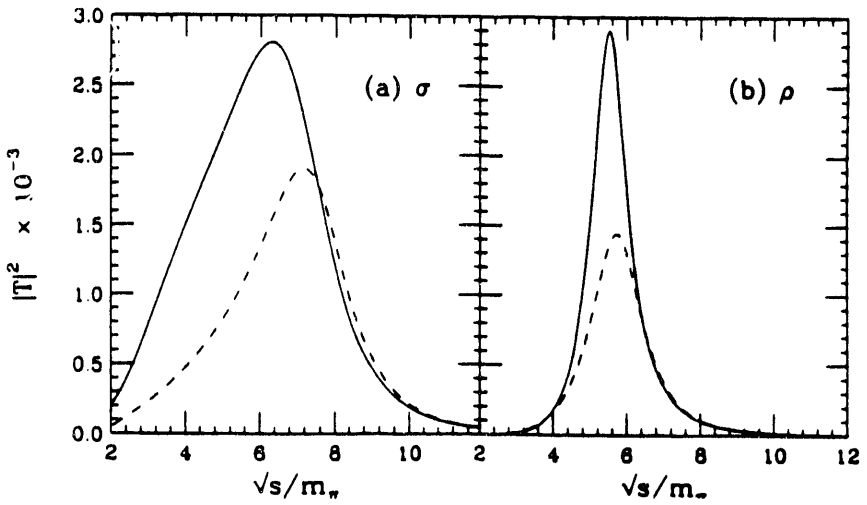

FIG. 2 (a) T_σ as a function of $\sqrt{s}$ for $P = 0$; solid line: free cross section, dashed line: including medium effects in a thermal bath with T = 150 MeV and μ = 130 MeV. (b) As for (a), but for the ρ-channel.

4. The case of a full resonance gas:[4] These decrease phase space occupation and reduce the quantum correlation effects yet further. Thus, at opposite extreme to the picture in above two sections, we have assumed string/Lund model initial occupation, *viz.*, $\pi : \eta : \rho : \omega \sim 3 : 1 : 9 : 3$. The in-medium $\pi\pi$ scattering and ρ-meson formation is described via the T-matrix above, and all other cross-sections via a Hauser-Feshbach formalism, as an estimate. Only a hadronization time of 1 fm/c now barely produces sufficient peaking.[4]

Our work has investigated if quantum correlations after hadronization could alone be responsible for observed low-$p_\perp$ peaking in pion spectra. We treat the effective pionization/hadronization time as a free parameter, and investigate two extreme initial particle composition scenarios. For pions only, the in-medium cross section implies an average pionization time of $\sim$ 4.5 fm/c, decidedly short for a strong first order phase transition. In the opposite extreme of string-type initial particle abundance, $\tau_{had} \sim 1$ fm/c, and a QGP is ruled out. The alternative is that the hadronization process itself, or some other hadronic mechanism, is responsible (at least in part)

for the "soft pion puzzle." The current work requires extension to investigate the effects of baryons, the mean field, and further possible medium-dependences of hadronic properties and cross sections. Specifically, we are investigating HBT data to compare to the current model, and the possibility of a σ-bound state. The work here also lends itself to RHIC physics, where the SVT will permit a measurement of particle spectra down to $p_\perp \sim 40$ MeV/c.

[1]ISP, ZfK Rossendorf, O-8051 Dresden, Federal Republic of Germany.
[2]NSCL/Cyclotron Laboratory, M.S.U., East Lansing, MI 48824-1321.
[3]IFT, Federal University of Rio de Janeiro, Rio de Janeiro, Brazil.
[4]Physics Department, SUNY at Stony Brook, NY 11794-3800
[5]ISN, IN2P3-CNRS/Université Joseph Fourier, F-38026 Grenoble Cédex, France.

References

1. G.M. Welke, G.F. Bertsch, S. Boggs, and M. Prakash, "Simulations of the Boltzmann equation for bosons," in Proceedings of the Seventh Winter Workshop on Nuclear Dynamics, page 189, Jan. 26 - Feb. 2, 1991, Key West, Florida; eds. W. Bauer and J. Kapusta (World Scientific Press).
2. G.M. Welke and G.F. Bertsch, Phys. Rev. C45 (1992) 1403.
3. Z. Aouissat, G. Chanfray, P. Schuck, and G.M. Welke, Z. Phys. A340 (1991) 347.
4. H.W. Barz, P. Danielewicz, H. Schulz, and G.M. Welke, Phys. Lett. B287 (1992) 40.
5. For example, The NA35 Collaboration: H. Ströbele et al., Z. Phys. C38 (1988) 89.
6. The EHS-NA22 collaboration: M. Adamus et al., Z. Phys. C39, 311 (1988).
7. J.A. Johnstone and T.-S.H. Lee, Phys.Rev. C34, (1986) 243.

V.2 Non-equilibrium properties of hadronic mixtures[1,2]

Gerd M. Welke, in collaboration with M. Prakash,[1] M. Prakash,[1] and R. Venugopalan.[2]

The equilibration of hot hadronic matter has been studied in the framework of relativistic kinetic theory. Various non-equilibrium properties of a mixture comprised of pions, kaons and nucleons were calculated in the dilute limit for small deviations from local thermal equilibrium. Interactions between these constituents are specified by two body empirical phase shifts. The properties calculated include the relaxation times, collision times and mean free paths associated with binary interactions. Transport properties such as the viscosity, the thermal conductivity, and the diffusion and thermal diffusion coefficients were calculated in the Chapman-Enskog formalism. This formalism was extended to extract relaxation times associated with shear and heat flows, drag flow and diffusion flow.

It was found that kaons and nucleons equilibrate significantly more slowly than pions. A calculation of persistence ratios explicitly shows that the degradation of momentum and energy in elastic collisions is smaller for heavier particles than for pions. This result is independently obtained by calculating the relaxation times associated with the drag and diffusion of these particles. Our results have important implications for the space-time description of ultrarelativistic heavy ion collisions. In particular, they give a plausible resolution to a longstanding puzzle concerning collective flow effects on the transverse momentum distributions of heavy particles such as kaons and nucleons versus those of pions.

[1]Physics Department, SUNY at Stony Brook, NY 11794-3800
[2]School of Physics and Astronomy, University of Minnesota,
Minneapolis, MN 55455.

References

1. M. Prakash, M. Prakash, R. Venugopalan and G. Welke, Stony Brook Preprint SUNY-NTG-92-22, and NSCL/MSU Preprint MSUCL-854; submitted.
2. M. Prakash, M. Prakash, R. Venugopalan and G. Welke, Stony Brook Preprint SUNY-NTG-92-23, and WSU Preprint WSU-NP-92-1; submitted.

END

DATE
FILMED
6/10/93